

NACARM A52B20

6378


NACA

TECH LIBRARY KAFB, NM

RESEARCH MEMORANDUM

THE EFFECTS OF REYNOLDS NUMBER AT MACH NUMBERS

UP TO 0.94 ON THE LOADING ON A 35° SWEPT-

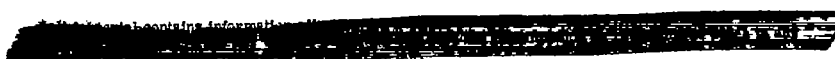
BACK WING HAVING NACA 65₁A012

STREAMWISE SECTIONS

By Bruce E. Tinling and Armando E. Lopez

Ames Aeronautical Laboratory
Moffett Field, Calif.

CLASSIFIED DOCUMENT



NATIONAL ADVISORY COMMITTEE
FOR AERONAUTICS

WASHINGTON

June 16, 1952

PERMANENT RECORD

319.98/39



0142903

1N

NACA RM A52B20

NATIONAL ADVISORY COMMITTEE FOR AERONAUTICS

RESEARCH MEMORANDUM

THE EFFECTS OF REYNOLDS NUMBER AT MACH NUMBERS

UP TO 0.94 ON THE LOADING ON A 35° SWEPT-

BACK WING HAVING NACA 65₁A012

STREAMWISE SECTIONS

By Bruce E. Tinling and Armando E. Lopez

SUMMARY

An investigation has been made of the effects of a variation of Reynolds number on the forces, moments, and surface pressures on a semi-span model of a wing having 35° of sweepback, an aspect ratio of 5, a taper ratio of 0.7, and the NACA 65₁A012 section in planes parallel to the plane of symmetry. Data are presented for a range of Reynolds numbers from 2,000,000 to 10,000,000 at a Mach number of 0.25, and from 2,000,000 to approximately 4,500,000 at Mach numbers from 0.60 to 0.94.

The results indicated that, in general, the effects of Reynolds number were greater toward the tip of the wing than near the root. At a Mach number of 0.25, the maximum normal-force coefficients for wing sections inboard of about 80 percent of the semispan were greater than predicted by applying simple sweep theory to two-dimensional section data. A lower value of maximum section normal-force coefficient than predicted from section data was obtained for sections at 90 and 95 percent of the semispan. At Mach numbers greater than that for drag divergence, a change in Reynolds number from 2,000,000 to 4,500,000 caused a change in loading at small lift coefficients which, at a Mach number of 0.94, was sufficient to shift the center of pressure rearward by 150 percent of the mean aerodynamic chord. This change in loading is believed to have resulted from a change in the type of boundary layer in the region of the shock.

INTRODUCTION

An investigation of the effects of Mach number and Reynolds number on the aerodynamic characteristics of several 12-percent-thick wings having 35° of sweepback and various amounts of camber has been reported in reference 1. The results of this investigation indicate that an abrupt decrease of lift-curve slope accompanied by a large reduction of static longitudinal stability occurred at the design lift coefficient at a Reynolds number of 2,000,000 when the Mach number for drag divergence was exceeded. Similar phenomena have been reported in reference 2 which presents results of tests at a Reynolds number of about 600,000 of several wings having 45° of sweepback and the NACA 63₁A012 section in planes parallel to the plane of symmetry. This reduction of static longitudinal stability is contrary to previous results from tests of swept-back wings having sections less than 12 percent thick. (See, for example, references 3 and 4.) The results of reference 1 also indicate the effects of Reynolds number on the aerodynamic characteristics of the wings at low Mach numbers to be large.

In order to determine the nature of the changes in loading which resulted in the above phenomena, a duplicate of one of the semispan models of reference 1 was constructed. This model was equipped with flush orifices for the measurement of surface pressures. High-speed tests were conducted in the Ames 12-foot pressure wind tunnel and in the Ames 16-foot high-speed wind tunnel in order that the effect of a variation of Reynolds number from 2,000,000 to about 4,500,000 could be assessed at high Mach numbers. Low-speed tests were conducted in the 12-foot wind tunnel over the same range of Reynolds numbers as reported in reference 1.

NOTATION

$\frac{b}{2}$	wing semispan perpendicular to the plane of symmetry, feet
C_D	drag coefficient $\left(\frac{\text{drag}}{qS} \right)$
C_{D_p}	pressure-drag coefficient $\left(\frac{\text{pressure drag}}{qS} \right)$
C_L	lift coefficient $\left(\frac{\text{lift}}{qS} \right)$

- C_m pitching-moment coefficient about the quarter point of the mean aerodynamic chord $\left(\frac{\text{pitching moment}}{qS\bar{c}} \right)$
- C_{m_s} span-load pitching-moment coefficient about the quarter point of the mean aerodynamic chord computed from the span loading assuming the section centers of pressure at 26.2 percent chord
- C_N normal-force coefficient $\left(\frac{\text{normal force}}{qS} \right)$
- c local wing chord parallel to the plane of symmetry, feet
- c_{av} average wing chord parallel to the plane of symmetry, feet
- \bar{c} mean aerodynamic chord $\left(\frac{\int_0^{b/2} c^2 dy}{\int_0^{b/2} c dy} \right)$, feet
- C_m section pitching-moment coefficient about the quarter point of the section chord $\left(\frac{\text{section pitching moment}}{qc^2} \right)$
- C_n section normal-force coefficient $\left(\frac{\text{section normal force}}{qc} \right)$
- M free-stream Mach number
- P pressure coefficient $\left(\frac{\text{local static pressure} - \text{free-stream static pressure}}{q} \right)$
- $P_{cr, \Delta=35^\circ}$ critical pressure coefficient, corresponding to a local Mach number of 1.0 in a direction perpendicular to the wing quarter-chord line
- $$\left[\frac{2}{\gamma M^2} \left\{ \left[\frac{2}{\gamma+1} \left(1 + \frac{\gamma-1}{2} M^2 \cos^2 35^\circ \right) \right]^{\frac{\gamma}{\gamma-1}} - 1 \right\} \right]$$
- (See reference 4 for derivation of this expression.)
- q free-stream dynamic pressure $\left(\frac{1}{2} \rho V^2 \right)$, pounds per square foot

R Reynolds number, based on the mean aerodynamic chord
S area of semispan wing, square feet
V free-stream velocity, feet per second
y lateral distance from the plane of symmetry, feet
α angle of attack, degrees
γ ratio of specific heats (1.400)
η fraction of semispan $\left(\frac{y}{b/2}\right)$
ρ free-stream mass density of air, slugs per cubic foot

MODEL

The semispan model represented a wing having an aspect ratio of 5 and had 35° of sweepback of the quarter-chord line, a taper ratio of 0.7, and the NACA 65₁A012 airfoil section parallel to the plane of symmetry. The plan form and section of this model are identical to one of those tested during the investigation reported in reference 1.

The surface of the model was an alloy of tin and bismuth which was bonded to a steel spar. In order to measure surface pressures, the model was equipped with flush orifices in rows oriented parallel to the plane of symmetry at 10, 20, 40, 60, 80, 90, and 95 percent of the semispan. The dimensions of the model are shown in figure 1, and the coordinates of the NACA 65₁A012 airfoil section are given in table I. Similar semi-span mountings were used in both the Ames 12-foot pressure wind tunnel and the Ames 16-foot high-speed wind tunnel as shown in the photographs of figure 2. In each case, the model was mounted with the root chord in the plane of the 4-foot-diameter turntable, and the juncture between the model and the turntable was sealed. The 1/8-inch gap around the edge of the turntable was not sealed.

TESTS

Ames 12-Foot Pressure Wind Tunnel

Two series of tests were conducted: one to evaluate the effects of Reynolds number at a Mach number of 0.25, and one to evaluate the effects

of Mach number at a Reynolds number of 2,000,000. (See fig. 3.) Surface pressures, lift, drag, and pitching moment were measured over an angle-of-attack range sufficient to obtain data for lift coefficients from zero to that for the stall, except where the maximum angle of attack was limited by wind-tunnel power or by the height of the multiple tube manometer which was used to measure surface pressures.

Ames 16-Foot High-Speed Wind Tunnel

Surface pressures were the only measurements made during the tests conducted in the Ames 16-foot high-speed wind tunnel. As shown in figure 3, the Reynolds number of these tests varied from 3,900,000 at a Mach number of 0.62 to 4,600,000 at a Mach number of 0.94.

CORRECTIONS TO DATA

Dynamic Pressure

The dynamic pressure measured in each wind tunnel was corrected for constriction effects due to the presence of the tunnel walls by the method of reference 5. These corrections have not been modified to allow for the effects of sweep. This correction and the corresponding correction to the Mach number are listed in the following table:

Corrected Mach number	12-foot pressure wind tunnel		16-foot high-speed wind tunnel	
	Uncorrected Mach number	$\frac{q_{corrected}}{q_{uncorrected}}$	Uncorrected Mach number	$\frac{q_{corrected}}{q_{uncorrected}}$
0.60	0.60	1.000	0.60	1.000
.80	.799	1.002	.799	1.001
.85	.849	1.002	.849	1.001
.875	.873	1.003	.874	1.002
.90	.897	1.004	.898	1.002
.92	.915	1.005	.918	1.003
.94	.934	1.006	.936	1.004

Force Measurements

The data obtained in the Ames 12-foot pressure wind tunnel were corrected for the effects of tunnel-wall interference originating from lift on the model by the method of reference 6 using the theoretical span load distribution for incompressible flow calculated by the method of reference 7. The corrections added to the drag and to the angle of attack were:

$$\Delta\alpha = 0.263 C_L$$

$$\Delta C_D = 0.00417 C_L^2$$

Since the turntable upon which the model was mounted was directly connected to the balance system, a tare correction to the drag was necessary. This correction was determined from tests with the model removed from the wind tunnel. The following corrections were subtracted from the measured drag coefficients:

$R \times 10^{-6}$	M	C_D tare
10	0.25	0.0066
6	.25	.0067
4	.25	.0069
2	.25	.0076
2	.60	.0085
2	.80	.0094
2	.85	.0097
2	.875	.0100
2	.90	.0102
2	.92	.0103
2	.94	.0105

No attempt has been made to evaluate tares due to interference between the model and the turntable or to compensate for the tunnel-floor boundary layer which, at the turntable, had a displacement thickness of 1/2 inch.

Integration of Surface Pressures

In order to evaluate the effects of Reynolds number on the aerodynamic characteristics of the wing at high subsonic speeds, it was

necessary to integrate the surface pressures measured in the 16-foot high-speed wind tunnel to obtain normal force, pitching moment, and pressure drag. In performing the integrations, the loading was extrapolated from 10 percent of the semispan toward the wing root. It was found that pitching moments obtained by integration of the surface pressures measured in the 12-foot wind tunnel agreed with the pitching moments obtained from force measurements if the loading curve was terminated 1/2 inch from the wing root, a distance equal to the tunnel boundary-layer displacement thickness. This procedure was followed when extrapolating the loading obtained from the 16-foot wind-tunnel tests since the results of the integrations were to be compared with force measurements made in the 12-foot wind tunnel.

The angle of attack measured during the tests in the 16-foot high-speed wind tunnel was corrected for the effects of tunnel-wall interference due to lift on the model by the method of reference 8. The following correction was added to the angle of attack:

$$\Delta\alpha = 0.135 C_L \approx 0.135 C_N$$

where C_N was obtained by integration of surface pressures.

RESULTS AND DISCUSSION

The aerodynamic characteristics of the model tested during the present investigation were similar at moderate lift coefficients to those reported in reference 1 for a model having the same section and plan form. However, at lift coefficients near that for the stall, differences in the aerodynamic characteristics occurred at Reynolds numbers of 2,000,000 and 10,000,000 at a Mach number of 0.25, which are believed to be attributable to small differences in both the surface contour near the leading edge and the condition of the surfaces of the two models.

The following discussion of the results of the present investigation has been divided into two parts: the effect of Reynolds number at a Mach number of 0.25, and the effect of Reynolds number at high subsonic Mach numbers. The surface pressures measured during the tests have been integrated to yield section normal-force and pitching-moment coefficients for streamwise sections at 10, 20, 40, 60, 80, 90, and 95 percent of semispan. Only a limited amount of the chordwise pressure-distribution data has been presented in plotted form. However, all the pressure data have been tabulated in tables II, III, and IV.

Effects of Reynolds Number at Mach Number of 0.25

The lift, drag, and pitching-moment characteristics and the corresponding section normal-force and section pitching-moment characteristics for a Reynolds number of 10,000,000 are presented in figure 4. Similar data are presented in figures 5, 6, and 7 for Reynolds numbers of 6,000,000, 4,000,000, and 2,000,000, respectively. The data obtained at a Reynolds number of 10,000,000 are included in each of the latter figures to show more clearly the effects of Reynolds number. Although data were not obtained beyond the stall at a Reynolds number of 10,000,000, the section normal-force data for the outer sections of the wing (fig. 4(b)) indicate that the stall was imminent at an angle of attack of 19° . The lift, drag, and pitching-moment data of figures 5(a), 6(a), and 7(a) show that the effects of Reynolds number were large, particularly in the upper lift-coefficient range. The section normal-force and section pitching-moment data shown in parts (b) and (c) of figures 5 through 7 indicate that the effects of Reynolds number were greater toward the tip than near the root of the wing.

It has been demonstrated by the results of an investigation reported in reference 9 that the aerodynamic characteristics of an infinite wing in oblique flow are determined by the aerodynamic characteristics of the sections normal to the quarter-chord line in accordance with the concepts of simple sweep theory. The section of the swept wing of this investigation was approximately 14 percent thick in planes normal to the quarter-chord line. Application of the simple sweep theory to section data of reference 10 indicates that the value of the maximum normal-force coefficient for a section of this wing should be about 0.91 and 0.84 for effective Reynolds numbers, based on the velocity and chord perpendicular to the quarter-chord line, of 6,700,000 and 4,000,000. These Reynolds numbers correspond to streamwise Reynolds numbers, based on the mean aerodynamic chord, of 10,000,000 and 6,000,000, respectively. Inspection of the data presented in figure 5(b) reveals that these values of maximum section normal-force coefficient correspond to those for a section at about 80 percent of the semispan; a higher value existing for sections nearer the root of the wing, and a lower value existing for sections nearer the tip. It must be noted that this correlation is not exact since the Mach numbers at which the section data of reference 10 were obtained are probably lower than the component of the Mach number perpendicular to the quarter-chord line of the wing. A correction to the two-dimensional section data for the decrease of maximum section normal-force coefficient with increasing Mach number (reference 11) would result in the point of correlation being moved farther toward the tip of the wing. The reduction in the value of the maximum section normal-force coefficient at 80 percent of the semispan with a reduction of Reynolds number to 2,000,000 is of the same magnitude as would be anticipated from the

results presented in reference 12 which show the effects of Reynolds number on NACA 6-series airfoil sections.

The chordwise distribution of static pressure at 20, 60, and 90 percent of the semispan for Reynolds numbers of 10,000,000 and 2,000,000 is presented in figure 8. These data indicate that the stall of the outer sections at a Reynolds number of 2,000,000 was preceded by a small amount of trailing-edge separation, as indicated by a decrease of the trailing-edge pressures, prior to complete separation from the leading edge. At a Reynolds number of 10,000,000 and an angle of attack of 16° , a definite loss of pressure recovery at 90 percent of the semispan occurred with little loss of leading-edge suction, indicating that the stall at this Reynolds number was predominantly of the turbulent or trailing-edge type. An analysis of the characteristics of a swept-back wing which stalled from the trailing edge has been presented in reference 13. The data of this reference show, as do those of the present investigation, that the maximum lift coefficients of the outer sections were approximately equal to those which can be predicted from section data. In reference 13, the increase in the value of the maximum section lift coefficient of the inner sections over that predicted from section data was attributed to a boundary-layer-control effect afforded by the drainage of the boundary-layer air away from the inner sections of the wing. This offers a partial explanation for the small effects of Reynolds number on the inner sections of the wing of this investigation in contrast to that which occurred at the outer sections. (See, for example, fig. 7(b).) The smaller effect of Reynolds number on the inner sections may also be due in part to the larger local Reynolds numbers of these sections as compared to the local Reynolds numbers of the outer sections.

At a Reynolds number of 2,000,000, a reduction in the lift-curve slope occurred at an angle of attack of about 3° , accompanied by a positive increase in the pitching moment. (See fig. 7.) Careful measurement of the slopes of the lift and pitching-moment curves of figures 5 and 6 indicates that a similar change in slope occurred at Reynolds numbers of 4,000,000 and 6,000,000, but to a lesser extent than at a Reynolds number of 2,000,000. As reported in reference 1, this increase in pitching moment and reduction in lift-curve slope occurred at the lift coefficient at which the low-drag range terminated. The low-drag range at a Reynolds number of 2,000,000 extended beyond the angle of attack at which an adverse gradient first existed near the leading edge as shown by the pressure data of figure 8(a). Such an extension of the low-drag range at low Reynolds numbers has been previously reported in reference 12.

On a swept wing, the changes in static longitudinal stability can be separated into that caused by changes in the distribution of loading along the section chords and that caused by changes in the distribution of loading along the span. The portion of the change in pitching moment

~~CONFIDENTIAL~~

NACA RM A52B20

with lift attributable to changes in the distribution of loading along the span is shown in figure 9. In this figure, the pitching-moment coefficients computed from force measurements are compared with those computed solely from the spanwise position of the center of pressure. In making this computation, the chordwise position of the center of pressure was assumed to be on the line joining the quarter-chord points of the sections perpendicular to the quarter-chord line. The pitching-moment coefficient about the quarter point of the mean aerodynamic chord calculated in this manner has been termed the span-load pitching-moment coefficient C_{m_s} . From the agreement of the slopes of the pitching-moment curves shown in figure 9, it may be seen that the spanwise center of pressure located on the line joining the quarter chords of the airfoil sections perpendicular to the quarter-chord line (26.2 percent local chord) proved to be the location of the wing center of pressure near zero lift. The smaller departure of C_{m_s} than of C_m from a linear variation with lift coefficient at lift coefficients below the stall signifies that much of the change in C_m was caused by movement of the section centers of pressure rather than by a change in the spanwise distribution of loading. Of particular interest is the abrupt increase in the pitching moment between 3° and 4° angle of attack at a Reynolds number of 2,000,000 which is indicated to be caused by a change in the section pitching moments and not by a change in the spanwise distribution of loading. At lift coefficients near the stall, a large positive increase in C_{m_s} occurred which is traceable to a reduction of the lift-curve slopes of the outer sections of the wing. This increase in span-load pitching-moment coefficient C_{m_s} was much greater than the increase in the pitching-moment coefficient C_m thereby indicating that rearward movement of the section centers of pressure occurred at these lift coefficients.

Effects of Reynolds Number at High Subsonic Mach Numbers

The data at high subsonic Mach numbers and a Reynolds number of 2,000,000 were obtained in the Ames 12-foot pressure wind tunnel. At Mach numbers greater than 0.875, measurements of the static pressure on the tunnel wall opposite the upper surface of the model indicated a local Mach number greater than 1.0 at some positive angles of attack. Since choking of the tunnel renders questionable the validity of data obtained under this condition, these data have been faired with a dotted line.

The data at the higher Reynolds numbers were obtained from tests in the Ames 16-foot high-speed wind tunnel. The Reynolds number of these tests varied from 3,900,000 at a Mach number of 0.62 to 4,600,000 at a Mach number of 0.94. (See fig. 3.) The Mach numbers of these tests were determined from a tunnel calibration which was conducted after the data

~~CONFIDENTIAL~~

for this report were obtained. Consequently, the values of Mach number for most of the data at the higher Reynolds number do not correspond exactly to the Mach numbers of the data obtained at a Reynolds number of 2,000,000. For this reason, actual data points at the higher Reynolds numbers are presented for comparison with those for a Reynolds number of 2,000,000 only at a Mach number of 0.94, where the Mach numbers for the two tests were identical, and at a Mach number of 0.62, where the difference of 0.02 in Mach number is not considered to be important. The remainder of the data presented from the tests conducted in the 16-foot wind tunnel were obtained from faired curves of the aerodynamic coefficients as a function of Mach number. No measurements to determine at what lift coefficient and Mach number the local Mach number at the tunnel wall exceeded unity were made during the tests in the 16-foot wind tunnel. Due to its larger test-section area, however, choking conditions can be expected to occur at lift coefficients somewhat greater than in the 12-foot tunnel for a given Mach number.

The normal-force and pitching-moment data for the higher Reynolds number tests were evaluated by integrating the measured surface pressures. The adequacy of this procedure is illustrated in figure 10. In this figure are presented data from the 12-foot pressure wind tunnel which were calculated from both force measurements and surface pressures. These data show that the indicated location of the center of pressure is the same in both instances since the slopes of the pitching-moment curves are nearly identical. However, integration of the surface pressures yielded a value of normal-force coefficient which at angles of attack greater than about 4° was several percent lower than that calculated from force measurements. It is not known whether this is a result of consistent errors in extrapolation and integration of surface pressures, or a result of unevaluated interference tares.

Data obtained in each wind tunnel at approximately the same Mach number and Reynolds number are presented in figure 11. The differences between the two sets of data are shown to be small except near the stall. Therefore, comparisons of the data obtained in each wind tunnel at higher Mach numbers, but at different Reynolds numbers, should indicate the effects of Reynolds number for moderate lift coefficients. These are presented in figures 12 through 17.

Effect of Reynolds number for normal-force coefficients near zero. The normal-force-curve slopes, the pitching-moment-curve slopes, and the pressure-drag coefficients for a normal-force coefficient of zero are presented as functions of Mach number in figure 18. These data indicate that the change in Reynolds number did not alter the Mach number for drag divergence. The Mach number for lift divergence, however, was greater by about 0.05 at the higher Reynolds number. A large effect of Reynolds number on the static longitudinal stability, as indicated by the value of $\frac{dC_m}{dC_N}$, is evident. At a Reynolds number of 2,000,000, no change

in stability occurred up to the Mach number for drag divergence, whereupon a large decrease of stability occurred with further increase of Mach number. At the higher Reynolds number the stability increased with increasing Mach number. At a Mach number of 0.94, the difference in the values of $\frac{dC_m}{dC_N}$ indicate the center of pressure at a Reynolds number of 2,000,000 to be roughly 1-1/2 mean aerodynamic chord lengths forward of its position at a Reynolds number of 4,600,000.

An estimate of the proportion of the change in stability caused by change in the spanwise distribution of loading may be made from inspection of the data of figure 19. In this figure, pitching-moment coefficients C_{m_s} which have been computed from the spanwise location of the center of pressure (chordwise center of pressure assumed to be at 26.2 percent of the local chord) are presented for comparison with the pitching-moment coefficients C_m calculated from force measurements. At a Reynolds number of 2,000,000 and a normal-force coefficient of zero (fig. 19(a)), the variation of the spanwise location of the center of pressure with Mach number was the predominant cause of the decrease in static longitudinal stability. At the higher Reynolds number (fig. 19(b)), spanwise movement of the center of pressure accounted for roughly half of the increase in static longitudinal stability with increasing Mach number; the remainder of the increase resulted from a rearward movement of the centers of pressure of the wing sections. The changes in the spanwise distribution of loading with Reynolds number, which are the principal cause of the changes in static longitudinal stability, are evident from the data of figure 20.

A tentative explanation can be offered for the large effects of Reynolds number on this wing at Mach numbers greater than that for drag divergence. The surface pressures on the upper surface of the wing at a Mach number of 0.94 and a normal-force coefficient of about zero are presented in figure 21. At 20 percent of the semispan, the compression immediately behind the position of minimum pressure was more abrupt at a Reynolds number of 4,600,000 than at a Reynolds number of 2,000,000. A similar difference is shown in reference 14 between the interaction of a shock wave with a turbulent boundary layer, and the interaction of a shock wave with a laminar boundary layer which does not separate from the surface. At the outer sections, 60 and 80 percent of the semispan for example, the minimum pressure is less and the pressure recovery is more nearly complete at a Reynolds number of 4,600,000 than at 2,000,000. These differences are again similar to those shown in reference 14 between interaction of shock waves with turbulent and with laminar boundary layers, except that at these sections the pressure distributions at the lower Reynolds number are similar to those which result when separation of the laminar boundary layer occurs ahead of the main shock wave. Additional evidence that the boundary layer has separated somewhere between 20 and 60 percent of the semispan at a Reynolds number of 2,000,000 is the more nearly complete pressure recovery at the

trailing edge at the inner section as compared to that at 60 and 90 percent of the semispan. From the foregoing, it is believed that at a Reynolds number of 4,600,000 the boundary layer near the location of the shock wave was turbulent. At a Reynolds number of 2,000,000 the boundary layer was laminar and separated ahead of the shock wave at sections outboard of 20 percent of the semispan.

The effect of a small angle of attack on the surface pressures may be seen from figures 22 and 23 where the chordwise pressure distributions at 20, 60, and 90 percent of the semispan are presented. At a Reynolds number of 2,000,000, and Mach numbers of 0.90 and 0.94, the point of minimum pressure on the upper surface outboard of about 20 percent of the semispan was ahead of that on the lower surface at an angle of attack of 1° . This is believed to have been caused by the relative movement of the point of laminar separation on the upper and lower surfaces with the increase in angle of attack from 0° . This relative movement of the points of minimum pressure on the upper and lower surfaces resulted in a positive normal force on the forward part of the sections, and a negative normal force on the rear of the sections. This resulted in low, and sometimes negative, section normal-force-curve slopes and large positive section pitching moments at small angles of attack for the outer sections at a Reynolds number of 2,000,000. At a Reynolds number of about 4,600,000, the movement of the point of minimum pressure caused by a small angle of attack was slight and, in general, positive normal forces existed over the entire chord for all sections of the wing.

Effects of Reynolds number at moderate normal-force coefficients. At Mach numbers of 0.60 and 0.80 the increase in Reynolds number had very little effect on the changes in stability and in normal-force-curve slope with increases in angle of attack up to 6° . (See figs. 11(a) and 12(a).) The reduction in longitudinal stability and the decrease in normal-force-curve slope which occurred between 3° and 4° angle of attack at these Mach numbers are similar to those previously noted for a Mach number of 0.25.

At higher Mach numbers, the pressure coefficient corresponding to a Mach number of 1 normal to the quarter-chord line ($P_{cr,A=35} = 0$) was exceeded at an angle of attack of 1° or less. (See figs. 22 and 23.) When this condition occurs, the existence of shock waves can be expected to have an influence on the effects of Reynolds number on the forces and pressures acting on the wing. The pitching-moment data for Mach numbers of 0.90, 0.92, and 0.94 (figs. 15(a), 16(a), and 17(a)) show that although an increase in Reynolds number eliminated the static longitudinal instability at a normal-force coefficient of zero, an equally drastic reduction of stability occurred at a positive normal-force coefficient at the higher Reynolds number. This reduction in stability occurred near a normal-force coefficient of 0.3 at Mach numbers of 0.90 and 0.92 (figs. 15(a) and 16(a)), and between 0.1 and 0.2 at a Mach number of 0.94.

(fig. 17(a)). These changes in stability were caused mostly by a change in the spanwise distribution of loading. (See fig. 19(b).) A reduction of the section normal-force-curve slopes of the sections comprising the outer 60 percent of the semispan caused this change in the spanwise distribution of loading as may be seen from the data of figures 14(b), 15(b), 16(b), and 17(b).

The pressure data for angles of attack from 2° to 5° at a Mach number of 0.90 and a Reynolds number of 2,000,000 are presented in figures 24(a) and 24(b). Similar data covering approximately the same range of angle of attack at a Mach number of 0.91 and a Reynolds number of 4,500,000 are presented in figures 24(c) and 24(d). The abrupt reduction of section normal-force-curve slope at 60 percent of the semispan at Mach numbers of both 0.90 and 0.92 at the higher Reynolds number (figs. 15(b) and 16(b)) is accompanied by the loss of pressure recovery indicated in figure 24(d). However, at 90 percent of the semispan very little loss of pressure recovery is indicated. At this section, the low section normal-force-curve slopes are associated with a region of negative normal force over the rear half of the section.

CONCLUDING REMARKS

The results of tests to evaluate the effects of Reynolds number on the loading on a 12-percent-thick wing having 35° of sweepback have been presented. In general, the results indicated that at all Mach numbers the effect of a change in Reynolds number was greater on the outer sections than on the inner sections of the wing. At a Mach number of 0.25, the maximum normal-force coefficients for wing sections inboard of about 80 percent of the semispan were greater than predicted by applying simple sweep theory to two-dimensional section data. A lower value of maximum section normal-force coefficient than predicted from section data was obtained for sections at 90 and 95 percent of the semispan. At Mach numbers greater than that for drag divergence, an increase in Reynolds number from 2,000,000 to 4,500,000 caused a change in loading which at a Mach number of 0.94 was sufficient to shift the center of pressure rearward by about 150 percent of the mean aerodynamic chord. This change in loading is believed to have resulted from a change in the type of boundary layer in the region of the shock wave from laminar at the lower Reynolds number to turbulent at the higher Reynolds number.

Ames Aeronautical Laboratory
National Advisory Committee for Aeronautics
Moffett Field, Calif.

[REDACTED]
REFERENCES

1. Tinling, Bruce E., and Kolk, W. Richard: The Effects of Mach Number and Reynolds Number on the Aerodynamic Characteristics of Several 12-Percent-Thick Wings Having 35° of Sweepback and Various Amounts of Camber. NACA RM A50K27, 1951.
2. Polhamus, Edward C., and King, Thomas J., Jr.: Aerodynamic Characteristics of Tapered Wings Having Aspect Ratios of 4, 6, and 8, Quarter-Chord Lines Swept Back 45°, and NACA 63₁A012 Airfoil Sections. Transonic-Bump Method. NACA RM L51C26, 1951.
3. Tinling, Bruce E., and Dickson, Jerald K.: Tests of a Model Horizontal Tail of Aspect Ratio 4.5 in the Ames 12-Foot Pressure Wind Tunnel. I - Quarter-Chord Line Swept Back 35°. NACA RM A9G13, 1949.
4. Edwards, George G., and Boltz, Frederick W.: An Analysis of the Forces and Pressure Distribution on a Wing With the Leading Edge Swept Back 37.25°. NACA RM A9K01, 1950.
5. Herriot, John G.: Blockage Corrections for Three-Dimensional-Flow Closed-Throat Wind Tunnels, with Consideration of the Effect of Compressibility. NACA Rep. 995, 1950. (Formerly NACA RM A7B28)
6. Sivells, James C., and Deters, Owen J.: Jet-Boundary and Plan-Form Corrections for Partial-Span Models with Reflection Plane, End Plate, or No End Plate in a Closed Circular Wind Tunnel. NACA Rep. 843, 1946. (Formerly NACA TN 1077)
7. DeYoung, John, and Harper, Charles W.: Theoretical Symmetric Span Loading at Subsonic Speeds for Wings Having Arbitrary Plan Form. NACA Rep. 921, 1948.
8. Swanson, Robert S., and Toll, Thomas A.: Jet-Boundary Corrections for Reflection-Plane Models in Rectangular Wind Tunnels. NACA Rep. 770, 1943. (Formerly NACA ARR 3E22)
9. Dannenberg, Robert E.: Measurements of Section Characteristics of a 45° Swept Wing Spanning a Rectangular Low-Speed Wind Tunnel as Affected by the Tunnel Walls. NACA TN 2160, 1950.
10. Abbott, Ira H., von Doenhoff, Albert E., and Stivers, Louis S. Jr.: Summary of Airfoil Data. NACA Rep. 824, 1945. (Formerly NACA ACR L5C05)

~~CONFIDENTIAL~~

11. Furlong, G. Chester, and Fitzpatrick, James E.: Effects of Mach Number up to 0.34 and Reynolds Number up to 8×10^6 on the Maximum Lift Coefficient of a Wing of NACA 66-Series Airfoil Sections. NACA TN 2251, 1950.
12. Loftin, Laurence K., Jr., and Smith, Hamilton A.: Aerodynamic Characteristics of 15 NACA Airfoil Sections at Seven Reynolds Numbers from 0.7×10^6 to 9.0×10^6 . NACA TN 1945, 1949.
13. Hunton, Lynn W., and Dew, Joseph K.: The Effects of Camber and Twist on the Aerodynamic Loading and Stalling Characteristics of a Large Scale 45° Swept-Back Wing. NACA RM A50J24, 1951.
14. Liepmann, Hans Wolfgang: Investigations of the Interaction Between Boundary Layer and Shockwaves in Transonic Flow. Jour. Aero. Sci. Vol. 3, no. 12, Dec. 1946, pp. 623-639.

~~CONFIDENTIAL~~

TABLE I.- COORDINATES OF THE NACA 65₁A012
AIRFOIL SECTION

[All dimensions given in percent chord]

Upper and lower surfaces	
Station	Ordinate
0	0
.5	.913
.75	1.106
1.25	1.414
2.5	1.942
5.0	2.614
7.5	3.176
10	3.647
15	4.392
20	4.956
25	5.383
30	5.693
35	5.897
40	5.995
45	5.997
50	5.828
55	5.544
60	5.143
65	4.654
70	4.091
75	3.467
80	2.798
85	2.106
90	1.413
95	.719
100	.025
L.E. radius: 0.922 percent chord	
T.E. radius: 0.029 percent chord	



TABLE II.- CONTINUED

(b) Concluded

		$\alpha = 0.00$													
		Angle of attack, α , degrees													
		0	1.0	2.0	3.0	4.0	5.0	6.0	8.1	10.1	12.1	14.1	16.1	18.1	20.1
Leading edge	0	.61	.43	.61	.73	.40	.31	-.03	-.69	-.55	-.95	-3.78	-5.00	-1.80	-9.08
Upper surface	1.7	-.06	-.98	-.03	-.68	-.98	-.18	-.16	-.96	-.67	-.30	-.72	-.86	-.96	-.01
	4.1	-.10	-.23	-.08	-.65	-.15	-.65	-.13	-.66	-.15	-.66	-.36	-.33	-.36	-.04
	7.0	-.13	-.23	-.15	-.65	-.23	-.73	-.02	-.68	-.18	-.74	-.95	-.95	-.10	-.85
	8.0	-.16	-.23	-.15	-.65	-.23	-.73	-.02	-.68	-.13	-.72	-.72	-.80	-.15	-.78
	11.7	-.23	-.23	-.15	-.65	-.23	-.73	-.02	-.68	-.13	-.72	-.86	-.86	-.15	-.85
	15.7	-.23	-.23	-.15	-.65	-.23	-.73	-.02	-.68	-.13	-.72	-.86	-.86	-.15	-.85
	18.6	-.23	-.23	-.15	-.65	-.23	-.73	-.02	-.68	-.13	-.72	-.86	-.86	-.15	-.85
	19.4	-.23	-.23	-.15	-.65	-.23	-.73	-.02	-.68	-.13	-.72	-.86	-.86	-.15	-.85
	19.7	-.23	-.23	-.15	-.65	-.23	-.73	-.02	-.68	-.13	-.72	-.86	-.86	-.15	-.85
	24.4	-.23	-.23	-.15	-.65	-.23	-.73	-.02	-.68	-.13	-.72	-.86	-.86	-.15	-.85
Lower surface	1.6	-.08	-.08	-.08	-.08	-.08	-.08	-.08	-.08	-.08	-.08	-.08	-.08	-.08	-.08
	4.1	-.15	-.09	-.15	-.09	-.15	-.09	-.15	-.09	-.15	-.09	-.15	-.09	-.15	-.09
	6.1	-.15	-.09	-.15	-.09	-.15	-.09	-.15	-.09	-.15	-.09	-.15	-.09	-.15	-.09
	9.1	-.15	-.09	-.15	-.09	-.15	-.09	-.15	-.09	-.15	-.09	-.15	-.09	-.15	-.09
	12.9	-.15	-.09	-.15	-.09	-.15	-.09	-.15	-.09	-.15	-.09	-.15	-.09	-.15	-.09
	15.7	-.15	-.09	-.15	-.09	-.15	-.09	-.15	-.09	-.15	-.09	-.15	-.09	-.15	-.09
	18.6	-.15	-.09	-.15	-.09	-.15	-.09	-.15	-.09	-.15	-.09	-.15	-.09	-.15	-.09
	19.4	-.15	-.09	-.15	-.09	-.15	-.09	-.15	-.09	-.15	-.09	-.15	-.09	-.15	-.09
	19.8	-.15	-.09	-.15	-.09	-.15	-.09	-.15	-.09	-.15	-.09	-.15	-.09	-.15	-.09
	24.4	-.15	-.09	-.15	-.09	-.15	-.09	-.15	-.09	-.15	-.09	-.15	-.09	-.15	-.09
		$\alpha = 0.05$													
		Angle of attack, α , degrees													
		0	1.0	2.0	3.0	4.0	5.0	6.0	8.1	10.1	12.1	14.1	16.1	18.1	20.1
Leading edge	0	.63	.63	.63	.73	.40	.31	-.03	-.69	-.55	-.95	-3.78	-5.00	-1.80	-9.08
Upper surface	1.7	-.05	-.98	-.03	-.68	-.98	-.18	-.16	-.96	-.67	-.30	-.72	-.86	-.96	-.01
	4.1	-.10	-.23	-.08	-.65	-.15	-.65	-.13	-.66	-.18	-.66	-.36	-.33	-.36	-.04
	7.0	-.13	-.23	-.15	-.65	-.23	-.73	-.02	-.68	-.18	-.74	-.95	-.95	-.10	-.85
	8.0	-.16	-.23	-.15	-.65	-.23	-.73	-.02	-.68	-.13	-.72	-.72	-.80	-.15	-.78
	11.7	-.23	-.23	-.15	-.65	-.23	-.73	-.02	-.68	-.13	-.72	-.86	-.86	-.15	-.85
	15.7	-.23	-.23	-.15	-.65	-.23	-.73	-.02	-.68	-.13	-.72	-.86	-.86	-.15	-.85
	18.6	-.23	-.23	-.15	-.65	-.23	-.73	-.02	-.68	-.13	-.72	-.86	-.86	-.15	-.85
	19.4	-.23	-.23	-.15	-.65	-.23	-.73	-.02	-.68	-.13	-.72	-.86	-.86	-.15	-.85
	24.4	-.23	-.23	-.15	-.65	-.23	-.73	-.02	-.68	-.13	-.72	-.86	-.86	-.15	-.85
	29.3	-.23	-.23	-.15	-.65	-.23	-.73	-.02	-.68	-.13	-.72	-.86	-.86	-.15	-.85
Lower surface	1.6	-.08	-.08	-.08	-.08	-.08	-.08	-.08	-.08	-.08	-.08	-.08	-.08	-.08	-.08
	4.1	-.15	-.09	-.15	-.09	-.15	-.09	-.15	-.09	-.15	-.09	-.15	-.09	-.15	-.09
	6.1	-.15	-.09	-.15	-.09	-.15	-.09	-.15	-.09	-.15	-.09	-.15	-.09	-.15	-.09
	9.1	-.15	-.09	-.15	-.09	-.15	-.09	-.15	-.09	-.15	-.09	-.15	-.09	-.15	-.09
	12.9	-.15	-.09	-.15	-.09	-.15	-.09	-.15	-.09	-.15	-.09	-.15	-.09	-.15	-.09
	15.7	-.15	-.09	-.15	-.09	-.15	-.09	-.15	-.09	-.15	-.09	-.15	-.09	-.15	-.09
	18.6	-.15	-.09	-.15	-.09	-.15	-.09	-.15	-.09	-.15	-.09	-.15	-.09	-.15	-.09
	19.4	-.15	-.09	-.15	-.09	-.15	-.09	-.15	-.09	-.15	-.09	-.15	-.09	-.15	-.09
	19.8	-.15	-.09	-.15	-.09	-.15	-.09	-.15	-.09	-.15	-.09	-.15	-.09	-.15	-.09
	24.4	-.15	-.09	-.15	-.09	-.15	-.09	-.15	-.09	-.15	-.09	-.15	-.09	-.15	-.09

NACA

TABLE II.- CONTINUED

(c) Concluded.

 $\alpha_r = 0.80$

Location	Per-	Angle of attack, α_r , degrees											
		0	1.0	2.0	3.0	4.0	5.0	6.0	8.1	10.1	12.1	14.1	16.1
Leading edge	0	.40	.53	.60	.68	.71	.78	.81	.85	.90	.94	.98	.99
	1.0	-0.05	-0.02	-0.04	-0.06	-0.08	-0.09	-0.10	-0.10	-0.10	-0.10	-0.10	-0.10
	2.0	-0.15	-0.12	-0.14	-0.16	-0.18	-0.19	-0.20	-0.20	-0.20	-0.20	-0.20	-0.20
	3.0	-0.25	-0.22	-0.24	-0.26	-0.28	-0.29	-0.30	-0.30	-0.30	-0.30	-0.30	-0.30
	4.0	-0.35	-0.32	-0.34	-0.36	-0.38	-0.39	-0.40	-0.40	-0.40	-0.40	-0.40	-0.40
	5.0	-0.45	-0.42	-0.44	-0.46	-0.48	-0.49	-0.50	-0.50	-0.50	-0.50	-0.50	-0.50
	6.0	-0.55	-0.52	-0.54	-0.56	-0.58	-0.59	-0.60	-0.60	-0.60	-0.60	-0.60	-0.60
	8.1	-0.75	-0.72	-0.74	-0.76	-0.78	-0.79	-0.80	-0.80	-0.80	-0.80	-0.80	-0.80
	10.1	-0.95	-0.92	-0.94	-0.96	-0.98	-0.99	-0.99	-0.99	-0.99	-0.99	-0.99	-0.99
	12.1	-1.00	-0.97	-0.99	-0.99	-0.99	-0.99	-0.99	-0.99	-0.99	-0.99	-0.99	-0.99
	14.1	-1.00	-0.97	-0.99	-0.99	-0.99	-0.99	-0.99	-0.99	-0.99	-0.99	-0.99	-0.99
	16.1	-1.00	-0.97	-0.99	-0.99	-0.99	-0.99	-0.99	-0.99	-0.99	-0.99	-0.99	-0.99
	18.1	-1.00	-0.97	-0.99	-0.99	-0.99	-0.99	-0.99	-0.99	-0.99	-0.99	-0.99	-0.99

 $\alpha_r = 0.90$

Location	Per-	Angle of attack, α_r , degrees											
		0	1.0	2.0	3.0	4.0	5.0	6.0	8.1	10.1	12.1	14.1	16.1
Leading edge	0	.48	.55	.60	.64	.68	.71	.74	.77	.81	.85	.88	.89
	1.0	-0.05	-0.02	-0.04	-0.06	-0.08	-0.09	-0.10	-0.10	-0.10	-0.10	-0.10	-0.10
	2.0	-0.15	-0.12	-0.14	-0.16	-0.18	-0.19	-0.20	-0.20	-0.20	-0.20	-0.20	-0.20
	3.0	-0.25	-0.22	-0.24	-0.26	-0.28	-0.29	-0.30	-0.30	-0.30	-0.30	-0.30	-0.30
	4.0	-0.35	-0.32	-0.34	-0.36	-0.38	-0.39	-0.40	-0.40	-0.40	-0.40	-0.40	-0.40
	5.0	-0.45	-0.42	-0.44	-0.46	-0.48	-0.49	-0.50	-0.50	-0.50	-0.50	-0.50	-0.50
	6.0	-0.55	-0.52	-0.54	-0.56	-0.58	-0.59	-0.60	-0.60	-0.60	-0.60	-0.60	-0.60
	8.1	-0.75	-0.72	-0.74	-0.76	-0.78	-0.79	-0.80	-0.80	-0.80	-0.80	-0.80	-0.80
	10.1	-0.95	-0.92	-0.94	-0.96	-0.98	-0.99	-0.99	-0.99	-0.99	-0.99	-0.99	-0.99
	12.1	-1.00	-0.97	-0.99	-0.99	-0.99	-0.99	-0.99	-0.99	-0.99	-0.99	-0.99	-0.99
	14.1	-1.00	-0.97	-0.99	-0.99	-0.99	-0.99	-0.99	-0.99	-0.99	-0.99	-0.99	-0.99
	16.1	-1.00	-0.97	-0.99	-0.99	-0.99	-0.99	-0.99	-0.99	-0.99	-0.99	-0.99	-0.99
	18.1	-1.00	-0.97	-0.99	-0.99	-0.99	-0.99	-0.99	-0.99	-0.99	-0.99	-0.99	-0.99

 $\alpha_r = 0.95$

Location	Per-	Angle of attack, α_r , degrees											
		0	1.0	2.0	3.0	4.0	5.0	6.0	8.1	10.1	12.1	14.1	16.1
Leading edge	0	.55	.68	.70	.76	.79	.85	.86	.91	.95	.98	.99	.99
	1.0	-0.05	-0.02	-0.04	-0.06	-0.08	-0.09	-0.10	-0.10	-0.10	-0.10	-0.10	-0.10
	2.0	-0.15	-0.12	-0.14	-0.16	-0.18	-0.19	-0.20	-0.20	-0.20	-0.20	-0.20	-0.20
	3.0	-0.25	-0.22	-0.24	-0.26	-0.28	-0.29	-0.30	-0.30	-0.30	-0.30	-0.30	-0.30
	4.0	-0.35	-0.32	-0.34	-0.36	-0.38	-0.39	-0.40	-0.40	-0.40	-0.40	-0.40	-0.40
	5.0	-0.45	-0.42	-0.44	-0.46	-0.48	-0.49	-0.50	-0.50	-0.50	-0.50	-0.50	-0.50
	6.0	-0.55	-0.52	-0.54	-0.56	-0.58	-0.59	-0.60	-0.60	-0.60	-0.60	-0.60	-0.60
	8.1	-0.75	-0.72	-0.74	-0.76	-0.78	-0.79	-0.80	-0.80	-0.80	-0.80	-0.80	-0.80
	10.1	-0.95	-0.92	-0.94	-0.96	-0.98	-0.99	-0.99	-0.99	-0.99	-0.99	-0.99	-0.99
	12.1	-1.00	-0.97	-0.99	-0.99	-0.99	-0.99	-0.99	-0.99	-0.99	-0.99	-0.99	-0.99
	14.1	-1.00	-0.97	-0.99	-0.99	-0.99	-0.99	-0.99	-0.99	-0.99	-0.99	-0.99	-0.99
	16.1	-1.00	-0.97	-0.99	-0.99	-0.99	-0.99	-0.99	-0.99	-0.99	-0.99	-0.99	-0.99
	18.1	-1.00	-0.97	-0.99	-0.99	-0.99	-0.99	-0.99	-0.99	-0.99	-0.99	-0.99	-0.99

NACA

TABLE II.— CONCLUDED

(d) Concluded



TABLE III.- CONTINUED

(b) Concluded

		$c_1 = 0.00$													
		Angle of attack, α , degrees													
Location along chord	Percent chord	-0.7	-0.2	0.3	0.8	1.6	2.8	3.8	4.9	5.9	7.9	9.9	11.9	13.8	15.8
		0	.87	.88	.70	.70	.68	.59	.54	.46	.38	.30	.21	0	-.10
Upper surface	1.7	.08	-.03	-0.11	-0.20	-0.46	-0.76	-1.16	-1.35	-1.33	-1.36	-1.28	-0.98	-0.92	.88
	1.7	.18	-.04	-0.12	-0.21	-0.47	-0.77	-1.17	-1.36	-1.34	-1.37	-1.29	-1.03	-0.97	.93
	1.7	.28	-.05	-0.13	-0.22	-0.48	-0.78	-1.18	-1.37	-1.35	-1.38	-1.30	-1.04	-0.98	.94
	1.7	.38	-.06	-0.14	-0.23	-0.49	-0.79	-1.19	-1.38	-1.36	-1.39	-1.31	-1.05	-0.99	.95
	1.7	.48	-.07	-0.15	-0.24	-0.50	-0.80	-1.20	-1.39	-1.37	-1.40	-1.32	-1.06	-1.00	.96
	1.7	.58	-.08	-0.16	-0.25	-0.51	-0.81	-1.21	-1.40	-1.38	-1.41	-1.33	-1.07	-1.01	.97
	1.7	.68	-.09	-0.17	-0.26	-0.52	-0.82	-1.22	-1.41	-1.39	-1.42	-1.34	-1.08	-1.02	.98
	1.7	.78	-.10	-0.18	-0.27	-0.53	-0.83	-1.23	-1.42	-1.40	-1.43	-1.35	-1.09	-1.03	.99
	1.7	.88	-.11	-0.19	-0.28	-0.54	-0.84	-1.24	-1.43	-1.41	-1.44	-1.36	-1.10	-1.04	.99
	1.7	.98	-.12	-0.20	-0.29	-0.55	-0.85	-1.25	-1.44	-1.42	-1.45	-1.37	-1.11	-1.05	.99
Lower surface	1.7	0	.87	.88	.70	.70	.68	.59	.54	.46	.38	.30	.21	0	-.10
	1.7	1.7	1.8	1.9	2.0	2.1	2.2	2.3	2.4	2.5	2.6	2.7	2.8	2.9	3.0
	1.7	2.7	2.8	2.9	3.0	3.1	3.2	3.3	3.4	3.5	3.6	3.7	3.8	3.9	4.0
	1.7	3.7	3.8	3.9	4.0	4.1	4.2	4.3	4.4	4.5	4.6	4.7	4.8	4.9	5.0
	1.7	4.9	5.0	5.1	5.2	5.3	5.4	5.5	5.6	5.7	5.8	5.9	6.0	6.1	6.2
	1.7	6.2	6.3	6.4	6.5	6.6	6.7	6.8	6.9	7.0	7.1	7.2	7.3	7.4	7.5
	1.7	7.5	7.6	7.7	7.8	7.9	8.0	8.1	8.2	8.3	8.4	8.5	8.6	8.7	8.8
	1.7	8.8	8.9	9.0	9.1	9.2	9.3	9.4	9.5	9.6	9.7	9.8	9.9	10.0	10.1
	1.7	10.1	10.2	10.3	10.4	10.5	10.6	10.7	10.8	10.9	11.0	11.1	11.2	11.3	11.4
	1.7	11.4	11.5	11.6	11.7	11.8	11.9	12.0	12.1	12.2	12.3	12.4	12.5	12.6	12.7
		$c_1 = 0.50$													
		Angle of attack, α , degrees													
Location along chord	Percent chord	-0.7	-0.2	0.3	0.8	1.6	2.8	3.8	4.9	5.9	7.9	9.9	11.9	13.8	15.8
		0	.87	.88	.69	.69	.61	.53	.45	.37	.30	.23	.16	.09	-.05
Upper surface	1.7	.08	-.05	-0.12	-0.20	-0.46	-0.76	-1.16	-1.35	-1.33	-1.36	-1.28	-0.98	-0.92	.88
	1.7	.18	-.06	-0.13	-0.21	-0.47	-0.77	-1.17	-1.36	-1.34	-1.37	-1.29	-1.03	-0.97	.93
	1.7	.28	-.07	-0.14	-0.22	-0.48	-0.78	-1.18	-1.37	-1.35	-1.38	-1.30	-1.04	-0.98	.94
	1.7	.38	-.08	-0.15	-0.23	-0.49	-0.79	-1.19	-1.38	-1.36	-1.39	-1.31	-1.05	-0.99	.95
	1.7	.48	-.09	-0.16	-0.24	-0.50	-0.80	-1.20	-1.39	-1.37	-1.40	-1.32	-1.06	-1.00	.96
	1.7	.58	-.10	-0.17	-0.25	-0.51	-0.81	-1.21	-1.40	-1.38	-1.41	-1.33	-1.07	-1.01	.97
	1.7	.68	-.11	-0.18	-0.26	-0.52	-0.82	-1.22	-1.41	-1.39	-1.42	-1.34	-1.08	-1.02	.98
	1.7	.78	-.12	-0.19	-0.27	-0.53	-0.83	-1.23	-1.42	-1.40	-1.43	-1.35	-1.09	-1.03	.99
	1.7	.88	-.13	-0.20	-0.28	-0.54	-0.84	-1.24	-1.43	-1.41	-1.44	-1.36	-1.10	-1.04	.99
	1.7	.98	-.14	-0.21	-0.29	-0.55	-0.85	-1.25	-1.44	-1.42	-1.45	-1.37	-1.11	-1.05	.99
Lower surface	1.7	0	.87	.88	.70	.70	.68	.59	.54	.46	.38	.30	.21	0	-.10
	1.7	1.7	1.8	1.9	2.0	2.1	2.2	2.3	2.4	2.5	2.6	2.7	2.8	2.9	3.0
	1.7	2.7	2.8	2.9	3.0	3.1	3.2	3.3	3.4	3.5	3.6	3.7	3.8	3.9	4.0
	1.7	3.7	3.8	3.9	4.0	4.1	4.2	4.3	4.4	4.5	4.6	4.7	4.8	4.9	5.0
	1.7	4.9	5.0	5.1	5.2	5.3	5.4	5.5	5.6	5.7	5.8	5.9	6.0	6.1	6.2
	1.7	6.2	6.3	6.4	6.5	6.6	6.7	6.8	6.9	7.0	7.1	7.2	7.3	7.4	7.5
	1.7	7.5	7.6	7.7	7.8	7.9	8.0	8.1	8.2	8.3	8.4	8.5	8.6	8.7	8.8
	1.7	8.8	8.9	9.0	9.1	9.2	9.3	9.4	9.5	9.6	9.7	9.8	9.9	10.0	10.1
	1.7	10.1	10.2	10.3	10.4	10.5	10.6	10.7	10.8	10.9	11.0	11.1	11.2	11.3	11.4
	1.7	11.4	11.5	11.6	11.7	11.8	11.9	12.0	12.1	12.2	12.3	12.4	12.5	12.6	12.7

NACA

Museum

TABLE III.—CONTINUED

(c) Concluded

		c_l , 0.80											c_l , 0.90															
		Angle of attack, α , degrees											Angle of attack, α , degrees															
Location along chord	Percent chord	-0.7 -0.2 0.3 0.5 1.0 2.0 3.0 4.0 5.0 7.0 9.0 11.0 13.0											-0.7 -0.2 0.3 0.6 1.0 2.0 3.0 4.0 5.0 7.0 9.0 11.0 13.0															
		.65	.69	.71	.71	.71	.65	.59	.54	.48	.39	.33	.26	.20	.15	.10	.05	.00	.-0.05	.-0.10	.-0.15	.-0.20	.-0.25					
Upper surface	Leading edge	-0.7	-0.2	0.3	0.5	1.0	2.0	3.0	4.0	5.0	7.0	9.0	11.0	13.0	-0.7	-0.2	0.3	0.6	1.0	2.0	3.0	4.0	5.0	7.0	9.0	11.0	13.0	
	1.7	0.03	-0.03	-0.05	-0.05	-0.05	-0.05	-0.05	-0.05	-0.05	-0.05	-0.05	-0.05	-0.05	0.07	0.09	0.13	0.17	0.21	0.25	0.29	0.33	0.37	0.41	0.45	0.49		
	2.1	-0.03	-0.05	-0.05	-0.05	-0.05	-0.05	-0.05	-0.05	-0.05	-0.05	-0.05	-0.05	-0.05	-0.05	-0.05	-0.05	-0.05	-0.05	-0.05	-0.05	-0.05	-0.05	-0.05	-0.05	-0.05		
	2.5	-0.10	-0.10	-0.10	-0.10	-0.10	-0.10	-0.10	-0.10	-0.10	-0.10	-0.10	-0.10	-0.10	-0.10	-0.10	-0.10	-0.10	-0.10	-0.10	-0.10	-0.10	-0.10	-0.10	-0.10	-0.10		
	2.9	-0.16	-0.16	-0.16	-0.16	-0.16	-0.16	-0.16	-0.16	-0.16	-0.16	-0.16	-0.16	-0.16	-0.16	-0.16	-0.16	-0.16	-0.16	-0.16	-0.16	-0.16	-0.16	-0.16	-0.16	-0.16		
	3.3	-0.20	-0.20	-0.20	-0.20	-0.20	-0.20	-0.20	-0.20	-0.20	-0.20	-0.20	-0.20	-0.20	-0.20	-0.20	-0.20	-0.20	-0.20	-0.20	-0.20	-0.20	-0.20	-0.20	-0.20	-0.20		
	3.7	-0.23	-0.23	-0.23	-0.23	-0.23	-0.23	-0.23	-0.23	-0.23	-0.23	-0.23	-0.23	-0.23	-0.23	-0.23	-0.23	-0.23	-0.23	-0.23	-0.23	-0.23	-0.23	-0.23	-0.23	-0.23		
	4.1	-0.25	-0.25	-0.25	-0.25	-0.25	-0.25	-0.25	-0.25	-0.25	-0.25	-0.25	-0.25	-0.25	-0.25	-0.25	-0.25	-0.25	-0.25	-0.25	-0.25	-0.25	-0.25	-0.25	-0.25	-0.25		
	4.5	-0.26	-0.26	-0.26	-0.26	-0.26	-0.26	-0.26	-0.26	-0.26	-0.26	-0.26	-0.26	-0.26	-0.26	-0.26	-0.26	-0.26	-0.26	-0.26	-0.26	-0.26	-0.26	-0.26	-0.26	-0.26		
	4.9	-0.27	-0.27	-0.27	-0.27	-0.27	-0.27	-0.27	-0.27	-0.27	-0.27	-0.27	-0.27	-0.27	-0.27	-0.27	-0.27	-0.27	-0.27	-0.27	-0.27	-0.27	-0.27	-0.27	-0.27	-0.27		
Lower surface	Upper face	-0.7	-0.2	0.3	0.5	1.0	2.0	3.0	4.0	5.0	7.0	9.0	11.0	13.0	-0.7	-0.2	0.3	0.6	1.0	2.0	3.0	4.0	5.0	7.0	9.0	11.0	13.0	
	1.7	0.07	0.09	0.11	0.13	0.15	0.17	0.19	0.21	0.23	0.25	0.27	0.29	0.31	0.35	0.37	0.41	0.45	0.49	0.53	0.57	0.61	0.65	0.69	0.73	0.77	0.81	
	2.1	0.09	0.11	0.13	0.15	0.17	0.19	0.21	0.23	0.25	0.27	0.29	0.31	0.33	0.37	0.39	0.43	0.47	0.51	0.55	0.59	0.63	0.67	0.71	0.75	0.79	0.83	
	2.5	0.11	0.13	0.15	0.17	0.19	0.21	0.23	0.25	0.27	0.29	0.31	0.33	0.35	0.39	0.41	0.45	0.49	0.53	0.57	0.61	0.65	0.69	0.73	0.77	0.81	0.85	
	2.9	0.12	0.14	0.16	0.18	0.20	0.22	0.24	0.26	0.28	0.30	0.32	0.34	0.36	0.40	0.42	0.46	0.50	0.54	0.58	0.62	0.66	0.70	0.74	0.78	0.82	0.86	
Lower surface	Lower face	-0.7	-0.2	0.3	0.5	1.0	2.0	3.0	4.0	5.0	7.0	9.0	11.0	13.0	-0.7	-0.2	0.3	0.6	1.0	2.0	3.0	4.0	5.0	7.0	9.0	11.0	13.0	
	1.7	0.05	0.06	0.08	0.10	0.12	0.14	0.16	0.18	0.20	0.22	0.24	0.26	0.28	0.32	0.34	0.38	0.42	0.46	0.50	0.54	0.58	0.62	0.66	0.70	0.74	0.78	
	2.1	0.06	0.07	0.09	0.11	0.13	0.15	0.17	0.19	0.21	0.23	0.25	0.27	0.29	0.33	0.35	0.39	0.43	0.47	0.51	0.55	0.59	0.63	0.67	0.71	0.75	0.79	0.83
	2.5	0.07	0.08	0.10	0.12	0.14	0.16	0.18	0.20	0.22	0.24	0.26	0.28	0.30	0.34	0.36	0.40	0.44	0.48	0.52	0.56	0.60	0.64	0.68	0.72	0.76	0.80	0.84
	2.9	0.08	0.09	0.11	0.13	0.15	0.17	0.19	0.21	0.23	0.25	0.27	0.29	0.31	0.35	0.37	0.41	0.45	0.49	0.53	0.57	0.61	0.65	0.69	0.73	0.77	0.81	0.85

NACA

TABLE III.- CONTINUED

(d) R, 4,500,000; M, 0.88

		$\eta = 0.10$													
		Angle of attack, α , degrees													
Location percent chord	Leading edge	-0.7	-0.6	-0.5	0.4	1.6	2.6	3.6	4.6	5.6	6.6	7.6	8.6	9.6	11.6
		0	.76	.75	.76	.76	.75	.74	.73	.70	.65	.70	.75	.75	.72
Upper surface	Leading edge	-0.7	-0.6	-0.5	0.4	1.6	2.6	3.6	4.6	5.6	6.6	7.6	8.6	9.6	11.6
		0	.76	.75	.76	.76	.75	.74	.73	.70	.65	.70	.75	.75	.72
Lower surface	Leading edge	-0.7	-0.6	-0.5	0.4	1.6	2.6	3.6	4.6	5.6	6.6	7.6	8.6	9.6	11.6
		0	.76	.75	.76	.76	.75	.74	.73	.70	.65	.70	.75	.75	.72
		$\eta = 0.20$													
		Angle of attack, α , degrees													
Location percent chord	Leading edge	-0.7	-0.6	-0.5	0.4	1.6	2.6	3.6	4.6	5.6	6.6	7.6	8.6	9.6	11.6
		0	.76	.75	.76	.76	.75	.74	.73	.70	.65	.70	.75	.75	.72
Upper surface	Leading edge	-0.7	-0.6	-0.5	0.4	1.6	2.6	3.6	4.6	5.6	6.6	7.6	8.6	9.6	11.6
		0	.76	.75	.76	.76	.75	.74	.73	.70	.65	.70	.75	.75	.72
Lower surface	Leading edge	-0.7	-0.6	-0.5	0.4	1.6	2.6	3.6	4.6	5.6	6.6	7.6	8.6	9.6	11.6
		0	.76	.75	.76	.76	.75	.74	.73	.70	.65	.70	.75	.75	.72
		$\eta = 0.40$													
		Angle of attack, α , degrees													
Location percent chord	Leading edge	-0.7	-0.2	0.3	0.8	1.6	2.6	3.6	4.6	5.6	6.6	7.6	8.6	9.6	11.6
		0	.71	.71	.71	.71	.69	.68	.66	.63	.59	.57	.57	.57	.55
Upper surface	Leading edge	-0.7	-0.2	0.3	0.8	1.6	2.6	3.6	4.6	5.6	6.6	7.6	8.6	9.6	11.6
		0	.71	.71	.71	.71	.69	.68	.66	.63	.59	.57	.57	.57	.55
Lower surface	Leading edge	-0.7	-0.2	0.3	0.8	1.6	2.6	3.6	4.6	5.6	6.6	7.6	8.6	9.6	11.6
		0	.71	.71	.71	.71	.69	.68	.66	.63	.59	.57	.57	.57	.55
		$\eta = 0.60$													
		Angle of attack, α , degrees													
Location percent chord	Leading edge	-0.7	-0.2	0.3	0.8	1.6	2.6	3.6	4.6	5.6	6.6	7.6	8.6	9.6	11.6
		0	.69	.70	.70	.70	.68	.66	.63	.59	.55	.53	.53	.53	.50
Upper surface	Leading edge	-0.7	-0.2	0.3	0.8	1.6	2.6	3.6	4.6	5.6	6.6	7.6	8.6	9.6	11.6
		0	.69	.70	.70	.70	.68	.66	.63	.59	.55	.53	.53	.53	.50
Lower surface	Leading edge	-0.7	-0.2	0.3	0.8	1.6	2.6	3.6	4.6	5.6	6.6	7.6	8.6	9.6	11.6
		0	.69	.70	.70	.70	.68	.66	.63	.59	.55	.53	.53	.53	.50

CONFIDENTIAL

TABLE III.—CONTINUED

(d) Concluded

Location	Per-	Angle of attack, α , degrees											
		-0.7	-0.8	0.3	0.8	1.8	2.0	3.8	4.8	5.9	7.9	9.9	
Landing edge	cent	0	.65	.69	.70	.70	.68	.67	.63	.47	.38	.36	.35
Upper surface	1.7	.07	-.03	-.09	-.19	-.14	-.07	-.08	-.03	-.11	-.03	-.06	-.02
	1.8	-.06	-.10	-.17	-.20	-.15	-.06	-.07	-.03	-.13	-.03	-.06	-.01
	6.9	-.13	-.18	-.25	-.29	-.21	-.15	-.16	-.09	-.21	-.03	-.16	-.07
	9.1	-.19	-.24	-.31	-.35	-.26	-.19	-.20	-.12	-.28	-.08	-.21	-.11
	14.9	-.33	-.35	-.40	-.45	-.37	-.28	-.30	-.19	-.57	-.20	-.33	-.16
	20.1	-.31	-.34	-.39	-.43	-.35	-.28	-.30	-.19	-.57	-.21	-.33	-.16
	25.9	-.31	-.34	-.39	-.43	-.35	-.28	-.30	-.19	-.57	-.21	-.33	-.16
	30.7	-.38	-.43	-.49	-.53	-.41	-.31	-.33	-.21	-.61	-.26	-.39	-.20
	45.6	-.38	-.43	-.49	-.53	-.41	-.31	-.33	-.21	-.61	-.26	-.39	-.20
	50.8	-.38	-.43	-.49	-.53	-.41	-.31	-.33	-.21	-.61	-.26	-.39	-.20
Lower surface	55.6	-.06	-.08	-.09	-.04	-.05	-.03	-.05	-.01	0.0	-.12	-.12	-.04
	59.5	-.03	-.05	-.06	-.03	-.04	-.02	-.04	-.01	0.0	-.12	-.12	-.04
	63.1	-.03	-.05	-.06	-.03	-.04	-.02	-.04	-.01	0.0	-.12	-.12	-.04
	67.1	-.03	-.05	-.06	-.03	-.04	-.02	-.04	-.01	0.0	-.12	-.12	-.04
	71.1	-.03	-.05	-.06	-.03	-.04	-.02	-.04	-.01	0.0	-.12	-.12	-.04
	75.1	-.03	-.05	-.06	-.03	-.04	-.02	-.04	-.01	0.0	-.12	-.12	-.04
	82.3	-.03	-.05	-.06	-.03	-.04	-.02	-.04	-.01	0.0	-.12	-.12	-.04



~~CONFIDENTIAL~~

NACA RM A52B20

TABLE III.- CONTINUED

(e) R_s , 4,500,000; M_∞ , 0.91

		a, 0.30											
		Angle of attack, α , degrees											
Location chord		-0.7	-0.2	0.3	0.8	1.8	2.8	3.8	4.9	5.9	7.9	9.9	11.9
Leading edge	0	.76	.77	.77	.77	.76	.75	.73	.70	.68	.66	.50	.38
Upper surface	1.3	.28	.19	.10	.04	.05	.25	.07	.06	.05	.04	.03	.03
Upper surface	2.2												
Upper surface	3.2												
Upper surface	4.3												
Upper surface	5.2												
Upper surface	7.7												
Upper surface	11.9												
Lower surface	20.1												
Lower surface	29.6												
Lower surface	39.3												
Lower surface	59.7												
Lower surface	80.3												
Lower surface	90.3												
Lower surface	95.0												

		a, 0.30											
		Angle of attack, α , degrees											
Location chord		-0.7	-0.2	0.3	0.8	1.8	2.8	3.8	4.9	5.9	7.9	9.9	11.9
Leading edge	0	.75	.75	.75	.75	.75	.75	.75	.75	.75	.75	.75	.75
Upper surface	0.7	.08	.08	.08	.08	.08	.08	.08	.08	.08	.08	.08	.08
Upper surface	1.3												
Upper surface	2.2												
Upper surface	3.2												
Upper surface	4.3												
Upper surface	5.2												
Upper surface	7.7												
Lower surface	20.1												
Lower surface	29.6												
Lower surface	39.3												
Lower surface	59.7												
Lower surface	80.3												
Lower surface	90.3												
Lower surface	95.0												

		a, 0.40											
		Angle of attack, α , degrees											
Location chord		-0.7	-0.2	0.3	0.8	1.8	2.8	3.8	4.9	5.9	7.9	9.9	11.9
Leading edge	0	.71	.70	.71	.71	.69	.68	.67	.66	.65	.64	.50	.38
Upper surface	1.3	.31	.07	.08	.10	.06	.06	.06	.06	.06	.06	.06	.06
Upper surface	2.2												
Upper surface	3.2												
Upper surface	4.3												
Upper surface	5.2												
Upper surface	7.7												
Upper surface	11.9												
Lower surface	20.1												
Lower surface	29.6												
Lower surface	39.3												
Lower surface	59.7												
Lower surface	80.3												
Lower surface	90.3												
Lower surface	95.0												

		a, 0.40											
		Angle of attack, α , degrees											
Location chord		-0.7	-0.2	0.3	0.8	1.8	2.8	3.8	4.9	5.9	7.9	9.9	11.9
Leading edge	0	.70	.70	.70	.70	.69	.68	.67	.66	.65	.64	.50	.38
Upper surface	1.3	.05	.05	.05	.05	.05	.05	.05	.05	.05	.05	.05	.05
Upper surface	2.2												
Upper surface	3.2												
Upper surface	4.3												
Upper surface	5.2												
Upper surface	7.7												
Upper surface	11.9												
Lower surface	20.1												
Lower surface	29.6												
Lower surface	39.3												
Lower surface	59.7												
Lower surface	80.3												
Lower surface	90.3												
Lower surface	95.0												

NACA

TABLE III.- CONTINUED

(f) R, 4,600,000; M, 0.93

		a, 0.10										
		Angle of attack, α , degrees										
		-0.7	-0.2	0.3	0.8	1.3	2.8	3.8	4.8	5.9	7.9	9.9
Leading edge		-0.7	-0.2	0.3	0.8	1.3	2.8	3.8	4.8	5.9	7.9	9.9
Upper surface		0	.76	.79	.77	.76	.74	.71	.69	.68	.59	.52
Lower surface		1.1	1.2	1.3	1.4	1.5	1.6	1.7	1.8	1.9	2.0	2.1
Per cent chord		0.31	0.36	0.48	0.51	0.53	0.57	0.63	0.67	0.71	0.76	0.86
Leading edge		0	.76	.79	.77	.76	.74	.71	.69	.68	.59	.52
Upper surface		1.1	1.2	1.3	1.4	1.5	1.6	1.7	1.8	1.9	2.0	2.1
Lower surface		1.1	1.2	1.3	1.4	1.5	1.6	1.7	1.8	1.9	2.0	2.1

		a, 0.20										
		Angle of attack, α , degrees										
		-0.7	-0.2	0.3	0.8	1.3	2.8	3.8	4.8	5.9	7.9	9.9
Leading edge		0	.76	.76	.76	.75	.72	.67	.63	.61	.49	.40
Upper surface		2.7	3.1	3.2	3.3	3.4	3.5	3.6	3.7	3.8	3.9	4.0
Lower surface		1.1	1.2	1.3	1.4	1.5	1.6	1.7	1.8	1.9	2.0	2.1
Per cent chord		0.31	0.36	0.48	0.51	0.53	0.57	0.63	0.67	0.71	0.76	0.86
Leading edge		0	.76	.76	.76	.75	.72	.67	.63	.61	.49	.40
Upper surface		2.7	3.1	3.2	3.3	3.4	3.5	3.6	3.7	3.8	3.9	4.0
Lower surface		1.1	1.2	1.3	1.4	1.5	1.6	1.7	1.8	1.9	2.0	2.1

		a, 0.40										
		Angle of attack, α , degrees										
		-0.7	-0.2	0.3	0.8	1.3	2.8	3.8	4.8	5.9	7.9	9.9
Leading edge		0	.71	.73	.73	—	.71	.67	.63	.59	.56	.43
Upper surface		1.1	1.2	1.3	1.4	1.5	1.6	1.7	1.8	1.9	2.0	2.1
Lower surface		1.1	1.2	1.3	1.4	1.5	1.6	1.7	1.8	1.9	2.0	2.1
Per cent chord		0.31	0.36	0.48	0.51	0.53	0.57	0.63	0.67	0.71	0.76	0.86
Leading edge		0	.71	.73	.73	—	.71	.67	.63	.59	.56	.43
Upper surface		1.1	1.2	1.3	1.4	1.5	1.6	1.7	1.8	1.9	2.0	2.1
Lower surface		1.1	1.2	1.3	1.4	1.5	1.6	1.7	1.8	1.9	2.0	2.1

		a, 0.60										
		Angle of attack, α , degrees										
		-0.7	-0.2	0.3	0.8	1.3	2.8	3.8	4.8	5.9	7.9	9.9
Leading edge		0	.70	.71	.72	—	.70	.67	.63	.59	.57	.46
Upper surface		1.1	1.2	1.3	1.4	1.5	1.6	1.7	1.8	1.9	2.0	2.1
Lower surface		1.1	1.2	1.3	1.4	1.5	1.6	1.7	1.8	1.9	2.0	2.1
Per cent chord		0.31	0.36	0.48	0.51	0.53	0.57	0.63	0.67	0.71	0.76	0.86
Leading edge		0	.70	.71	.72	—	.70	.67	.63	.59	.57	.46
Upper surface		1.1	1.2	1.3	1.4	1.5	1.6	1.7	1.8	1.9	2.0	2.1
Lower surface		1.1	1.2	1.3	1.4	1.5	1.6	1.7	1.8	1.9	2.0	2.1

NACA

TABLE III.- CONTINUED

(f) Concluded

		$\eta_1 = 0.80$										
Location	Per- cent chord	Angle of attack, α , degrees										
		-0.7	-0.8	0.3	0.8	1.8	2.8	3.8	4.8	5.9	7.9	9.9
Leading edge	0	.66	.68	.69	.70	.70	.66	.64	.63	.61	.51	.40
Upper surface	1.7	0.05	0	-0.06	-0.14	-0.19	-0.26	-0.33	-0.43	-0.51	-1.03	-1.14
	4.1	-0.05	-0.10	-0.15	-0.20	-0.30	-0.36	-0.42	-0.50	-0.58	-0.79	-1.02
	7.0	-0.11	-0.16	-0.20	-0.25	-0.33	-0.40	-0.47	-0.53	-0.60	-0.73	-1.10
	9.0	-0.17	-0.21	-0.26	-0.30	-0.37	-0.43	-0.50	-0.56	-0.62	-0.71	-1.08
	13.7	-0.27	-0.30	-0.35	-0.38	-0.42	-0.47	-0.53	-0.58	-0.63	-0.70	-1.07
	19.1	-0.35	-0.38	-0.42	-0.45	-0.49	-0.53	-0.58	-0.63	-0.68	-0.75	-1.04
	29.3	-0.45	-0.48	-0.51	-0.54	-0.58	-0.61	-0.65	-0.69	-0.73	-0.78	-1.02
	39.5	-0.55	-0.58	-0.61	-0.64	-0.67	-0.70	-0.73	-0.76	-0.80	-0.83	-1.06
	49.7	-0.60	-0.63	-0.66	-0.69	-0.72	-0.75	-0.78	-0.81	-0.84	-0.87	-1.07
	59.8	-0.65	-0.68	-0.71	-0.74	-0.77	-0.80	-0.83	-0.86	-0.89	-0.92	-1.08
Lower surface	1.6	1.02	1.04	1.05	1.06	1.07	1.08	1.09	1.10	1.11	1.12	1.10
	4.0	-1.02	-1.04	-1.05	-1.06	-1.07	-1.08	-1.09	-1.10	-1.11	-1.12	-1.03
	6.6	-1.02	-1.04	-1.05	-1.06	-1.07	-1.08	-1.09	-1.10	-1.11	-1.12	-1.03
	9.3	-1.02	-1.04	-1.05	-1.06	-1.07	-1.08	-1.09	-1.10	-1.11	-1.12	-1.03
	14.9	-1.02	-1.04	-1.05	-1.06	-1.07	-1.08	-1.09	-1.10	-1.11	-1.12	-1.03
	19.3	-1.02	-1.04	-1.05	-1.06	-1.07	-1.08	-1.09	-1.10	-1.11	-1.12	-1.03
	29.5	-1.02	-1.04	-1.05	-1.06	-1.07	-1.08	-1.09	-1.10	-1.11	-1.12	-1.03
	39.7	-1.02	-1.04	-1.05	-1.06	-1.07	-1.08	-1.09	-1.10	-1.11	-1.12	-1.03
	49.8	-1.02	-1.04	-1.05	-1.06	-1.07	-1.08	-1.09	-1.10	-1.11	-1.12	-1.03
	59.9	-1.02	-1.04	-1.05	-1.06	-1.07	-1.08	-1.09	-1.10	-1.11	-1.12	-1.03

NACA

		$\eta_1 = 0.90$										
Location	Per- cent chord	Angle of attack, α , degrees										
		-0.7	-0.8	0.3	0.8	1.8	2.8	3.8	4.8	5.9	7.9	9.9
Leading edge	0	.66	.68	.69	.70	.66	.64	.63	.62	.59	.51	.42
Upper surface	1.8	0.02	0	-0.17	-0.23	-0.31	-0.38	-0.45	-0.52	-0.58	-0.68	-1.10
	4.6	-0.18	-0.27	-0.35	-0.42	-0.49	-0.56	-0.63	-0.70	-0.77	-0.85	-1.07
	7.6	-0.19	-0.28	-0.36	-0.43	-0.50	-0.57	-0.64	-0.71	-0.78	-0.86	-1.03
	9.3	-0.23	-0.32	-0.40	-0.47	-0.54	-0.61	-0.68	-0.75	-0.82	-0.90	-1.00
	14.9	-0.23	-0.32	-0.40	-0.47	-0.54	-0.61	-0.68	-0.75	-0.82	-0.90	-1.00
	19.3	-0.23	-0.32	-0.40	-0.47	-0.54	-0.61	-0.68	-0.75	-0.82	-0.90	-1.00
	29.5	-0.23	-0.32	-0.40	-0.47	-0.54	-0.61	-0.68	-0.75	-0.82	-0.90	-1.00
	39.7	-0.23	-0.32	-0.40	-0.47	-0.54	-0.61	-0.68	-0.75	-0.82	-0.90	-1.00
	49.8	-0.23	-0.32	-0.40	-0.47	-0.54	-0.61	-0.68	-0.75	-0.82	-0.90	-1.00
	59.9	-0.23	-0.32	-0.40	-0.47	-0.54	-0.61	-0.68	-0.75	-0.82	-0.90	-1.00
Lower surface	1.4	-1.02	-1.04	-1.05	-1.06	-1.07	-1.08	-1.09	-1.10	-1.11	-1.12	-1.03
	4.1	-1.02	-1.04	-1.05	-1.06	-1.07	-1.08	-1.09	-1.10	-1.11	-1.12	-1.03
	6.1	-1.02	-1.04	-1.05	-1.06	-1.07	-1.08	-1.09	-1.10	-1.11	-1.12	-1.03
	9.6	-1.02	-1.04	-1.05	-1.06	-1.07	-1.08	-1.09	-1.10	-1.11	-1.12	-1.03
	13.7	-1.02	-1.04	-1.05	-1.06	-1.07	-1.08	-1.09	-1.10	-1.11	-1.12	-1.03
	20.2	-1.02	-1.04	-1.05	-1.06	-1.07	-1.08	-1.09	-1.10	-1.11	-1.12	-1.03
	29.7	-1.02	-1.04	-1.05	-1.06	-1.07	-1.08	-1.09	-1.10	-1.11	-1.12	-1.03
	39.6	-1.02	-1.04	-1.05	-1.06	-1.07	-1.08	-1.09	-1.10	-1.11	-1.12	-1.03
	49.5	-1.02	-1.04	-1.05	-1.06	-1.07	-1.08	-1.09	-1.10	-1.11	-1.12	-1.03
	59.6	-1.02	-1.04	-1.05	-1.06	-1.07	-1.08	-1.09	-1.10	-1.11	-1.12	-1.03

TABLE III.- CONTINUED

(g) $R = 4,600,000$; $M = 0.94$

		$\alpha = 0.10$									$\alpha = 0.20$														
		Angle of attack, α , degrees									Angle of attack, α , degrees														
Location		Percent chord	-0.7	-0.2	0.3	0.8	1.6	2.8	3.8	4.8	5.9	7.9	9.9	0	-0.7	-0.2	0.3	0.8	1.6	2.8	3.8	4.8	5.9	7.9	9.9
Leading edge		0	0	-70	-70	-70	-70	-70	-70	-70	-65	-65	-55	0	0	-70	-70	-70	-70	-70	-70	-65	-65	-55	
Upper surface	0	0.11	0.36	0.13	0.40	-0.03	-0.15	-0.27	-0.30	-0.33	-0.33	-0.33	-0.33	0.11	0.09	0.11	0.12	0.13	0.15	0.16	0.16	0.16	0.16	0.16	
	0.15	0.26	0.26	0.26	0.26	0.26	0.26	0.26	0.26	0.26	0.26	0.26	0.26	0.15	0.15	0.15	0.15	0.15	0.15	0.15	0.15	0.15	0.15	0.15	
Lower surface	0	0.29	0.29	0.29	0.29	0.29	0.29	0.29	0.29	0.29	0.29	0.29	0.29	0.29	0.29	0.29	0.29	0.29	0.29	0.29	0.29	0.29	0.29	0.29	
	0.15	0.29	0.29	0.29	0.29	0.29	0.29	0.29	0.29	0.29	0.29	0.29	0.29	0.29	0.29	0.29	0.29	0.29	0.29	0.29	0.29	0.29	0.29	0.29	
Upper surface	0	0.11	0.11	0.11	0.11	0.11	0.11	0.11	0.11	0.11	0.11	0.11	0.11	0.11	0.11	0.11	0.11	0.11	0.11	0.11	0.11	0.11	0.11	0.11	
	0.15	0.15	0.15	0.15	0.15	0.15	0.15	0.15	0.15	0.15	0.15	0.15	0.15	0.15	0.15	0.15	0.15	0.15	0.15	0.15	0.15	0.15	0.15	0.15	
Lower surface	0	0.29	0.29	0.29	0.29	0.29	0.29	0.29	0.29	0.29	0.29	0.29	0.29	0.29	0.29	0.29	0.29	0.29	0.29	0.29	0.29	0.29	0.29	0.29	
	0.15	0.29	0.29	0.29	0.29	0.29	0.29	0.29	0.29	0.29	0.29	0.29	0.29	0.29	0.29	0.29	0.29	0.29	0.29	0.29	0.29	0.29	0.29	0.29	
		$\alpha = 0.10$									$\alpha = 0.20$														
		Angle of attack, α , degrees									Angle of attack, α , degrees														
Location		Percent chord	-0.7	-0.2	0.3	0.8	1.6	2.8	3.8	4.8	5.9	7.9	9.9	0	-0.7	-0.2	0.3	0.8	1.6	2.8	3.8	4.8	5.9	7.9	9.9
Leading edge		0	0	-73	-73	-73	-73	-73	-73	-68	-68	-60	-55	-55	0	0	-73	-73	-73	-73	-73	-73	-68	-68	-60
Upper surface	0	0.13	0.08	0.08	0.08	0.08	0.08	0.08	0.08	0.08	0.08	0.08	0.08	0.13	0.08	0.08	0.08	0.08	0.08	0.08	0.08	0.08	0.08	0.08	
	0.15	0.15	0.15	0.15	0.15	0.15	0.15	0.15	0.15	0.15	0.15	0.15	0.15	0.15	0.15	0.15	0.15	0.15	0.15	0.15	0.15	0.15	0.15	0.15	
Lower surface	0	0.29	0.29	0.29	0.29	0.29	0.29	0.29	0.29	0.29	0.29	0.29	0.29	0.29	0.29	0.29	0.29	0.29	0.29	0.29	0.29	0.29	0.29	0.29	
	0.15	0.29	0.29	0.29	0.29	0.29	0.29	0.29	0.29	0.29	0.29	0.29	0.29	0.29	0.29	0.29	0.29	0.29	0.29	0.29	0.29	0.29	0.29	0.29	
		$\alpha = 0.10$									$\alpha = 0.20$														
		Angle of attack, α , degrees									Angle of attack, α , degrees														
Location		Percent chord	-0.7	-0.2	0.3	0.8	1.6	2.8	3.8	4.8	5.9	7.9	9.9	0	-0.7	-0.2	0.3	0.8	1.6	2.8	3.8	4.8	5.9	7.9	9.9
Leading edge		0	0	-73	-73	-73	-73	-73	-73	-68	-68	-60	-55	-55	0	0	-73	-73	-73	-73	-73	-73	-68	-68	-60
Upper surface	0	0.13	0.08	0.08	0.08	0.08	0.08	0.08	0.08	0.08	0.08	0.08	0.08	0.13	0.08	0.08	0.08	0.08	0.08	0.08	0.08	0.08	0.08	0.08	
	0.15	0.15	0.15	0.15	0.15	0.15	0.15	0.15	0.15	0.15	0.15	0.15	0.15	0.15	0.15	0.15	0.15	0.15	0.15	0.15	0.15	0.15	0.15	0.15	
Lower surface	0	0.29	0.29	0.29	0.29	0.29	0.29	0.29	0.29	0.29	0.29	0.29	0.29	0.29	0.29	0.29	0.29	0.29	0.29	0.29	0.29	0.29	0.29	0.29	
	0.15	0.29	0.29	0.29	0.29	0.29	0.29	0.29	0.29	0.29	0.29	0.29	0.29	0.29	0.29	0.29	0.29	0.29	0.29	0.29	0.29	0.29	0.29	0.29	

CONFIDENTIAL

CONFIDENTIAL

TABLE III.- CONCLUDED

(g) Concluded

		$\alpha_0 = 0.80$									$\alpha_0 = 0.90$												
		Angle of attack, α , degrees									Angle of attack, α , degrees												
Location	Percent chord	-0.7	-0.2	0.3	0.8	1.8	2.8	3.8	4.8	5.9	7.9	9.9	-0.7	-0.2	0.3	0.8	1.8	2.8	3.8	4.8	5.9	7.9	9.9
		0	.68	.69	.69	.69	.71	.70	.67	.63	.60	.58	.56	0	.70	.70	.71	.69	.65	.63	.60	.51	.47
Upper surface	0	1.7	0.68	0.91	-0.05	-0.13	-0.87	-0.45	-0.66	-0.87	-0.88	-1.04	-1.11	1.7	0.67	0	-0.15	-0.55	-0.85	-0.88	-1.05	-1.12	-1.15
	0.1	1.7	-0.93	-0.99	-0.17	-0.19	-0.85	-0.47	-0.67	-0.88	-0.89	-1.05	-1.12	1.7	-0.94	-0.95	-0.96	-1.05	-1.12	-1.13	-1.14	-1.15	
	0.2	1.7	-0.89	-0.92	-0.19	-0.19	-0.85	-0.47	-0.67	-0.88	-0.89	-1.05	-1.12	1.7	-0.89	-0.92	-0.95	-1.05	-1.12	-1.13	-1.14	-1.15	
	0.3	1.7	-0.75	-0.84	-0.21	-0.21	-0.85	-0.47	-0.67	-0.88	-0.89	-1.05	-1.12	1.7	-0.75	-0.84	-0.95	-1.05	-1.12	-1.13	-1.14	-1.15	
	0.4	1.7	-0.71	-0.79	-0.23	-0.23	-0.85	-0.47	-0.67	-0.88	-0.89	-1.05	-1.12	1.7	-0.71	-0.79	-0.95	-1.05	-1.12	-1.13	-1.14	-1.15	
	0.5	1.7	-0.67	-0.74	-0.25	-0.25	-0.85	-0.47	-0.67	-0.88	-0.89	-1.05	-1.12	1.7	-0.67	-0.74	-0.95	-1.05	-1.12	-1.13	-1.14	-1.15	
	0.6	1.7	-0.63	-0.69	-0.27	-0.27	-0.85	-0.47	-0.67	-0.88	-0.89	-1.05	-1.12	1.7	-0.63	-0.69	-0.95	-1.05	-1.12	-1.13	-1.14	-1.15	
	0.7	1.7	-0.59	-0.64	-0.29	-0.29	-0.85	-0.47	-0.67	-0.88	-0.89	-1.05	-1.12	1.7	-0.59	-0.64	-0.95	-1.05	-1.12	-1.13	-1.14	-1.15	
	0.8	1.7	-0.55	-0.59	-0.31	-0.31	-0.85	-0.47	-0.67	-0.88	-0.89	-1.05	-1.12	1.7	-0.55	-0.59	-0.95	-1.05	-1.12	-1.13	-1.14	-1.15	
	0.9	1.7	-0.51	-0.54	-0.33	-0.33	-0.85	-0.47	-0.67	-0.88	-0.89	-1.05	-1.12	1.7	-0.51	-0.54	-0.95	-1.05	-1.12	-1.13	-1.14	-1.15	
Lower surface	0	1.6	0.59	0.84	0.19	0.19	0.85	0.47	0.67	0.88	0.89	1.05	1.12	1.6	0.58	0.83	0.18	0.18	0.85	0.47	0.67	0.88	0.89
	0.1	1.6	0.55	0.79	0.21	0.21	0.85	0.47	0.67	0.88	0.89	1.05	1.12	1.6	0.54	0.78	0.20	0.20	0.85	0.47	0.67	0.88	0.89
	0.2	1.6	0.51	0.74	0.23	0.23	0.85	0.47	0.67	0.88	0.89	1.05	1.12	1.6	0.51	0.73	0.21	0.21	0.85	0.47	0.67	0.88	0.89
	0.3	1.6	0.47	0.69	0.25	0.25	0.85	0.47	0.67	0.88	0.89	1.05	1.12	1.6	0.47	0.68	0.23	0.23	0.85	0.47	0.67	0.88	0.89
	0.4	1.6	0.43	0.64	0.27	0.27	0.85	0.47	0.67	0.88	0.89	1.05	1.12	1.6	0.43	0.63	0.25	0.25	0.85	0.47	0.67	0.88	0.89
	0.5	1.6	0.39	0.59	0.29	0.29	0.85	0.47	0.67	0.88	0.89	1.05	1.12	1.6	0.39	0.58	0.27	0.27	0.85	0.47	0.67	0.88	0.89
	0.6	1.6	0.35	0.54	0.31	0.31	0.85	0.47	0.67	0.88	0.89	1.05	1.12	1.6	0.35	0.53	0.29	0.29	0.85	0.47	0.67	0.88	0.89
	0.7	1.6	0.31	0.49	0.33	0.33	0.85	0.47	0.67	0.88	0.89	1.05	1.12	1.6	0.31	0.48	0.27	0.27	0.85	0.47	0.67	0.88	0.89
	0.8	1.6	0.27	0.44	0.35	0.35	0.85	0.47	0.67	0.88	0.89	1.05	1.12	1.6	0.27	0.43	0.25	0.25	0.85	0.47	0.67	0.88	0.89
	0.9	1.6	0.23	0.39	0.37	0.37	0.85	0.47	0.67	0.88	0.89	1.05	1.12	1.6	0.23	0.38	0.23	0.23	0.85	0.47	0.67	0.88	0.89

NACA

TABLE IV.- TABULATED PRESSURE COEFFICIENTS FROM HIGH-SPEED TESTS IN THE 12-FOOT WIND TUNNEL AT A REYNOLDS NUMBER OF 2,000,000

(a) R, 2,000,000; M, 0.60

		C _L 0.10											
		Angle of attack, α , degrees											
		0	1.0	2.0	3.0	4.0	5.0	6.0	8.1	10.1	12.1	14.0	16.0
Location along chord		0	.70	.71	.69	.67	.65	.63	.58	.53	.48	.43	.38
Leading edge													
Upper surface													
Lower surface													

		C _L 0.30											
		Angle of attack, α , degrees											
		0	1.0	2.0	3.0	4.0	5.0	6.0	8.1	10.1	12.1	14.0	16.0
Location along chord		0	.50	.49	.48	.47	.46	.45	.44	.43	.42	.41	.40
Leading edge													
Upper surface													
Lower surface													

		C _L 0.40											
		Angle of attack, α , degrees											
		0	1.0	2.0	3.0	4.0	5.0	6.0	8.1	10.1	12.1	14.0	16.0
Location along chord		0	.57	.56	.55	.54	.53	.52	.51	.50	.49	.48	.47
Leading edge													
Upper surface													
Lower surface													

		C _L 0.60											
		Angle of attack, α , degrees											
		0	1.0	2.0	3.0	4.0	5.0	6.0	8.1	10.1	12.1	14.0	16.0
Location along chord		0	.59	.58	.57	.56	.55	.54	.53	.52	.51	.50	.49
Leading edge													
Upper surface													
Lower surface													

TABLE IV.- CONTINUED

(b) Concluded

		$\alpha_0 = 0.80$											
		Angle of attack, α , degrees											
Location	Percent chord	-0.5	0	0.5	1.0	2.0	3.0	4.0	5.1	6.1	8.1	10.1	12.1
Leading edge	0	.04	.06	.08	.08	.07	.08	.05	.11	.11	.05	.19	.21
Upper surface	1.7	0.00	-0.11	-0.11	-0.10	-0.09	-0.08	-0.17	-1.21	-1.21	-1.07	-0.11	-0.11
	4.1	-0.13	-0.19	-0.21	-0.20	-0.19	-0.18	-0.18	-1.19	-1.19	-1.13	-0.15	-0.15
	7.0	-0.19	-0.23	-0.24	-0.23	-0.22	-0.21	-0.21	-1.15	-1.15	-1.13	-0.17	-0.17
	9.0	-0.21	-0.23	-0.24	-0.23	-0.22	-0.21	-0.21	-1.13	-1.13	-1.13	-0.17	-0.17
	13.7	-0.21	-0.23	-0.24	-0.23	-0.22	-0.21	-0.21	-1.13	-1.13	-1.13	-0.17	-0.17
	19.1	-0.21	-0.23	-0.24	-0.23	-0.22	-0.21	-0.21	-1.13	-1.13	-1.13	-0.17	-0.17
	25.6	-0.21	-0.23	-0.24	-0.23	-0.22	-0.21	-0.21	-1.13	-1.13	-1.13	-0.17	-0.17
	34.6	-0.21	-0.23	-0.24	-0.23	-0.22	-0.21	-0.21	-1.13	-1.13	-1.13	-0.17	-0.17
	44.4	-0.21	-0.23	-0.24	-0.23	-0.22	-0.21	-0.21	-1.13	-1.13	-1.13	-0.17	-0.17
	55.0	-0.21	-0.23	-0.24	-0.23	-0.22	-0.21	-0.21	-1.13	-1.13	-1.13	-0.17	-0.17
Lower surface	1.6	-0.01	-0.10	-0.10	-0.10	-0.09	-0.09	-0.01	-1.20	-1.20	-1.18	-0.10	-0.10
	4.1	-0.14	-0.20	-0.20	-0.20	-0.19	-0.19	-0.14	-1.19	-1.19	-1.18	-0.10	-0.10
	7.0	-0.16	-0.21	-0.21	-0.21	-0.20	-0.20	-0.16	-1.19	-1.19	-1.18	-0.10	-0.10
	9.0	-0.17	-0.21	-0.21	-0.21	-0.20	-0.20	-0.17	-1.19	-1.19	-1.18	-0.10	-0.10
	13.7	-0.17	-0.21	-0.21	-0.21	-0.20	-0.20	-0.17	-1.19	-1.19	-1.18	-0.10	-0.10
	19.1	-0.17	-0.21	-0.21	-0.21	-0.20	-0.20	-0.17	-1.19	-1.19	-1.18	-0.10	-0.10
	25.6	-0.17	-0.21	-0.21	-0.21	-0.20	-0.20	-0.17	-1.19	-1.19	-1.18	-0.10	-0.10
	34.6	-0.17	-0.21	-0.21	-0.21	-0.20	-0.20	-0.17	-1.19	-1.19	-1.18	-0.10	-0.10
	44.4	-0.17	-0.21	-0.21	-0.21	-0.20	-0.20	-0.17	-1.19	-1.19	-1.18	-0.10	-0.10
	55.0	-0.17	-0.21	-0.21	-0.21	-0.20	-0.20	-0.17	-1.19	-1.19	-1.18	-0.10	-0.10

		$\alpha_0 = 0.90$											
		Angle of attack, α , degrees											
Location	Percent chord	-0.5	0	0.5	1.0	2.0	3.0	4.0	5.1	6.1	8.1	10.1	12.1
Leading edge	0	.06	.08	.08	.08	.08	.08	.05	.11	.11	.05	.19	.21
Upper surface	1.7	0.05	-0.10	-0.10	-0.10	-0.09	-0.09	-0.01	-1.20	-1.20	-1.18	-0.10	-0.10
	4.1	-0.15	-0.20	-0.20	-0.20	-0.19	-0.19	-0.15	-1.19	-1.19	-1.18	-0.10	-0.10
	7.0	-0.16	-0.21	-0.21	-0.21	-0.20	-0.20	-0.16	-1.19	-1.19	-1.18	-0.10	-0.10
	9.0	-0.17	-0.21	-0.21	-0.21	-0.20	-0.20	-0.17	-1.19	-1.19	-1.18	-0.10	-0.10
	13.7	-0.17	-0.21	-0.21	-0.21	-0.20	-0.20	-0.17	-1.19	-1.19	-1.18	-0.10	-0.10
	19.1	-0.17	-0.21	-0.21	-0.21	-0.20	-0.20	-0.17	-1.19	-1.19	-1.18	-0.10	-0.10
	25.6	-0.17	-0.21	-0.21	-0.21	-0.20	-0.20	-0.17	-1.19	-1.19	-1.18	-0.10	-0.10
	34.6	-0.17	-0.21	-0.21	-0.21	-0.20	-0.20	-0.17	-1.19	-1.19	-1.18	-0.10	-0.10
	44.4	-0.17	-0.21	-0.21	-0.21	-0.20	-0.20	-0.17	-1.19	-1.19	-1.18	-0.10	-0.10
	55.0	-0.17	-0.21	-0.21	-0.21	-0.20	-0.20	-0.17	-1.19	-1.19	-1.18	-0.10	-0.10
Lower surface	1.6	-0.01	-0.10	-0.10	-0.10	-0.09	-0.09	-0.01	-1.20	-1.20	-1.18	-0.10	-0.10
	4.1	-0.14	-0.20	-0.20	-0.20	-0.19	-0.19	-0.14	-1.19	-1.19	-1.18	-0.10	-0.10
	7.0	-0.16	-0.21	-0.21	-0.21	-0.20	-0.20	-0.16	-1.19	-1.19	-1.18	-0.10	-0.10
	9.0	-0.17	-0.21	-0.21	-0.21	-0.20	-0.20	-0.17	-1.19	-1.19	-1.18	-0.10	-0.10
	13.7	-0.17	-0.21	-0.21	-0.21	-0.20	-0.20	-0.17	-1.19	-1.19	-1.18	-0.10	-0.10
	19.1	-0.17	-0.21	-0.21	-0.21	-0.20	-0.20	-0.17	-1.19	-1.19	-1.18	-0.10	-0.10
	25.6	-0.17	-0.21	-0.21	-0.21	-0.20	-0.20	-0.17	-1.19	-1.19	-1.18	-0.10	-0.10
	34.6	-0.17	-0.21	-0.21	-0.21	-0.20	-0.20	-0.17	-1.19	-1.19	-1.18	-0.10	-0.10
	44.4	-0.17	-0.21	-0.21	-0.21	-0.20	-0.20	-0.17	-1.19	-1.19	-1.18	-0.10	-0.10
	55.0	-0.17	-0.21	-0.21	-0.21	-0.20	-0.20	-0.17	-1.19	-1.19	-1.18	-0.10	-0.10

NACA

TABLE IV.- CONTINUED

(c) $R, 2,000,000$; $M, 0.85$

		$\alpha, 0.30$												
		Angle of attack, α , degrees												
Position Percent chord	Leading edge	-0.5	0	0.5	1.0	2.0	3.0	4.1	5.1	6.1	8.1	10.1	12.1	
		.16	.17	.17	.17	.17	.17	.17	.17	.17	.17	.17	.17	.17
Upper surface	0	0.18	0.13	0.07	0.03	-0.10	-0.16	-0.21	-0.27	-0.33	-0.38	-0.43	-0.48	-0.53
	1.0	0.18	0.13	0.07	0.03	-0.10	-0.16	-0.21	-0.27	-0.33	-0.38	-0.43	-0.48	-0.53
Lower surface	0	0.18	0.13	0.07	0.03	-0.10	-0.16	-0.21	-0.27	-0.33	-0.38	-0.43	-0.48	-0.53
	1.0	0.18	0.13	0.07	0.03	-0.10	-0.16	-0.21	-0.27	-0.33	-0.38	-0.43	-0.48	-0.53

		$\alpha, 0.30$												
		Angle of attack, α , degrees												
Position Percent chord	Leading edge	-0.5	0	0.5	1.0	2.0	3.0	4.1	5.1	6.1	8.1	10.1	12.1	
		.17	.17	.17	.17	.17	.17	.17	.17	.17	.17	.17	.17	.17
Upper surface	0	0.18	0.13	0.07	0.03	-0.10	-0.16	-0.21	-0.27	-0.33	-0.38	-0.43	-0.48	-0.53
	1.0	0.18	0.13	0.07	0.03	-0.10	-0.16	-0.21	-0.27	-0.33	-0.38	-0.43	-0.48	-0.53
Lower surface	0	0.18	0.13	0.07	0.03	-0.10	-0.16	-0.21	-0.27	-0.33	-0.38	-0.43	-0.48	-0.53
	1.0	0.18	0.13	0.07	0.03	-0.10	-0.16	-0.21	-0.27	-0.33	-0.38	-0.43	-0.48	-0.53

		$\alpha, 0.40$												
		Angle of attack, α , degrees												
Position Percent chord	Leading edge	-0.5	0	0.5	1.0	2.0	3.0	4.1	5.1	6.1	8.1	10.1	12.1	
		.70	.70	.70	.70	.70	.70	.70	.70	.70	.70	.70	.70	.70
Upper surface	0	0.18	0.13	0.07	0.03	-0.10	-0.16	-0.21	-0.27	-0.33	-0.38	-0.43	-0.48	-0.53
	1.0	0.18	0.13	0.07	0.03	-0.10	-0.16	-0.21	-0.27	-0.33	-0.38	-0.43	-0.48	-0.53
Lower surface	0	0.18	0.13	0.07	0.03	-0.10	-0.16	-0.21	-0.27	-0.33	-0.38	-0.43	-0.48	-0.53
	1.0	0.18	0.13	0.07	0.03	-0.10	-0.16	-0.21	-0.27	-0.33	-0.38	-0.43	-0.48	-0.53

		$\alpha, 0.40$												
		Angle of attack, α , degrees												
Position Percent chord	Leading edge	-0.5	0	0.5	1.0	2.0	3.0	4.1	5.1	6.1	8.1	10.1	12.1	
		.70	.70	.70	.70	.70	.70	.70	.70	.70	.70	.70	.70	.70
Upper surface	0	0.18	0.13	0.07	0.03	-0.10	-0.16	-0.21	-0.27	-0.33	-0.38	-0.43	-0.48	-0.53
	1.0	0.18	0.13	0.07	0.03	-0.10	-0.16	-0.21	-0.27	-0.33	-0.38	-0.43	-0.48	-0.53
Lower surface	0	0.18	0.13	0.07	0.03	-0.10	-0.16	-0.21	-0.27	-0.33	-0.38	-0.43	-0.48	-0.53
	1.0	0.18	0.13	0.07	0.03	-0.10	-0.16	-0.21	-0.27	-0.33	-0.38	-0.43	-0.48	-0.53

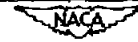


TABLE IV.- CONTINUED

(c) Concluded

		$\eta, 0.80$												$\eta, 0.90$												
		Angle of attack, a_t , degrees												Angle of attack, a_t , degrees												
Location	Percent chord	-0.5	0	0.5	1.0	2.0	3.0	4.1	5.1	6.1	8.1	10.1	12.1	-0.5	0	0.5	1.0	2.0	3.0	4.1	5.1	6.1	8.1	10.1	12.1	
Leading edge	0	.66	.67	.69	.69	.68	.64	.59	.53	.48	.39	.31	.23	0	.66	.68	.69	.71	.74	.76	.79	.81	.83	.85	.87	.89
Upper surface	-0.5	.06	-0.03	-0.17	-0.24	-0.30	-0.38	-0.45	-0.52	-0.59	-0.65	-0.72	-0.78	0	.06	-0.03	-0.17	-0.24	-0.30	-0.38	-0.45	-0.52	-0.59	-0.65	-0.72	-0.78
	0	-1.7	-1.7	-1.7	-1.7	-1.7	-1.7	-1.7	-1.7	-1.7	-1.7	-1.7	-1.7	-1.7	-1.7	-1.7	-1.7	-1.7	-1.7	-1.7	-1.7	-1.7	-1.7	-1.7	-1.7	
	.5	-2.9	-2.9	-2.9	-2.9	-2.9	-2.9	-2.9	-2.9	-2.9	-2.9	-2.9	-2.9	-2.9	-2.9	-2.9	-2.9	-2.9	-2.9	-2.9	-2.9	-2.9	-2.9	-2.9	-2.9	
	1.0	-3.9	-3.9	-3.9	-3.9	-3.9	-3.9	-3.9	-3.9	-3.9	-3.9	-3.9	-3.9	-3.9	-3.9	-3.9	-3.9	-3.9	-3.9	-3.9	-3.9	-3.9	-3.9	-3.9	-3.9	
	2.0	-5.1	-5.1	-5.1	-5.1	-5.1	-5.1	-5.1	-5.1	-5.1	-5.1	-5.1	-5.1	-5.1	-5.1	-5.1	-5.1	-5.1	-5.1	-5.1	-5.1	-5.1	-5.1	-5.1	-5.1	
	3.0	-6.5	-6.5	-6.5	-6.5	-6.5	-6.5	-6.5	-6.5	-6.5	-6.5	-6.5	-6.5	-6.5	-6.5	-6.5	-6.5	-6.5	-6.5	-6.5	-6.5	-6.5	-6.5	-6.5	-6.5	
	4.1	-7.7	-7.7	-7.7	-7.7	-7.7	-7.7	-7.7	-7.7	-7.7	-7.7	-7.7	-7.7	-7.7	-7.7	-7.7	-7.7	-7.7	-7.7	-7.7	-7.7	-7.7	-7.7	-7.7	-7.7	
	5.1	-8.7	-8.7	-8.7	-8.7	-8.7	-8.7	-8.7	-8.7	-8.7	-8.7	-8.7	-8.7	-8.7	-8.7	-8.7	-8.7	-8.7	-8.7	-8.7	-8.7	-8.7	-8.7	-8.7	-8.7	
	6.1	-9.4	-9.4	-9.4	-9.4	-9.4	-9.4	-9.4	-9.4	-9.4	-9.4	-9.4	-9.4	-9.4	-9.4	-9.4	-9.4	-9.4	-9.4	-9.4	-9.4	-9.4	-9.4	-9.4	-9.4	
	8.1	-10.0	-10.0	-10.0	-10.0	-10.0	-10.0	-10.0	-10.0	-10.0	-10.0	-10.0	-10.0	-10.0	-10.0	-10.0	-10.0	-10.0	-10.0	-10.0	-10.0	-10.0	-10.0	-10.0		
	10.1	-10.5	-10.5	-10.5	-10.5	-10.5	-10.5	-10.5	-10.5	-10.5	-10.5	-10.5	-10.5	-10.5	-10.5	-10.5	-10.5	-10.5	-10.5	-10.5	-10.5	-10.5	-10.5	-10.5		
	12.1	-11.0	-11.0	-11.0	-11.0	-11.0	-11.0	-11.0	-11.0	-11.0	-11.0	-11.0	-11.0	-11.0	-11.0	-11.0	-11.0	-11.0	-11.0	-11.0	-11.0	-11.0	-11.0	-11.0		
Lower surface	-0.5	-1.7	-1.7	-1.7	-1.7	-1.7	-1.7	-1.7	-1.7	-1.7	-1.7	-1.7	-1.7	-1.7	-1.7	-1.7	-1.7	-1.7	-1.7	-1.7	-1.7	-1.7	-1.7	-1.7	-1.7	
	0	-2.9	-2.9	-2.9	-2.9	-2.9	-2.9	-2.9	-2.9	-2.9	-2.9	-2.9	-2.9	-2.9	-2.9	-2.9	-2.9	-2.9	-2.9	-2.9	-2.9	-2.9	-2.9	-2.9	-2.9	
	.5	-4.1	-4.1	-4.1	-4.1	-4.1	-4.1	-4.1	-4.1	-4.1	-4.1	-4.1	-4.1	-4.1	-4.1	-4.1	-4.1	-4.1	-4.1	-4.1	-4.1	-4.1	-4.1	-4.1	-4.1	
	1.0	-5.1	-5.1	-5.1	-5.1	-5.1	-5.1	-5.1	-5.1	-5.1	-5.1	-5.1	-5.1	-5.1	-5.1	-5.1	-5.1	-5.1	-5.1	-5.1	-5.1	-5.1	-5.1	-5.1	-5.1	
	2.0	-6.5	-6.5	-6.5	-6.5	-6.5	-6.5	-6.5	-6.5	-6.5	-6.5	-6.5	-6.5	-6.5	-6.5	-6.5	-6.5	-6.5	-6.5	-6.5	-6.5	-6.5	-6.5	-6.5	-6.5	
	3.0	-7.7	-7.7	-7.7	-7.7	-7.7	-7.7	-7.7	-7.7	-7.7	-7.7	-7.7	-7.7	-7.7	-7.7	-7.7	-7.7	-7.7	-7.7	-7.7	-7.7	-7.7	-7.7	-7.7	-7.7	
	4.1	-8.7	-8.7	-8.7	-8.7	-8.7	-8.7	-8.7	-8.7	-8.7	-8.7	-8.7	-8.7	-8.7	-8.7	-8.7	-8.7	-8.7	-8.7	-8.7	-8.7	-8.7	-8.7	-8.7	-8.7	
	5.1	-9.4	-9.4	-9.4	-9.4	-9.4	-9.4	-9.4	-9.4	-9.4	-9.4	-9.4	-9.4	-9.4	-9.4	-9.4	-9.4	-9.4	-9.4	-9.4	-9.4	-9.4	-9.4	-9.4	-9.4	
	6.1	-10.0	-10.0	-10.0	-10.0	-10.0	-10.0	-10.0	-10.0	-10.0	-10.0	-10.0	-10.0	-10.0	-10.0	-10.0	-10.0	-10.0	-10.0	-10.0	-10.0	-10.0	-10.0	-10.0		
	8.1	-10.5	-10.5	-10.5	-10.5	-10.5	-10.5	-10.5	-10.5	-10.5	-10.5	-10.5	-10.5	-10.5	-10.5	-10.5	-10.5	-10.5	-10.5	-10.5	-10.5	-10.5	-10.5	-10.5		
	10.1	-11.0	-11.0	-11.0	-11.0	-11.0	-11.0	-11.0	-11.0	-11.0	-11.0	-11.0	-11.0	-11.0	-11.0	-11.0	-11.0	-11.0	-11.0	-11.0	-11.0	-11.0	-11.0	-11.0		
	12.1	-11.5	-11.5	-11.5	-11.5	-11.5	-11.5	-11.5	-11.5	-11.5	-11.5	-11.5	-11.5	-11.5	-11.5	-11.5	-11.5	-11.5	-11.5	-11.5	-11.5	-11.5	-11.5	-11.5		

NACA

TABLE IV.- CONTINUED

(d) Concluded

		$R_0 = 0.80$													
		Angle of attack, α , degrees													
Location	Per cent chord	-0.5 0 .5 1.0 2.0 3.0 4.1 5.1 6.1 8.1 10.1 12.1 14.0													
		Leading edge	0	.59	.68	.63	.69	.60	.65	.61	.66	.61	.51	.41	.39
Upper surface	1.7	0.61	-0.04	-0.14	-0.12	-0.17	-0.13	-0.09	-1.10	-1.17	-1.31	-0.90	-0.50	-0.47	
	4.1	-1.38	-1.13	-1.20	-1.05	-1.17	-1.29	-1.03	-1.03	-1.14	-1.08	-1.78	-1.45	-1.18	
	7.0	-1.11	-1.09	-1.13	-1.05	-1.12	-1.18	-1.03	-1.03	-1.14	-1.08	-1.78	-1.45	-1.21	
	9.0	-1.28	-1.21	-1.24	-1.17	-1.23	-1.29	-1.19	-1.03	-1.14	-1.08	-1.78	-1.45	-1.38	
	12.1	-1.28	-1.21	-1.24	-1.17	-1.23	-1.29	-1.19	-1.03	-1.14	-1.08	-1.78	-1.45	-1.40	
	15.1	-1.17	-1.13	-1.17	-1.12	-1.17	-1.19	-1.03	-1.03	-1.14	-1.08	-1.78	-1.45	-1.38	
	18.6	-1.17	-1.13	-1.17	-1.12	-1.17	-1.19	-1.03	-1.03	-1.14	-1.08	-1.78	-1.45	-1.38	
	22.4	-1.28	-1.21	-1.24	-1.17	-1.23	-1.29	-1.19	-1.03	-1.14	-1.08	-1.78	-1.45	-1.38	
	26.9	-1.28	-1.21	-1.24	-1.17	-1.23	-1.29	-1.19	-1.03	-1.14	-1.08	-1.78	-1.45	-1.38	
	29.4	-1.28	-1.21	-1.24	-1.17	-1.23	-1.29	-1.19	-1.03	-1.14	-1.08	-1.78	-1.45	-1.38	
Lower surface	29.7	-1.28	-1.21	-1.24	-1.17	-1.23	-1.29	-1.19	-1.03	-1.14	-1.08	-1.78	-1.45	-1.38	
	39.1	-1.17	-1.13	-1.17	-1.12	-1.17	-1.19	-1.03	-1.03	-1.14	-1.08	-1.78	-1.45	-1.38	
	49.6	-1.17	-1.13	-1.17	-1.12	-1.17	-1.19	-1.03	-1.03	-1.14	-1.08	-1.78	-1.45	-1.38	
	59.6	-1.17	-1.13	-1.17	-1.12	-1.17	-1.19	-1.03	-1.03	-1.14	-1.08	-1.78	-1.45	-1.38	
	69.7	-1.17	-1.13	-1.17	-1.12	-1.17	-1.19	-1.03	-1.03	-1.14	-1.08	-1.78	-1.45	-1.38	
	79.5	-1.17	-1.13	-1.17	-1.12	-1.17	-1.19	-1.03	-1.03	-1.14	-1.08	-1.78	-1.45	-1.38	
Lower surface	89.3	-1.17	-1.13	-1.17	-1.12	-1.17	-1.19	-1.03	-1.03	-1.14	-1.08	-1.78	-1.45	-1.38	
	95.4	-1.17	-1.13	-1.17	-1.12	-1.17	-1.19	-1.03	-1.03	-1.14	-1.08	-1.78	-1.45	-1.38	
		$R_0 = 0.90$													
		Angle of attack, α , degrees													
Location	Per cent chord	-0.5 0 .5 1.0 2.0 3.0 4.1 5.1 6.1 8.1 10.1 12.1 14.0													
Leading edge	0	.67	.69	.68	.69	.60	.65	.60	.59	.53	.49	.36	.28	.19	
Upper surface	1.7	0.61	-0.04	-0.14	-0.12	-0.17	-0.13	-0.09	-1.10	-1.17	-1.31	-0.90	-0.50	-0.47	
	4.1	-1.38	-1.13	-1.20	-1.05	-1.17	-1.29	-1.03	-1.03	-1.14	-1.08	-1.78	-1.45	-1.21	
	7.0	-1.11	-1.09	-1.13	-1.05	-1.12	-1.18	-1.03	-1.03	-1.14	-1.08	-1.78	-1.45	-1.38	
	9.0	-1.28	-1.21	-1.24	-1.17	-1.23	-1.29	-1.19	-1.03	-1.14	-1.08	-1.78	-1.45	-1.38	
	12.1	-1.28	-1.21	-1.24	-1.17	-1.23	-1.29	-1.19	-1.03	-1.14	-1.08	-1.78	-1.45	-1.38	
	15.1	-1.28	-1.21	-1.24	-1.17	-1.23	-1.29	-1.19	-1.03	-1.14	-1.08	-1.78	-1.45	-1.38	
	18.6	-1.28	-1.21	-1.24	-1.17	-1.23	-1.29	-1.19	-1.03	-1.14	-1.08	-1.78	-1.45	-1.38	
	22.4	-1.28	-1.21	-1.24	-1.17	-1.23	-1.29	-1.19	-1.03	-1.14	-1.08	-1.78	-1.45	-1.38	
	26.9	-1.28	-1.21	-1.24	-1.17	-1.23	-1.29	-1.19	-1.03	-1.14	-1.08	-1.78	-1.45	-1.38	
	29.4	-1.28	-1.21	-1.24	-1.17	-1.23	-1.29	-1.19	-1.03	-1.14	-1.08	-1.78	-1.45	-1.38	
Lower surface	29.7	-1.28	-1.21	-1.24	-1.17	-1.23	-1.29	-1.19	-1.03	-1.14	-1.08	-1.78	-1.45	-1.38	
	39.1	-1.17	-1.13	-1.17	-1.12	-1.17	-1.19	-1.03	-1.03	-1.14	-1.08	-1.78	-1.45	-1.38	
	49.6	-1.17	-1.13	-1.17	-1.12	-1.17	-1.19	-1.03	-1.03	-1.14	-1.08	-1.78	-1.45	-1.38	
	59.6	-1.17	-1.13	-1.17	-1.12	-1.17	-1.19	-1.03	-1.03	-1.14	-1.08	-1.78	-1.45	-1.38	
	69.7	-1.17	-1.13	-1.17	-1.12	-1.17	-1.19	-1.03	-1.03	-1.14	-1.08	-1.78	-1.45	-1.38	
	79.5	-1.17	-1.13	-1.17	-1.12	-1.17	-1.19	-1.03	-1.03	-1.14	-1.08	-1.78	-1.45	-1.38	
Lower surface	89.3	-1.17	-1.13	-1.17	-1.12	-1.17	-1.19	-1.03	-1.03	-1.14	-1.08	-1.78	-1.45	-1.38	
	95.4	-1.17	-1.13	-1.17	-1.12	-1.17	-1.19	-1.03	-1.03	-1.14	-1.08	-1.78	-1.45	-1.38	
		$R_0 = 0.95$													
		Angle of attack, α , degrees													
Location	Per cent chord	-0.5 0 .5 1.0 2.0 3.0 4.1 5.1 6.1 8.1 10.1 12.1 14.0													
Leading edge	0	.63	.65	.66	.65	.63	.60	.54	.51	.41	.36	.31	.26		
Upper surface	1.7	0	-0.05	-0.18	-0.15	-0.18	-0.15	-0.09	-0.99	-1.11	-1.16	-1.03	-0.76	-0.43	
	4.1	-1.35	-1.11	-1.18	-1.05	-1.17	-1.29	-1.03	-1.03	-1.14	-1.08	-1.78	-1.45	-1.21	
	7.0	-1.15	-1.11	-1.18	-1.05	-1.17	-1.29	-1.03	-1.03	-1.14	-1.08	-1.78	-1.45	-1.38	
	9.0	-1.25	-1.21	-1.24	-1.17	-1.23	-1.29	-1.19	-1.03	-1.14	-1.08	-1.78	-1.45	-1.38	
	12.1	-1.25	-1.21	-1.24	-1.17	-1.23	-1.29	-1.19	-1.03	-1.14	-1.08	-1.78	-1.45	-1.38	
	15.1	-1.25	-1.21	-1.24	-1.17	-1.23	-1.29	-1.19	-1.03	-1.14	-1.08	-1.78	-1.45	-1.38	
	18.6	-1.25	-1.21	-1.24	-1.17	-1.23	-1.29	-1.19	-1.03	-1.14	-1.08	-1.78	-1.45	-1.38	
	22.4	-1.25	-1.21	-1.24	-1.17	-1.23	-1.29	-1.19	-1.03	-1.14	-1.08	-1.78	-1.45	-1.38	
	26.9	-1.25	-1.21	-1.24	-1.17	-1.23	-1.29	-1.19	-1.03	-1.14	-1.08	-1.78	-1.45	-1.38	
	29.4	-1.25	-1.21	-1.24	-1.17	-1.23	-1.29	-1.19	-1.03	-1.14	-1.08	-1.78	-1.45	-1.38	
Lower surface	29.7	-1.25	-1.21	-1.24	-1.17	-1.23	-1.29	-1.19	-1.03	-1.14	-1.08	-1.78	-1.45	-1.38	
	39.1	-1.25	-1.21	-1.24	-1.17	-1.23	-1.29	-1.19	-1.03	-1.14	-1.08	-1.78	-1.45	-1.38	
	49.6	-1.25	-1.21	-1.24	-1.17	-1.23	-1.29	-1.19	-1.03	-1.14	-1.08	-1.78	-1.45	-1.38	
	59.6	-1.25	-1.21	-1.24	-1.17	-1.23	-1.29	-1.19	-1.03	-1.14	-1.08	-1.78	-1.45	-1.38	
	69.7	-1.25	-1.21	-1.24	-1.17	-1.23	-1.29	-1.19	-1.03	-1.14	-1.08	-1.78	-1.45	-1.38	
	79.5	-1.25	-1.21	-1.24	-1.17	-1.23	-1.29	-1.19	-1.03	-1.14	-1.08	-1.78	-1.45	-1.38	



TABLE IV.- CONTINUED

(e) $R, 2,000,000$; $M, 0.90$

		0, 0.20										1, 0.20											
Location	Per cent chord	Angle of attack, α_1 , degrees											Angle of attack, α_1 , degrees										
		-0.5	0	0.5	1.0	2.0	3.0	4.0	5.1	6.1	10.1	12.1	-0.5	0	0.5	1.0	2.0	3.0	4.0	5.1	6.1	10.1	12.1
Leading edge	0	.79	.79	.79	.79	.79	.79	.79	.79	.79	.79	.79	.79	.79	.79	.79	.79	.79	.79	.79	.79	.79	.79
	2.7	-.12	-.12	-.12	-.12	-.12	-.12	-.12	-.12	-.12	-.12	-.12	-.12	-.12	-.12	-.12	-.12	-.12	-.12	-.12	-.12	-.12	-.12
	5.1	-.12	-.12	-.12	-.12	-.12	-.12	-.12	-.12	-.12	-.12	-.12	-.12	-.12	-.12	-.12	-.12	-.12	-.12	-.12	-.12	-.12	-.12
	7.5	-.12	-.12	-.12	-.12	-.12	-.12	-.12	-.12	-.12	-.12	-.12	-.12	-.12	-.12	-.12	-.12	-.12	-.12	-.12	-.12	-.12	-.12
	10.1	-.12	-.12	-.12	-.12	-.12	-.12	-.12	-.12	-.12	-.12	-.12	-.12	-.12	-.12	-.12	-.12	-.12	-.12	-.12	-.12	-.12	-.12
	12.1	-.12	-.12	-.12	-.12	-.12	-.12	-.12	-.12	-.12	-.12	-.12	-.12	-.12	-.12	-.12	-.12	-.12	-.12	-.12	-.12	-.12	-.12
		0, 0.40										1, 0.40											
Location	Per cent chord	Angle of attack, α_1 , degrees											Angle of attack, α_1 , degrees										
		-0.5	0	0.5	1.0	2.0	3.0	4.0	5.1	6.1	10.1	12.1	-0.5	0	0.5	1.0	2.0	3.0	4.0	5.1	6.1	10.1	12.1
Leading edge	0	.79	.79	.79	.79	.79	.79	.79	.79	.79	.79	.79	.79	.79	.79	.79	.79	.79	.79	.79	.79	.79	.79
	2.7	-.12	-.12	-.12	-.12	-.12	-.12	-.12	-.12	-.12	-.12	-.12	-.12	-.12	-.12	-.12	-.12	-.12	-.12	-.12	-.12	-.12	-.12
	5.1	-.12	-.12	-.12	-.12	-.12	-.12	-.12	-.12	-.12	-.12	-.12	-.12	-.12	-.12	-.12	-.12	-.12	-.12	-.12	-.12	-.12	-.12
	7.5	-.12	-.12	-.12	-.12	-.12	-.12	-.12	-.12	-.12	-.12	-.12	-.12	-.12	-.12	-.12	-.12	-.12	-.12	-.12	-.12	-.12	-.12
	10.1	-.12	-.12	-.12	-.12	-.12	-.12	-.12	-.12	-.12	-.12	-.12	-.12	-.12	-.12	-.12	-.12	-.12	-.12	-.12	-.12	-.12	-.12
	12.1	-.12	-.12	-.12	-.12	-.12	-.12	-.12	-.12	-.12	-.12	-.12	-.12	-.12	-.12	-.12	-.12	-.12	-.12	-.12	-.12	-.12	-.12
		0, 0.60										1, 0.60											
Location	Per cent chord	Angle of attack, α_1 , degrees											Angle of attack, α_1 , degrees										
		-0.5	0	0.5	1.0	2.0	3.0	4.0	5.1	6.1	10.1	12.1	-0.5	0	0.5	1.0	2.0	3.0	4.0	5.1	6.1	10.1	12.1
Leading edge	0	.79	.79	.79	.79	.79	.79	.79	.79	.79	.79	.79	.79	.79	.79	.79	.79	.79	.79	.79	.79	.79	.79
	2.7	-.12	-.12	-.12	-.12	-.12	-.12	-.12	-.12	-.12	-.12	-.12	-.12	-.12	-.12	-.12	-.12	-.12	-.12	-.12	-.12	-.12	-.12
	5.1	-.12	-.12	-.12	-.12	-.12	-.12	-.12	-.12	-.12	-.12	-.12	-.12	-.12	-.12	-.12	-.12	-.12	-.12	-.12	-.12	-.12	-.12
	7.5	-.12	-.12	-.12	-.12	-.12	-.12	-.12	-.12	-.12	-.12	-.12	-.12	-.12	-.12	-.12	-.12	-.12	-.12	-.12	-.12	-.12	-.12
	10.1	-.12	-.12	-.12	-.12	-.12	-.12	-.12	-.12	-.12	-.12	-.12	-.12	-.12	-.12	-.12	-.12	-.12	-.12	-.12	-.12	-.12	-.12
	12.1	-.12	-.12	-.12	-.12	-.12	-.12	-.12	-.12	-.12	-.12	-.12	-.12	-.12	-.12	-.12	-.12	-.12	-.12	-.12	-.12	-.12	-.12

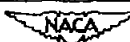
NACA

TABLE IV.—CONTINUED

(e) Concluded

Location	Reynolds number	Angle of attack, α , degrees												
		-0.5	0	0.5	1.0	1.5	2.0	2.5	3.0	4.0	5.1	6.1	10.1	18.1
Leading edge	0	.66	.67	.69	.69	.69	.69	.69	.69	.69	.69	.69	.69	.69
	1.7	.65	.65	.63	.61	.59	.56	.53	.50	.47	.44	.41	.38	.35
	7.0	.66	.66	.64	.62	.60	.57	.54	.51	.48	.45	.42	.39	.36
	19.4	.66	.66	.64	.62	.60	.57	.54	.51	.48	.45	.42	.39	.36
	39.4	.66	.66	.64	.62	.60	.57	.54	.51	.48	.45	.42	.39	.36
	59.6	.66	.66	.64	.62	.60	.57	.54	.51	.48	.45	.42	.39	.36
	89.7	.66	.66	.64	.62	.60	.57	.54	.51	.48	.45	.42	.39	.36
	99.7	.66	.66	.64	.62	.60	.57	.54	.51	.48	.45	.42	.39	.36
	94.1	.66	.66	.64	.62	.60	.57	.54	.51	.48	.45	.42	.39	.36
Upper surface	1.6	.66	.66	.64	.62	.60	.57	.54	.51	.48	.45	.42	.39	.36
	2.7	.66	.66	.64	.62	.60	.57	.54	.51	.48	.45	.42	.39	.36
	3.7	.66	.66	.64	.62	.60	.57	.54	.51	.48	.45	.42	.39	.36
	5.0	.66	.66	.64	.62	.60	.57	.54	.51	.48	.45	.42	.39	.36
	8.0	.66	.66	.64	.62	.60	.57	.54	.51	.48	.45	.42	.39	.36
	12.0	.66	.66	.64	.62	.60	.57	.54	.51	.48	.45	.42	.39	.36
	19.0	.66	.66	.64	.62	.60	.57	.54	.51	.48	.45	.42	.39	.36
	31.0	.66	.66	.64	.62	.60	.57	.54	.51	.48	.45	.42	.39	.36
	51.0	.66	.66	.64	.62	.60	.57	.54	.51	.48	.45	.42	.39	.36
	85.0	.66	.66	.64	.62	.60	.57	.54	.51	.48	.45	.42	.39	.36
Lower surface	1.6	.66	.66	.64	.62	.60	.57	.54	.51	.48	.45	.42	.39	.36
	2.7	.66	.66	.64	.62	.60	.57	.54	.51	.48	.45	.42	.39	.36
	3.7	.66	.66	.64	.62	.60	.57	.54	.51	.48	.45	.42	.39	.36
	5.0	.66	.66	.64	.62	.60	.57	.54	.51	.48	.45	.42	.39	.36
	8.0	.66	.66	.64	.62	.60	.57	.54	.51	.48	.45	.42	.39	.36
	12.0	.66	.66	.64	.62	.60	.57	.54	.51	.48	.45	.42	.39	.36
	19.0	.66	.66	.64	.62	.60	.57	.54	.51	.48	.45	.42	.39	.36
	31.0	.66	.66	.64	.62	.60	.57	.54	.51	.48	.45	.42	.39	.36
	51.0	.66	.66	.64	.62	.60	.57	.54	.51	.48	.45	.42	.39	.36
	85.0	.66	.66	.64	.62	.60	.57	.54	.51	.48	.45	.42	.39	.36

		Angle of attack, α , degrees										
Laminar flow		-0.5	0	0.5	1.0	2.0	3.0	4.0	5.1	6.1	10.1	12.1
Leading edge	Upper surface	0	.68	.69	.69	.69	.68	.67	.61	.56	.39	.34
	Upper surface	1.7	.68	.69	.69	.69	.68	.67	.61	.56	.39	.34
	Upper surface	3.0	.68	.69	.69	.69	.68	.67	.61	.56	.39	.34
	Upper surface	4.0	.68	.69	.69	.69	.68	.67	.61	.56	.39	.34
	Upper surface	5.1	.68	.69	.69	.69	.68	.67	.61	.56	.39	.34
	Upper surface	6.1	.68	.69	.69	.69	.68	.67	.61	.56	.39	.34
	Upper surface	10.1	.68	.69	.69	.69	.68	.67	.61	.56	.39	.34
	Upper surface	12.1	.68	.69	.69	.69	.68	.67	.61	.56	.39	.34
	Lower surface	0	.68	.69	.69	.69	.68	.67	.61	.56	.39	.34
	Lower surface	1.7	.68	.69	.69	.69	.68	.67	.61	.56	.39	.34
	Lower surface	3.0	.68	.69	.69	.69	.68	.67	.61	.56	.39	.34
	Lower surface	4.0	.68	.69	.69	.69	.68	.67	.61	.56	.39	.34
	Lower surface	5.1	.68	.69	.69	.69	.68	.67	.61	.56	.39	.34
	Lower surface	6.1	.68	.69	.69	.69	.68	.67	.61	.56	.39	.34
	Lower surface	10.1	.68	.69	.69	.69	.68	.67	.61	.56	.39	.34
	Lower surface	12.1	.68	.69	.69	.69	.68	.67	.61	.56	.39	.34



		Angle of attack, α , degrees										
		-0.5	0	0.5	1.0	2.0	3.0	4.0	5.1	6.1	10.1	18.1
Location forward chord		Leading edge	0	.64	.65	.66	.66	.66	.66	.66	.66	.67
Wing surface		1.8	0.01	-0.07	-0.15	-0.23	-0.31	-0.39	-0.47	-0.55	-0.63	-0.71
		1.8	-0.15	-0.29	-0.43	-0.57	-0.71	-0.85	-0.99	-1.13	-1.27	-1.41
		6.6	-0.15	-0.29	-0.43	-0.57	-0.71	-0.85	-0.99	-1.13	-1.27	-1.41
		9.3	-0.15	-0.29	-0.43	-0.57	-0.71	-0.85	-0.99	-1.13	-1.27	-1.41
		11.9	-0.15	-0.29	-0.43	-0.57	-0.71	-0.85	-0.99	-1.13	-1.27	-1.41
		19.2	-0.15	-0.29	-0.43	-0.57	-0.71	-0.85	-0.99	-1.13	-1.27	-1.41
		23.4	-0.15	-0.29	-0.43	-0.57	-0.71	-0.85	-0.99	-1.13	-1.27	-1.41
		30.0	-0.15	-0.29	-0.43	-0.57	-0.71	-0.85	-0.99	-1.13	-1.27	-1.41
		39.4	-0.15	-0.29	-0.43	-0.57	-0.71	-0.85	-0.99	-1.13	-1.27	-1.41
		49.9	-0.15	-0.29	-0.43	-0.57	-0.71	-0.85	-0.99	-1.13	-1.27	-1.41
		59.3	-0.15	-0.29	-0.43	-0.57	-0.71	-0.85	-0.99	-1.13	-1.27	-1.41
		69.7	-0.15	-0.29	-0.43	-0.57	-0.71	-0.85	-0.99	-1.13	-1.27	-1.41
		79.0	-0.15	-0.29	-0.43	-0.57	-0.71	-0.85	-0.99	-1.13	-1.27	-1.41
Lower surface		1.8	-0.15	-0.29	-0.43	-0.57	-0.71	-0.85	-0.99	-1.13	-1.27	-1.41
		1.8	-0.15	-0.29	-0.43	-0.57	-0.71	-0.85	-0.99	-1.13	-1.27	-1.41
		6.6	-0.15	-0.29	-0.43	-0.57	-0.71	-0.85	-0.99	-1.13	-1.27	-1.41
		9.6	-0.15	-0.29	-0.43	-0.57	-0.71	-0.85	-0.99	-1.13	-1.27	-1.41
		13.7	-0.15	-0.29	-0.43	-0.57	-0.71	-0.85	-0.99	-1.13	-1.27	-1.41
		18.9	-0.15	-0.29	-0.43	-0.57	-0.71	-0.85	-0.99	-1.13	-1.27	-1.41
		23.7	-0.15	-0.29	-0.43	-0.57	-0.71	-0.85	-0.99	-1.13	-1.27	-1.41
		28.9	-0.15	-0.29	-0.43	-0.57	-0.71	-0.85	-0.99	-1.13	-1.27	-1.41
		34.0	-0.15	-0.29	-0.43	-0.57	-0.71	-0.85	-0.99	-1.13	-1.27	-1.41
		39.1	-0.15	-0.29	-0.43	-0.57	-0.71	-0.85	-0.99	-1.13	-1.27	-1.41
		44.2	-0.15	-0.29	-0.43	-0.57	-0.71	-0.85	-0.99	-1.13	-1.27	-1.41
		49.3	-0.15	-0.29	-0.43	-0.57	-0.71	-0.85	-0.99	-1.13	-1.27	-1.41
		54.5	-0.15	-0.29	-0.43	-0.57	-0.71	-0.85	-0.99	-1.13	-1.27	-1.41
		59.6	-0.15	-0.29	-0.43	-0.57	-0.71	-0.85	-0.99	-1.13	-1.27	-1.41
		64.8	-0.15	-0.29	-0.43	-0.57	-0.71	-0.85	-0.99	-1.13	-1.27	-1.41
		69.9	-0.15	-0.29	-0.43	-0.57	-0.71	-0.85	-0.99	-1.13	-1.27	-1.41
		75.0	-0.15	-0.29	-0.43	-0.57	-0.71	-0.85	-0.99	-1.13	-1.27	-1.41
		80.2	-0.15	-0.29	-0.43	-0.57	-0.71	-0.85	-0.99	-1.13	-1.27	-1.41
		85.3	-0.15	-0.29	-0.43	-0.57	-0.71	-0.85	-0.99	-1.13	-1.27	-1.41
		90.5	-0.15	-0.29	-0.43	-0.57	-0.71	-0.85	-0.99	-1.13	-1.27	-1.41
		95.6	-0.15	-0.29	-0.43	-0.57	-0.71	-0.85	-0.99	-1.13	-1.27	-1.41
		100.8	-0.15	-0.29	-0.43	-0.57	-0.71	-0.85	-0.99	-1.13	-1.27	-1.41

TABLE IV.- CONTINUED

(f) R, 2,000,000; M, 0.92

Location Percent chord	$\alpha_0 = 0.10$											
	Angle of attack, α , degrees											
Leading edge	0	.10	.20	.30	.40	.50	.60	.70	.80	.90	10.1	
Upper surface	1.1	0.62	0.71	0.73	0.65	0.56	-0.23	-0.43	-0.35	-0.47	-0.76	-0.93
	2.1	0.12	-0.08	0.10	0.01	-0.09	-0.20	-0.30	-0.30	-0.43	-0.56	-0.66
	3.1	-0.51	-0.58	-0.60	-0.51	-0.50	-0.40	-0.50	-0.50	-0.50	-0.50	-0.50
	4.1	-0.06	0	-0.03	-0.01	-0.01	-0.08	-0.10	-0.10	-0.10	-0.10	-0.10
	5.1	-0.19	-0.26	-0.28	-0.19	-0.18	-0.17	-0.18	-0.18	-0.18	-0.18	-0.18
	6.1	-0.38	-0.45	-0.47	-0.38	-0.37	-0.36	-0.36	-0.36	-0.36	-0.36	-0.36
	7.1	-0.53	-0.60	-0.62	-0.53	-0.52	-0.51	-0.51	-0.51	-0.51	-0.51	-0.51
	8.1	-0.68	-0.75	-0.77	-0.68	-0.67	-0.66	-0.66	-0.66	-0.66	-0.66	-0.66
	9.1	-0.83	-0.88	-0.90	-0.83	-0.82	-0.81	-0.81	-0.81	-0.81	-0.81	-0.81
	10.1	-0.98	-1.03	-1.05	-0.98	-0.97	-0.96	-0.96	-0.96	-0.96	-0.96	-0.96
	11.1	-1.13	-1.18	-1.20	-1.13	-1.12	-1.11	-1.11	-1.11	-1.11	-1.11	-1.11
	12.1	-1.28	-1.33	-1.35	-1.28	-1.27	-1.26	-1.26	-1.26	-1.26	-1.26	-1.26
	13.1	-1.43	-1.48	-1.50	-1.43	-1.42	-1.41	-1.41	-1.41	-1.41	-1.41	-1.41
	14.1	-1.58	-1.63	-1.65	-1.58	-1.57	-1.56	-1.56	-1.56	-1.56	-1.56	-1.56
	15.1	-1.73	-1.78	-1.80	-1.73	-1.72	-1.71	-1.71	-1.71	-1.71	-1.71	-1.71
	16.1	-1.88	-1.93	-1.95	-1.88	-1.87	-1.86	-1.86	-1.86	-1.86	-1.86	-1.86
	17.1	-2.03	-2.08	-2.10	-2.03	-2.02	-2.01	-2.01	-2.01	-2.01	-2.01	-2.01
	18.1	-2.18	-2.23	-2.25	-2.18	-2.17	-2.16	-2.16	-2.16	-2.16	-2.16	-2.16
	19.1	-2.33	-2.38	-2.40	-2.33	-2.32	-2.31	-2.31	-2.31	-2.31	-2.31	-2.31
	20.1	-2.48	-2.53	-2.55	-2.48	-2.47	-2.46	-2.46	-2.46	-2.46	-2.46	-2.46
	21.1	-2.63	-2.68	-2.70	-2.63	-2.62	-2.61	-2.61	-2.61	-2.61	-2.61	-2.61
	22.1	-2.78	-2.83	-2.85	-2.78	-2.77	-2.76	-2.76	-2.76	-2.76	-2.76	-2.76
	23.1	-2.93	-2.98	-3.00	-2.93	-2.92	-2.91	-2.91	-2.91	-2.91	-2.91	-2.91
	24.1	-3.08	-3.13	-3.15	-3.08	-3.07	-3.06	-3.06	-3.06	-3.06	-3.06	-3.06
	25.1	-3.23	-3.28	-3.30	-3.23	-3.22	-3.21	-3.21	-3.21	-3.21	-3.21	-3.21
	26.1	-3.38	-3.43	-3.45	-3.38	-3.37	-3.36	-3.36	-3.36	-3.36	-3.36	-3.36
	27.1	-3.53	-3.58	-3.60	-3.53	-3.52	-3.51	-3.51	-3.51	-3.51	-3.51	-3.51
	28.1	-3.68	-3.73	-3.75	-3.68	-3.67	-3.66	-3.66	-3.66	-3.66	-3.66	-3.66
	29.1	-3.83	-3.88	-3.90	-3.83	-3.82	-3.81	-3.81	-3.81	-3.81	-3.81	-3.81
	30.1	-3.98	-4.03	-4.05	-3.98	-3.97	-3.96	-3.96	-3.96	-3.96	-3.96	-3.96
	31.1	-4.13	-4.18	-4.20	-4.13	-4.12	-4.11	-4.11	-4.11	-4.11	-4.11	-4.11
	32.1	-4.28	-4.33	-4.35	-4.28	-4.27	-4.26	-4.26	-4.26	-4.26	-4.26	-4.26
	33.1	-4.43	-4.48	-4.50	-4.43	-4.42	-4.41	-4.41	-4.41	-4.41	-4.41	-4.41
	34.1	-4.58	-4.63	-4.65	-4.58	-4.57	-4.56	-4.56	-4.56	-4.56	-4.56	-4.56
	35.1	-4.73	-4.78	-4.80	-4.73	-4.72	-4.71	-4.71	-4.71	-4.71	-4.71	-4.71
	36.1	-4.88	-4.93	-4.95	-4.88	-4.87	-4.86	-4.86	-4.86	-4.86	-4.86	-4.86
	37.1	-5.03	-5.08	-5.10	-5.03	-5.02	-5.01	-5.01	-5.01	-5.01	-5.01	-5.01
	38.1	-5.18	-5.23	-5.25	-5.18	-5.17	-5.16	-5.16	-5.16	-5.16	-5.16	-5.16
	39.1	-5.33	-5.38	-5.40	-5.33	-5.32	-5.31	-5.31	-5.31	-5.31	-5.31	-5.31
	40.1	-5.48	-5.53	-5.55	-5.48	-5.47	-5.46	-5.46	-5.46	-5.46	-5.46	-5.46
	41.1	-5.63	-5.68	-5.70	-5.63	-5.62	-5.61	-5.61	-5.61	-5.61	-5.61	-5.61
	42.1	-5.78	-5.83	-5.85	-5.78	-5.77	-5.76	-5.76	-5.76	-5.76	-5.76	-5.76
	43.1	-5.93	-5.98	-6.00	-5.93	-5.92	-5.91	-5.91	-5.91	-5.91	-5.91	-5.91
	44.1	-6.08	-6.13	-6.15	-6.08	-6.07	-6.06	-6.06	-6.06	-6.06	-6.06	-6.06
	45.1	-6.23	-6.28	-6.30	-6.23	-6.22	-6.21	-6.21	-6.21	-6.21	-6.21	-6.21
	46.1	-6.38	-6.43	-6.45	-6.38	-6.37	-6.36	-6.36	-6.36	-6.36	-6.36	-6.36
	47.1	-6.53	-6.58	-6.60	-6.53	-6.52	-6.51	-6.51	-6.51	-6.51	-6.51	-6.51
	48.1	-6.68	-6.73	-6.75	-6.68	-6.67	-6.66	-6.66	-6.66	-6.66	-6.66	-6.66
	49.1	-6.83	-6.88	-6.90	-6.83	-6.82	-6.81	-6.81	-6.81	-6.81	-6.81	-6.81
	50.1	-6.98	-7.03	-7.05	-6.98	-6.97	-6.96	-6.96	-6.96	-6.96	-6.96	-6.96
	51.1	-7.13	-7.18	-7.20	-7.13	-7.12	-7.11	-7.11	-7.11	-7.11	-7.11	-7.11
	52.1	-7.28	-7.33	-7.35	-7.28	-7.27	-7.26	-7.26	-7.26	-7.26	-7.26	-7.26
	53.1	-7.43	-7.48	-7.50	-7.43	-7.42	-7.41	-7.41	-7.41	-7.41	-7.41	-7.41
	54.1	-7.58	-7.63	-7.65	-7.58	-7.57	-7.56	-7.56	-7.56	-7.56	-7.56	-7.56
	55.1	-7.73	-7.78	-7.80	-7.73	-7.72	-7.71	-7.71	-7.71	-7.71	-7.71	-7.71
	56.1	-7.88	-7.93	-7.95	-7.88	-7.87	-7.86	-7.86	-7.86	-7.86	-7.86	-7.86
	57.1	-8.03	-8.08	-8.10	-8.03	-8.02	-8.01	-8.01	-8.01	-8.01	-8.01	-8.01
	58.1	-8.18	-8.23	-8.25	-8.18	-8.17	-8.16	-8.16	-8.16	-8.16	-8.16	-8.16
	59.1	-8.33	-8.38	-8.40	-8.33	-8.32	-8.31	-8.31	-8.31	-8.31	-8.31	-8.31
	60.1	-8.48	-8.53	-8.55	-8.48	-8.47	-8.46	-8.46	-8.46	-8.46	-8.46	-8.46
	61.1	-8.63	-8.68	-8.70	-8.63	-8.62	-8.61	-8.61	-8.61	-8.61	-8.61	-8.61
	62.1	-8.78	-8.83	-8.85	-8.78	-8.77	-8.76	-8.76	-8.76	-8.76	-8.76	-8.76
	63.1	-8.93	-8.98	-9.00	-8.93	-8.92	-8.91	-8.91	-8.91	-8.91	-8.91	-8.91
	64.1	-9.08	-9.13	-9.15	-9.08	-9.07	-9.06	-9.06	-9.06	-9.06	-9.06	-9.06
	65.1	-9.23	-9.28	-9.30	-9.23	-9.22	-9.21	-9.21	-9.21	-9.21	-9.21	-9.21
	66.1	-9.38	-9.43	-9.45	-9.38	-9.37	-9.36	-9.36	-9.36	-9.36	-9.36	-9.36
	67.1	-9.53	-9.58	-9.60	-9.53	-9.52	-9.51	-9.51	-9.51	-9.51	-9.51	-9.51
	68.1	-9.68	-9.73	-9.75	-9.68	-9.67	-9.66	-9.66	-9.66	-9.66	-9.66	-9.66
	69.1	-9.83	-9.88	-9.90	-9.83	-9.82	-9.81	-9.81	-9.81	-9.81	-9.81	-9.81
	70.1	-9.98	-10.03	-10.05	-9.98	-9.97	-9.96	-9.96	-9.96	-9.96	-9.96	-9.96
	71.1	-10.13	-10.18	-10.20	-10.13	-10.12	-10.11	-10.11	-10.11	-10.11	-10.11	-10.11
	72.1	-10.28	-10.33	-10.35	-10.28	-10.27	-10.26	-10.26	-10.26	-10.26	-10.26	-10.26
	73.1	-10.43	-10.48	-10.50	-10.43	-10.42	-10.41	-10.41	-10.41	-10.41	-10.41	-10.41
	74.1	-10.58	-10.63	-10.65	-10.58	-10.57	-10.56	-10.56	-10.56	-10.56	-10.56	-10.56
	75.1	-10.73	-10.78	-10.80	-10.73	-10.72	-10.71	-10.71	-10.71	-10.71	-10.71	-10.71
	76.1	-10.88	-10.93	-10.95	-10.88	-10.87	-10.86	-10.86	-10.86	-10.86	-10.86	-10.86
	77.1	-11.03	-11.08	-11.10	-11.03	-11.02	-11.01	-11.01	-11.01	-11.01	-11.01	-11.01
	78.1	-11.18	-11.23	-11.25	-11.18	-11.17	-11.16	-11.16	-11.16	-11.16	-11.16	-11.16
	79.1	-11.33	-11.38	-11.40	-11.33	-11.32	-11.31	-11.31	-11.31	-11.31	-11.31	-11.31
	80.1	-11.48	-11.53	-11.55	-11.48	-11.47	-11.46	-11.46	-11.46	-11.46	-11.46	-11.46
	81.1	-11.63	-11.68	-11.70	-11.63	-11.62	-11.61	-11.61	-11.61	-11.61	-11.61	-11.61
	82.1	-11.78	-11.83	-11.85	-11.78	-11.77	-11.76	-11.76	-11.76	-11.76	-11.76	-11.76
	83.1	-11.93	-11.98	-12.00	-11.93	-11.92	-11.91	-11.91	-11.91	-11.91	-11.91	-11.91
	84.1	-12.08	-12.13	-12.15	-12.08	-12.07	-12.06	-12.06	-12.06	-12.06	-12.06	-12.06
	85.1	-12.23	-12.28	-12.30	-12.23	-12.22	-12.21	-12.21	-12.21	-12.21	-12.21	-12.21
	86.1	-12.38	-12.43	-12.45	-12.38	-12.37	-12.36	-12.36	-12.36	-12.36	-12.36	-12.36
	87.1	-12.53	-12.58	-12.60	-12.53	-12.52	-12.51	-12.51	-12.51	-12.51	-12.51	-12.51
	88.1	-12.68	-12.73	-12.75	-12.68							

TABLE IV.- CONTINUED

(f) Concluded

		$\eta_2 = 0.80$										
		Angle of attack, α , degrees										
		-0.5	0	0.5	1.0	2.0	3.0	4.0	5.0	6.1	8.1	10.1
Leading edge	0	.66	.68	.69	.69	.69	.67	.68	.61	.57	.48	.39
Upper surface	1.7	-0.06	-0.05	-0.10	-0.17	-0.34	-0.53	-0.76	-0.89	-0.97	-1.11	-1.19
	4.1	-0.15	-0.18	-0.17	-0.28	-0.34	-0.47	-0.69	-0.81	-0.91	-1.05	-1.17
	7.0	-0.11	-0.19	-0.24	-0.37	-0.47	-0.67	-0.86	-0.96	-1.05	-1.15	-1.25
	9.0	-0.15	-0.18	-0.26	-0.38	-0.47	-0.70	-0.88	-0.96	-1.05	-1.15	-1.25
	15.7	-0.02	-0.05	-0.12	-0.21	-0.32	-0.47	-0.67	-0.81	-0.91	-1.05	-1.15
	19.1	-0.02	-0.05	-0.12	-0.21	-0.32	-0.47	-0.67	-0.81	-0.91	-1.05	-1.15
	29.6	-0.02	-0.05	-0.12	-0.21	-0.32	-0.47	-0.67	-0.81	-0.91	-1.05	-1.15
	39.4	-0.02	-0.05	-0.12	-0.21	-0.32	-0.47	-0.67	-0.81	-0.91	-1.05	-1.15
	49.6	-0.02	-0.05	-0.12	-0.21	-0.32	-0.47	-0.67	-0.81	-0.91	-1.05	-1.15
	69.7	-0.02	-0.05	-0.12	-0.21	-0.32	-0.47	-0.67	-0.81	-0.91	-1.05	-1.15
Lower surface	79.1	-0.02	-0.05	-0.12	-0.21	-0.32	-0.47	-0.67	-0.81	-0.91	-1.05	-1.15
	89.8	-0.02	-0.05	-0.12	-0.21	-0.32	-0.47	-0.67	-0.81	-0.91	-1.05	-1.15
	94.4	-0.02	-0.05	-0.12	-0.21	-0.32	-0.47	-0.67	-0.81	-0.91	-1.05	-1.15
Lower surface	1.6	-0.02	-0.05	-0.12	-0.21	-0.32	-0.47	-0.67	-0.81	-0.91	-1.05	-1.15
	4.3	-0.02	-0.05	-0.12	-0.21	-0.32	-0.47	-0.67	-0.81	-0.91	-1.05	-1.15
	7.9	-0.02	-0.05	-0.12	-0.21	-0.32	-0.47	-0.67	-0.81	-0.91	-1.05	-1.15
	11.8	-0.02	-0.05	-0.12	-0.21	-0.32	-0.47	-0.67	-0.81	-0.91	-1.05	-1.15
	20.0	-0.02	-0.05	-0.12	-0.21	-0.32	-0.47	-0.67	-0.81	-0.91	-1.05	-1.15
	30.3	-0.02	-0.05	-0.12	-0.21	-0.32	-0.47	-0.67	-0.81	-0.91	-1.05	-1.15
	39.5	-0.02	-0.05	-0.12	-0.21	-0.32	-0.47	-0.67	-0.81	-0.91	-1.05	-1.15
	49.2	-0.02	-0.05	-0.12	-0.21	-0.32	-0.47	-0.67	-0.81	-0.91	-1.05	-1.15
	59.3	-0.02	-0.05	-0.12	-0.21	-0.32	-0.47	-0.67	-0.81	-0.91	-1.05	-1.15
	69.0	-0.02	-0.05	-0.12	-0.21	-0.32	-0.47	-0.67	-0.81	-0.91	-1.05	-1.15
Lower surface	79.8	-0.02	-0.05	-0.12	-0.21	-0.32	-0.47	-0.67	-0.81	-0.91	-1.05	-1.15
	89.0	-0.02	-0.05	-0.12	-0.21	-0.32	-0.47	-0.67	-0.81	-0.91	-1.05	-1.15
	94.4	-0.02	-0.05	-0.12	-0.21	-0.32	-0.47	-0.67	-0.81	-0.91	-1.05	-1.15
		$\eta_2 = 0.75$										
		Angle of attack, α , degrees										
		-0.5	0	0.5	1.0	2.0	3.0	4.0	5.0	6.1	8.1	10.1
Leading edge	0	.64	.66	.67	.67	.67	.66	.63	.60	.56	.48	.39
Upper surface	1.8	-0.09	-0.06	-0.23	-0.42	-0.63	-0.76	-0.93	-0.97	-1.05	-1.11	-1.26
	4.1	-0.11	-0.15	-0.20	-0.30	-0.43	-0.53	-0.69	-0.86	-0.96	-1.10	-1.19
	6.5	-0.13	-0.18	-0.24	-0.34	-0.47	-0.57	-0.73	-0.89	-0.99	-1.03	-1.13
	9.0	-0.13	-0.18	-0.24	-0.34	-0.47	-0.57	-0.73	-0.89	-0.99	-1.03	-1.13
	14.7	-0.09	-0.12	-0.19	-0.29	-0.42	-0.52	-0.68	-0.84	-0.94	-1.00	-1.09
	19.1	-0.09	-0.12	-0.19	-0.29	-0.42	-0.52	-0.68	-0.84	-0.94	-1.00	-1.09
	29.6	-0.09	-0.12	-0.19	-0.29	-0.42	-0.52	-0.68	-0.84	-0.94	-1.00	-1.09
	39.4	-0.09	-0.12	-0.19	-0.29	-0.42	-0.52	-0.68	-0.84	-0.94	-1.00	-1.09
	49.6	-0.09	-0.12	-0.19	-0.29	-0.42	-0.52	-0.68	-0.84	-0.94	-1.00	-1.09
	69.7	-0.09	-0.12	-0.19	-0.29	-0.42	-0.52	-0.68	-0.84	-0.94	-1.00	-1.09
Lower surface	79.1	-0.09	-0.12	-0.19	-0.29	-0.42	-0.52	-0.68	-0.84	-0.94	-1.00	-1.09
	89.8	-0.09	-0.12	-0.19	-0.29	-0.42	-0.52	-0.68	-0.84	-0.94	-1.00	-1.09
	94.4	-0.09	-0.12	-0.19	-0.29	-0.42	-0.52	-0.68	-0.84	-0.94	-1.00	-1.09

NACA

TABLE IV.- CONTINUED

(g) $R, 2,000,000$; $M, 0.94$

Position Percent chord		$\alpha, 0.10$										$\alpha, 0.20$									
		Angle of attack, α , degrees										Angle of attack, α , degrees									
Leading edge	0	0.5	1.0	2.0	3.0	4.0	5.0	6.1	8.1	10.1	0	0.5	1.0	2.0	3.0	4.0	5.0	6.1	8.1	10.1	
Upper surface	0	.81	.83	.86	.89	.91	.90	.79	.76	.78	0	.71	.75	.77	.75	.70	.65	.61	.51	.41	.31
	.13	.19	.23	.26	.29	.32	.35	.32	.29	.26	.0	.03	.05	.07	.09	.06	.03	.01	.01	.01	.01
	.25	.39	.43	.46	.49	.52	.55	.52	.49	.46	.0	.08	.11	.14	.17	.14	.11	.08	.05	.03	.02
	.37	.59	.63	.66	.69	.72	.75	.72	.69	.66	.0	.18	.21	.24	.27	.24	.21	.18	.15	.12	.10
	.49	.79	.83	.86	.89	.92	.95	.92	.89	.86	.0	.38	.41	.44	.47	.44	.41	.38	.35	.32	.30
	.61	.98	.102	.105	.108	.111	.114	.111	.108	.105	.0	.58	.61	.64	.67	.64	.61	.58	.55	.52	.50
	.73	.122	.126	.129	.132	.135	.138	.135	.132	.129	.0	.78	.81	.84	.87	.84	.81	.78	.75	.72	.70
	.85	.142	.146	.149	.152	.155	.158	.155	.152	.149	.0	.98	.101	.104	.107	.104	.101	.98	.95	.92	.90
	.97	.162	.166	.169	.172	.175	.178	.175	.172	.169	.0	.118	.121	.124	.127	.124	.121	.118	.115	.112	.110
	1.0	.182	.186	.189	.192	.195	.198	.195	.192	.189	.0	.138	.141	.144	.147	.144	.141	.138	.135	.132	.130
Lower surface	0	.9	.11	.13	.15	.17	.19	.17	.15	.13	.0	.37	.40	.43	.46	.43	.40	.37	.34	.31	.28
	.12	.15	.17	.19	.21	.23	.25	.23	.21	.19	.0	.57	.60	.63	.66	.63	.60	.57	.54	.51	.48
	.24	.25	.27	.29	.31	.33	.35	.33	.31	.29	.0	.77	.80	.83	.86	.83	.80	.77	.74	.71	.68
	.36	.35	.37	.39	.41	.43	.45	.43	.41	.39	.0	.97	.100	.103	.106	.103	.100	.97	.94	.91	.88
	.48	.47	.49	.51	.53	.55	.57	.55	.53	.51	.0	.118	.121	.124	.127	.124	.121	.118	.115	.112	.110
	.60	.49	.51	.53	.55	.57	.59	.57	.55	.53	.0	.77	.80	.83	.86	.83	.80	.77	.74	.71	.68
Lower surface	0	.9	.11	.13	.15	.17	.19	.17	.15	.13	.0	.37	.40	.43	.46	.43	.40	.37	.34	.31	.28
	.12	.15	.17	.19	.21	.23	.25	.23	.21	.19	.0	.57	.60	.63	.66	.63	.60	.57	.54	.51	.48
	.24	.25	.27	.29	.31	.33	.35	.33	.31	.29	.0	.77	.80	.83	.86	.83	.80	.77	.74	.71	.68
	.36	.35	.37	.39	.41	.43	.45	.43	.41	.39	.0	.97	.100	.103	.106	.103	.100	.97	.94	.91	.88
	.48	.47	.49	.51	.53	.55	.57	.55	.53	.51	.0	.118	.121	.124	.127	.124	.121	.118	.115	.112	.110

NACA

TABLE IV.- CONCLUDED

(g) Concluded

		$\mu = 0.80$										
		Angle of attack, α , degrees										
Position chord		-0.5	0	0.5	1.0	2.0	3.0	4.0	5.0	6.1	8.1	10.1
Landing edge	0	.45	.45	.50	.49	.49	.50	.50	.51	.51	.51	.51
Upper surface	1.7	0.63	-0.03	-0.09	-0.13	-0.21	-0.49	-0.68	-0.83	-0.98	-1.03	-1.15
	1.9	0.62	-0.02	-0.08	-0.13	-0.21	-0.48	-0.67	-0.82	-0.97	-1.02	-1.14
	2.1	0.61	-0.01	-0.07	-0.12	-0.20	-0.47	-0.66	-0.81	-0.96	-1.01	-1.13
	2.3	0.60	0.00	-0.06	-0.11	-0.19	-0.46	-0.65	-0.80	-0.95	-1.00	-1.12
	2.5	0.59	0.01	-0.05	-0.10	-0.18	-0.45	-0.64	-0.79	-0.94	-0.99	-1.11
	2.7	0.58	0.02	-0.04	-0.09	-0.17	-0.44	-0.63	-0.78	-0.93	-0.98	-1.09
	2.9	0.57	0.03	-0.03	-0.08	-0.16	-0.43	-0.62	-0.77	-0.92	-0.97	-1.08
	3.1	0.56	0.04	-0.02	-0.07	-0.15	-0.42	-0.61	-0.76	-0.91	-0.96	-1.07
	3.3	0.55	0.05	-0.01	-0.06	-0.14	-0.41	-0.60	-0.75	-0.90	-0.95	-1.06
	3.5	0.54	0.06	0.00	-0.05	-0.13	-0.40	-0.59	-0.74	-0.89	-0.94	-1.05
Lower surface	3.7	0.53	0.07	0.01	-0.04	-0.12	-0.39	-0.58	-0.73	-0.88	-0.93	-1.04
	3.9	0.52	0.08	0.02	-0.03	-0.11	-0.38	-0.57	-0.72	-0.87	-0.92	-1.03
	4.1	0.51	0.09	0.03	-0.02	-0.10	-0.37	-0.56	-0.71	-0.86	-0.91	-1.02
	4.3	0.50	0.10	0.04	-0.01	-0.09	-0.36	-0.55	-0.70	-0.85	-0.90	-1.01
	4.5	0.49	0.11	0.05	0.00	-0.08	-0.35	-0.54	-0.69	-0.84	-0.89	-0.99
	4.7	0.48	0.12	0.06	0.01	-0.07	-0.34	-0.53	-0.68	-0.83	-0.88	-0.98
	4.9	0.47	0.13	0.07	0.02	-0.06	-0.33	-0.52	-0.67	-0.82	-0.87	-0.97
	5.1	0.46	0.14	0.08	0.03	-0.05	-0.32	-0.51	-0.66	-0.81	-0.86	-0.96
	5.3	0.45	0.15	0.09	0.04	-0.04	-0.31	-0.50	-0.65	-0.80	-0.85	-0.95
	5.5	0.44	0.16	0.10	0.05	-0.03	-0.30	-0.49	-0.64	-0.79	-0.84	-0.94

		$\mu = 0.90$										
		Angle of attack, α , degrees										
Position chord		-0.5	0	0.5	1.0	2.0	3.0	4.0	5.0	6.1	8.1	10.1
Landing edge	0	.85	.85	.85	.85	.85	.85	.85	.85	.85	.85	.85
Upper surface	1.7	0.86	-0.01	-0.07	-0.13	-0.21	-0.49	-0.68	-0.83	-0.98	-1.03	-1.15
	1.9	0.85	-0.02	-0.08	-0.14	-0.22	-0.50	-0.69	-0.84	-0.99	-1.04	-1.16
	2.1	0.84	-0.03	-0.09	-0.15	-0.23	-0.51	-0.70	-0.85	-1.00	-1.05	-1.17
	2.3	0.83	-0.04	-0.10	-0.16	-0.24	-0.52	-0.71	-0.86	-1.01	-1.06	-1.18
	2.5	0.82	-0.05	-0.11	-0.17	-0.25	-0.53	-0.72	-0.87	-1.02	-1.07	-1.19
	2.7	0.81	-0.06	-0.12	-0.18	-0.26	-0.54	-0.73	-0.88	-1.03	-1.08	-1.20
	2.9	0.80	-0.07	-0.13	-0.19	-0.27	-0.55	-0.74	-0.89	-1.04	-1.09	-1.21
	3.1	0.79	-0.08	-0.14	-0.20	-0.28	-0.56	-0.75	-0.90	-1.05	-1.10	-1.22
	3.3	0.78	-0.09	-0.15	-0.21	-0.29	-0.57	-0.76	-0.91	-1.06	-1.11	-1.23
	3.5	0.77	-0.10	-0.16	-0.22	-0.30	-0.58	-0.77	-0.92	-1.07	-1.12	-1.24
Lower surface	3.7	0.76	-0.11	-0.17	-0.23	-0.31	-0.59	-0.78	-0.93	-1.08	-1.13	-1.25
	3.9	0.75	-0.12	-0.18	-0.24	-0.32	-0.60	-0.79	-0.94	-1.09	-1.14	-1.26
	4.1	0.74	-0.13	-0.19	-0.25	-0.33	-0.61	-0.80	-0.95	-1.10	-1.15	-1.27
	4.3	0.73	-0.14	-0.20	-0.26	-0.34	-0.62	-0.81	-0.96	-1.11	-1.16	-1.28
	4.5	0.72	-0.15	-0.21	-0.27	-0.35	-0.63	-0.82	-0.97	-1.12	-1.17	-1.29
	4.7	0.71	-0.16	-0.22	-0.28	-0.36	-0.64	-0.83	-0.98	-1.13	-1.18	-1.30
	4.9	0.70	-0.17	-0.23	-0.29	-0.37	-0.65	-0.84	-0.99	-1.14	-1.19	-1.31
	5.1	0.69	-0.18	-0.24	-0.30	-0.38	-0.66	-0.85	-1.00	-1.15	-1.20	-1.32
	5.3	0.68	-0.19	-0.25	-0.31	-0.39	-0.67	-0.86	-1.01	-1.16	-1.21	-1.33
	5.5	0.67	-0.20	-0.26	-0.32	-0.40	-0.68	-0.87	-1.02	-1.17	-1.22	-1.34

		$\mu = 0.95$										
		Angle of attack, α , degrees										
Position chord		-0.5	0	0.5	1.0	2.0	3.0	4.0	5.0	6.1	8.1	10.1
Landing edge	0	.85	.85	.85	.85	.85	.85	.85	.85	.85	.85	.85
Upper surface	1.5	0.86	-0.11	-0.21	-0.31	-0.41	-0.51	-0.61	-0.71	-0.81	-0.91	-1.01
	1.6	0.85	-0.12	-0.22	-0.32	-0.42	-0.52	-0.62	-0.72	-0.82	-0.92	-1.02
	1.8	0.84	-0.13	-0.23	-0.33	-0.43	-0.53	-0.63	-0.73	-0.83	-0.93	-1.03
	2.0	0.83	-0.14	-0.24	-0.34	-0.44	-0.54	-0.64	-0.74	-0.84	-0.94	-1.04
	2.2	0.82	-0.15	-0.25	-0.35	-0.45	-0.55	-0.65	-0.75	-0.85	-0.95	-1.05
	2.4	0.81	-0.16	-0.26	-0.36	-0.46	-0.56	-0.66	-0.76	-0.86	-0.96	-1.06
	2.6	0.80	-0.17	-0.27	-0.37	-0.47	-0.57	-0.67	-0.77	-0.87	-0.97	-1.07
	2.8	0.79	-0.18	-0.28	-0.38	-0.48	-0.58	-0.68	-0.78	-0.88	-0.98	-1.08
	3.0	0.78	-0.19	-0.29	-0.39	-0.49	-0.59	-0.69	-0.79	-0.89	-0.99	-1.09
	3.2	0.77	-0.20	-0.30	-0.40	-0.50	-0.60	-0.70	-0.80	-0.90	-1.00	-1.10
Lower surface	3.4	0.76	-0.21	-0.31	-0.41	-0.51	-0.61	-0.71	-0.81	-0.91	-1.01	-1.11
	3.6	0.75	-0.22	-0.32	-0.42	-0.52	-0.62	-0.72	-0.82	-0.92	-1.02	-1.12
	3.8	0.74	-0.23	-0.33	-0.43	-0.53	-0.63	-0.73	-0.83	-0.93	-1.03	-1.13
	4.0	0.73	-0.24	-0.34	-0.44	-0.54	-0.64	-0.74	-0.84	-0.94	-1.04	-1.14
	4.2	0.72	-0.25	-0.35	-0.45	-0.55	-0.65	-0.75	-0.85	-0.95	-1.05	-1.15
	4.4	0.71	-0.26	-0.36	-0.46	-0.56	-0.66	-0.76	-0.86	-0.96	-1.06	-1.16
	4.6	0.70	-0.27	-0.37	-0.47	-0.57	-0.67	-0.77	-0.87	-0.97	-1.07	-1.17
	4.8	0.69	-0.28	-0.38	-0.48	-0.58	-0.68	-0.78	-0.88	-0.98	-1.08	-1.18
	5.0	0.68	-0.29	-0.39	-0.49	-0.59	-0.69	-0.79	-0.89	-0.99	-1.09	-1.19
	5.2	0.67	-0.30	-0.40	-0.50	-0.60	-0.70	-0.80	-0.90	-1.00	-1.10	-1.20

NACA



Aspect ratio 5.14

Taper ratio 0.713

Area 3.389 ft²

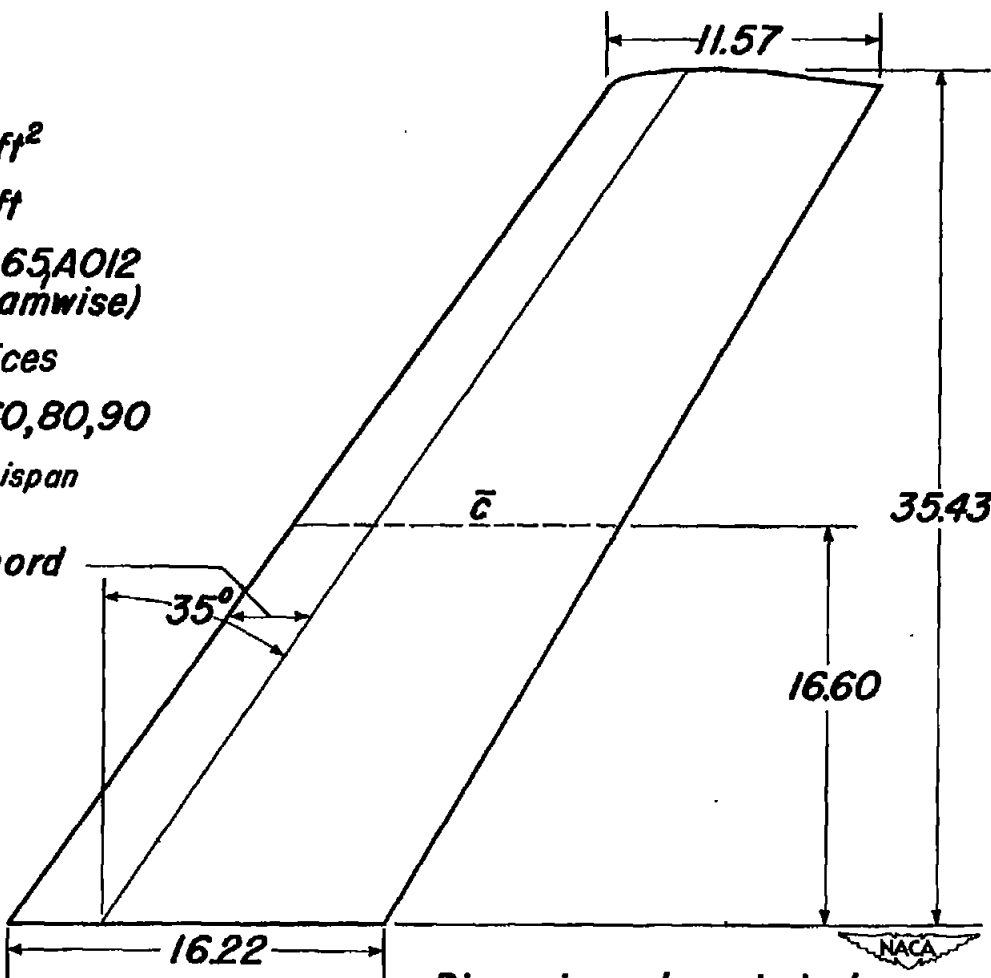
\bar{c} 1.166 ft

Section NACA 65A012
(streamwise)

Streamwise rows of orifices
located at 10, 20, 40, 60, 80, 90
and 95 percent of semispan

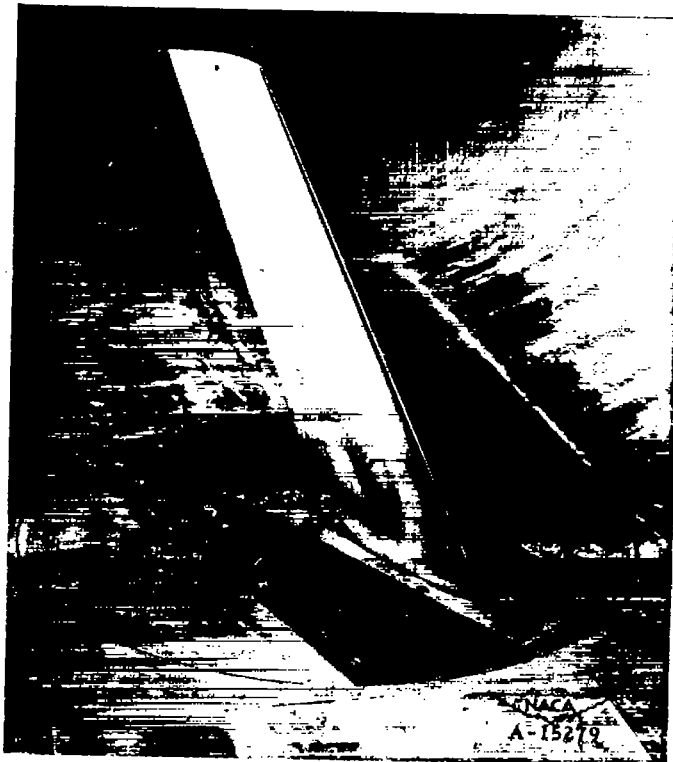
0.25-chord

35°

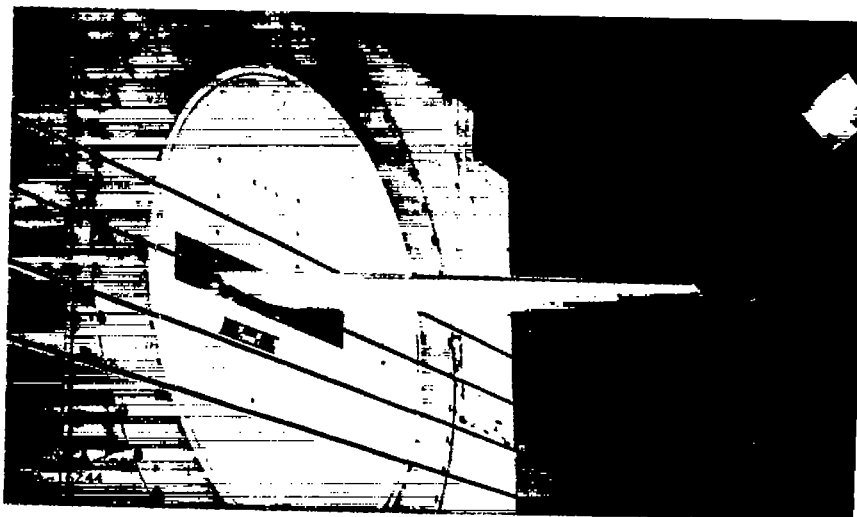


Dimensions shown in inches
unless otherwise noted

Figure 1.— Geometry of the model.



(a) Ames 12-foot pressure wind tunnel.



(b) Ames 16-foot high-speed wind tunnel.

Figure 2.— Photographs of the semispan model wing mounted in the Ames wind tunnels.

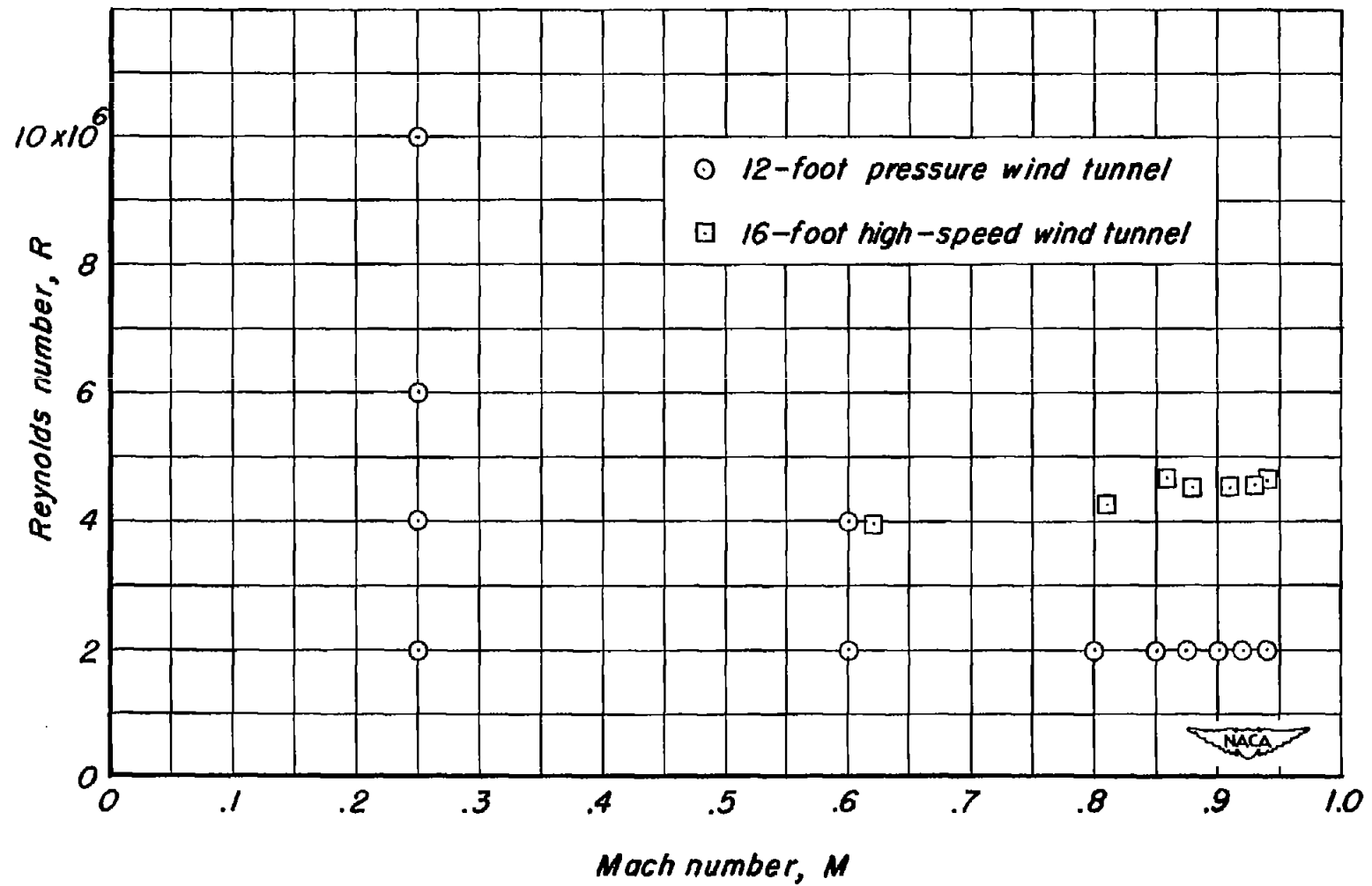
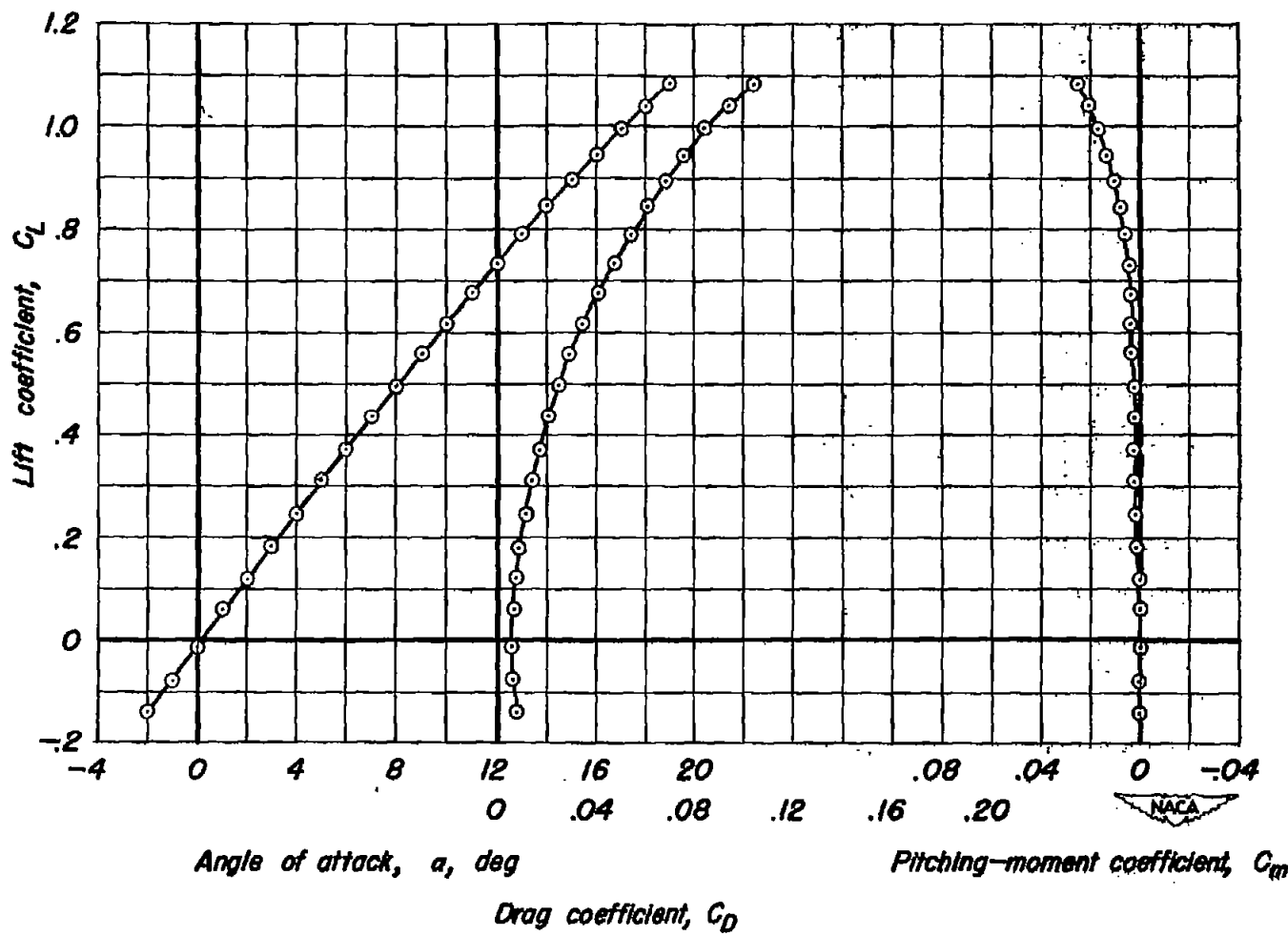
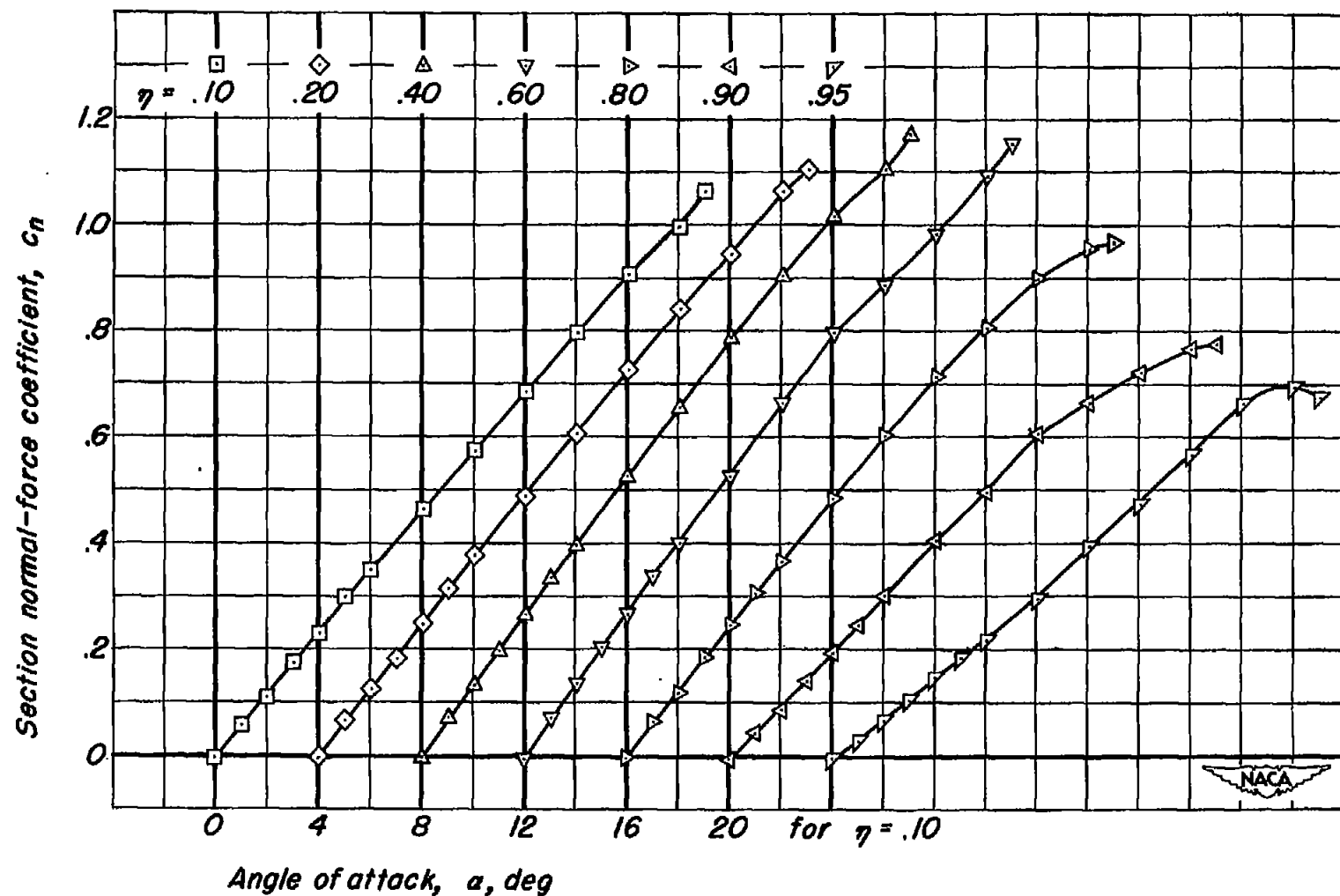


Figure 3.- The Reynolds numbers and Mach numbers of the tests.



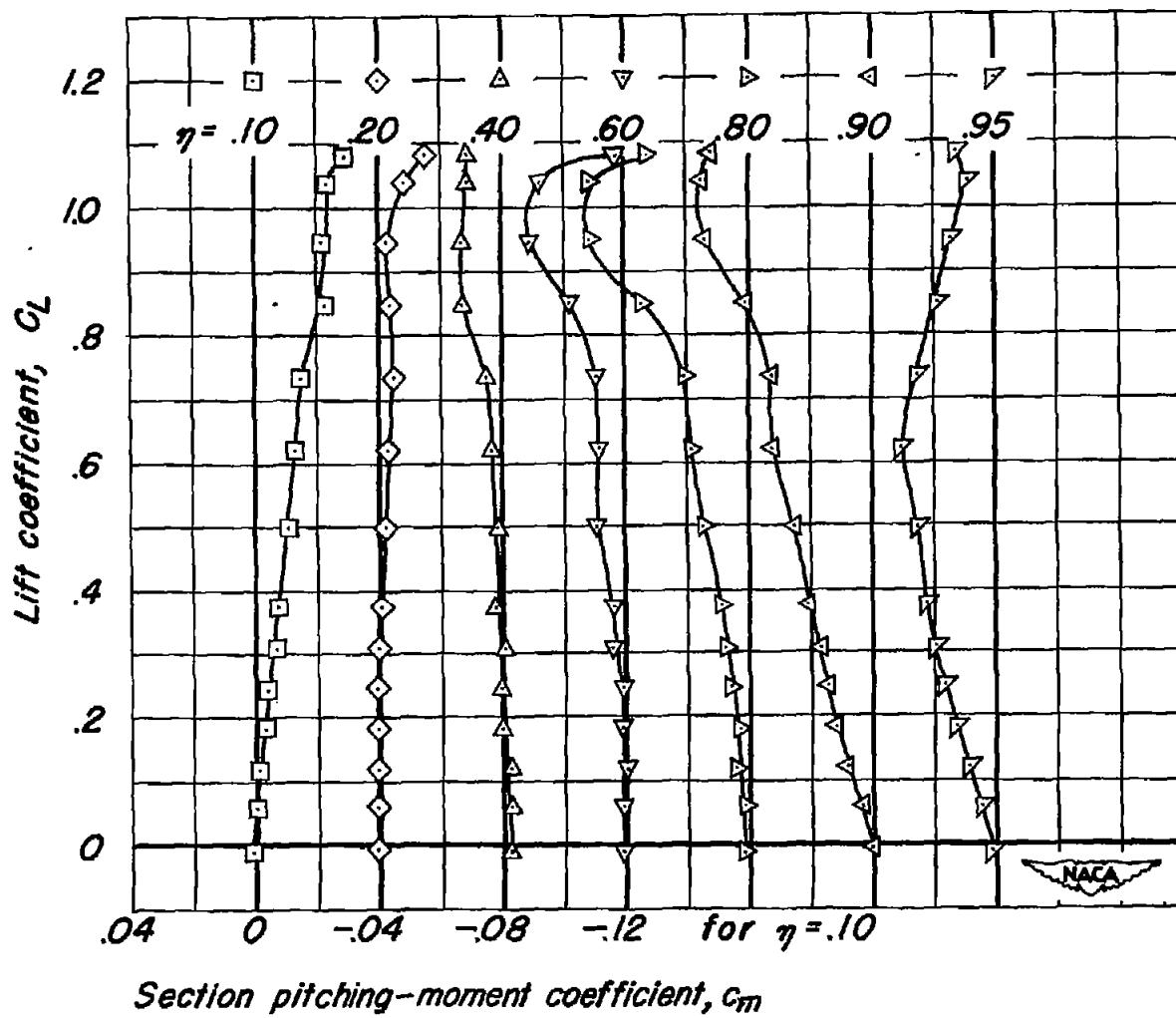
(a) Lift, drag, and pitching-moment characteristics.

Figure 4.- The lift, drag, and pitching-moment characteristics and the corresponding section normal-force and pitching-moment characteristics for seven sections of the wing. $R, 10,000,000$; $M, 0.25$.



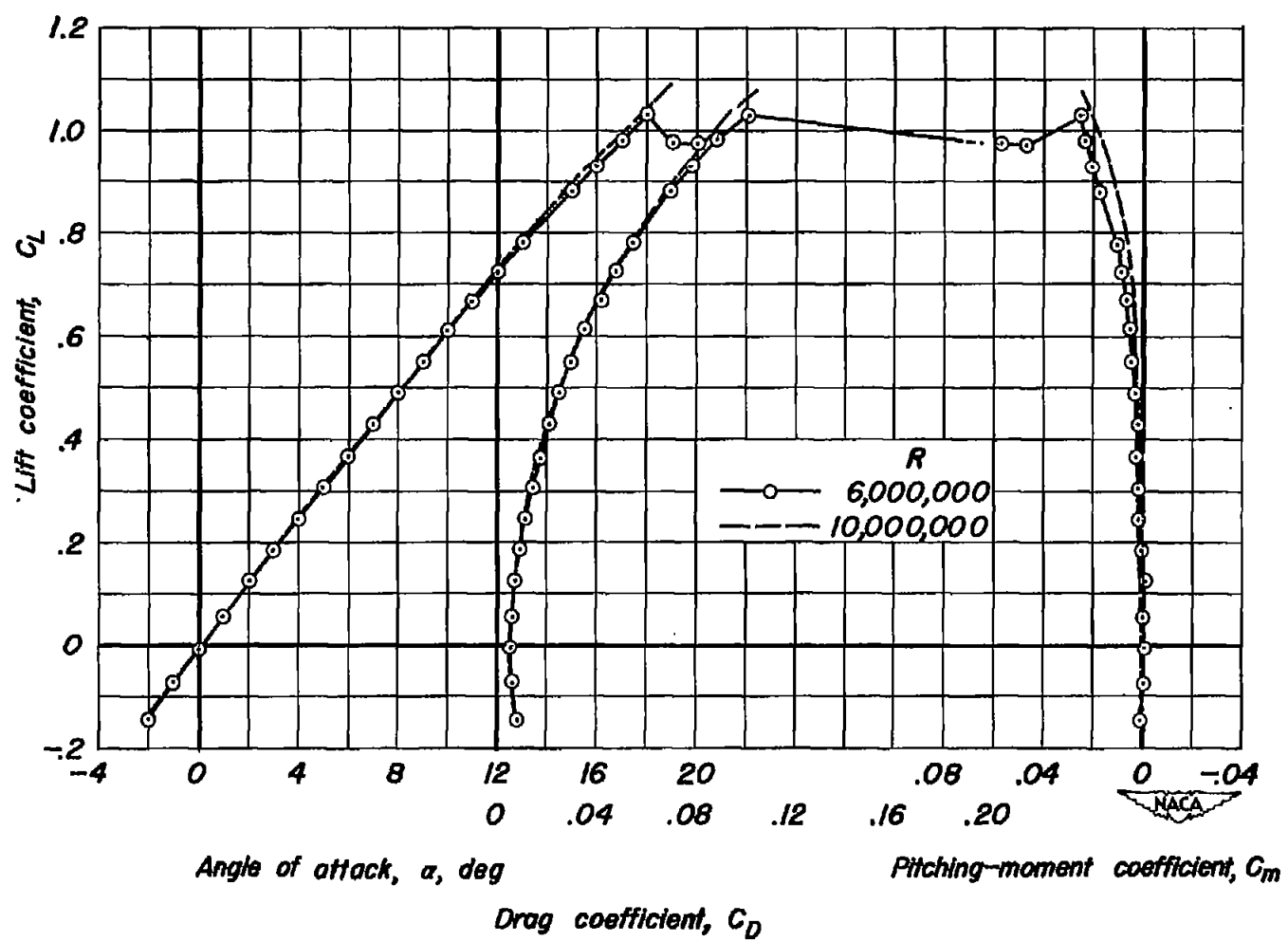
(b) Section normal-force characteristics.

Figure 4.—Continued. $R, 10,000,000$; $M, 0.25$.



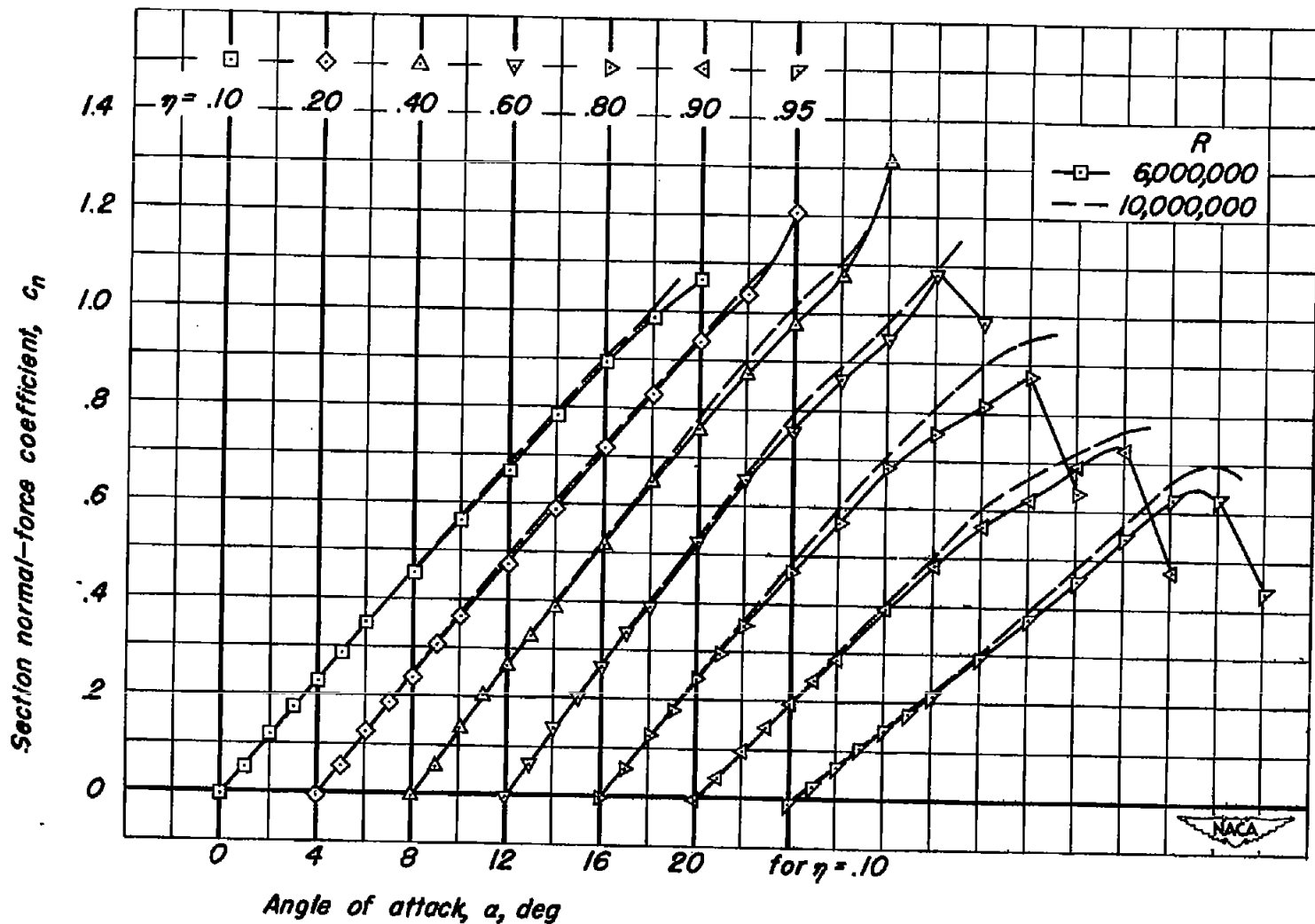
(c) Section pitching-moment characteristics.

Figure 4.—Concluded. $R, 10,000,000$; $M, 0.25$.



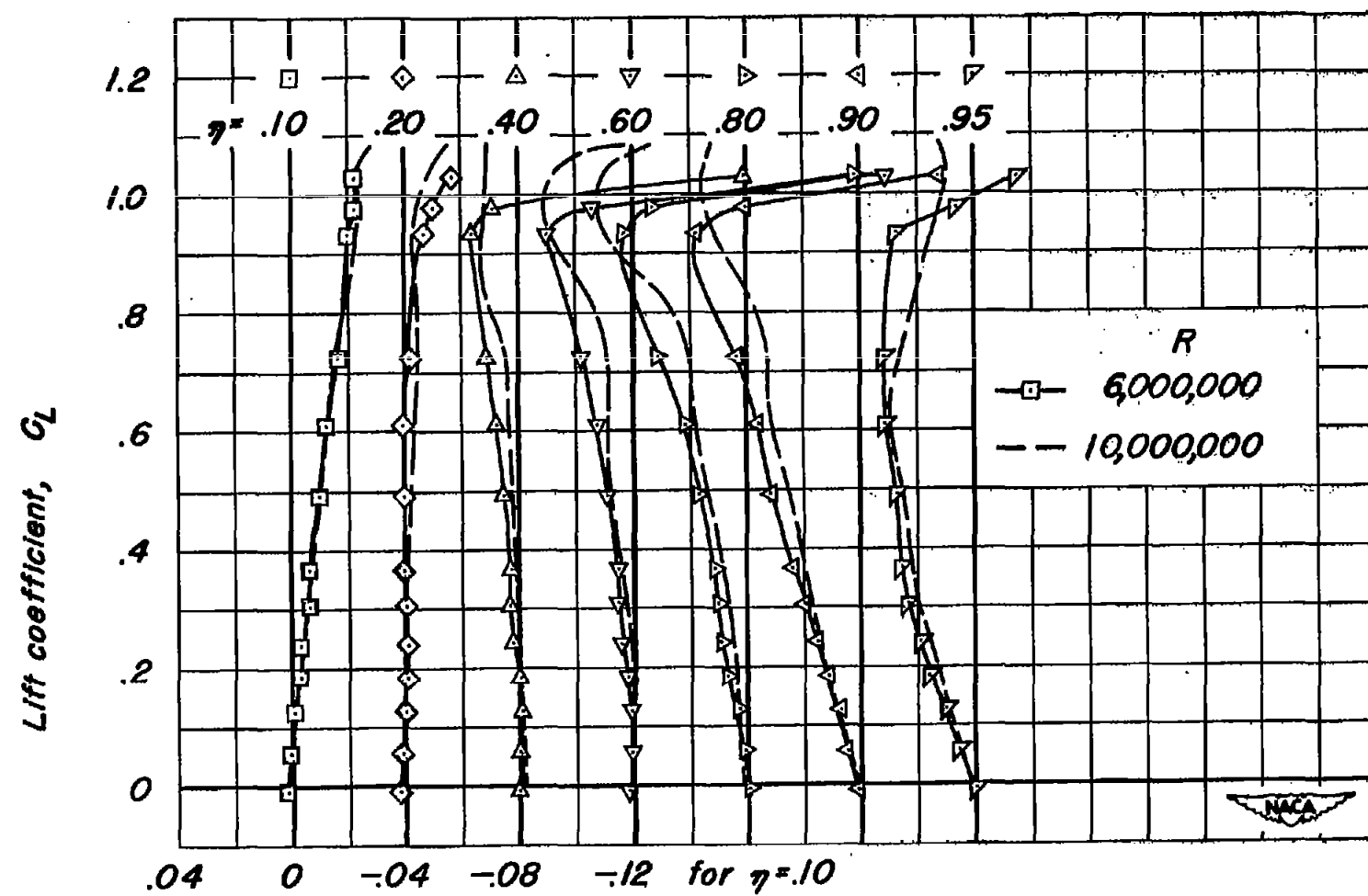
(a) Lift, drag, and pitching-moment characteristics.

Figure 5.— The lift, drag, and pitching-moment characteristics and the corresponding section normal-force and pitching-moment characteristics for seven sections of the wing. $M = 0.25$.



(b) Section normal-force characteristics.

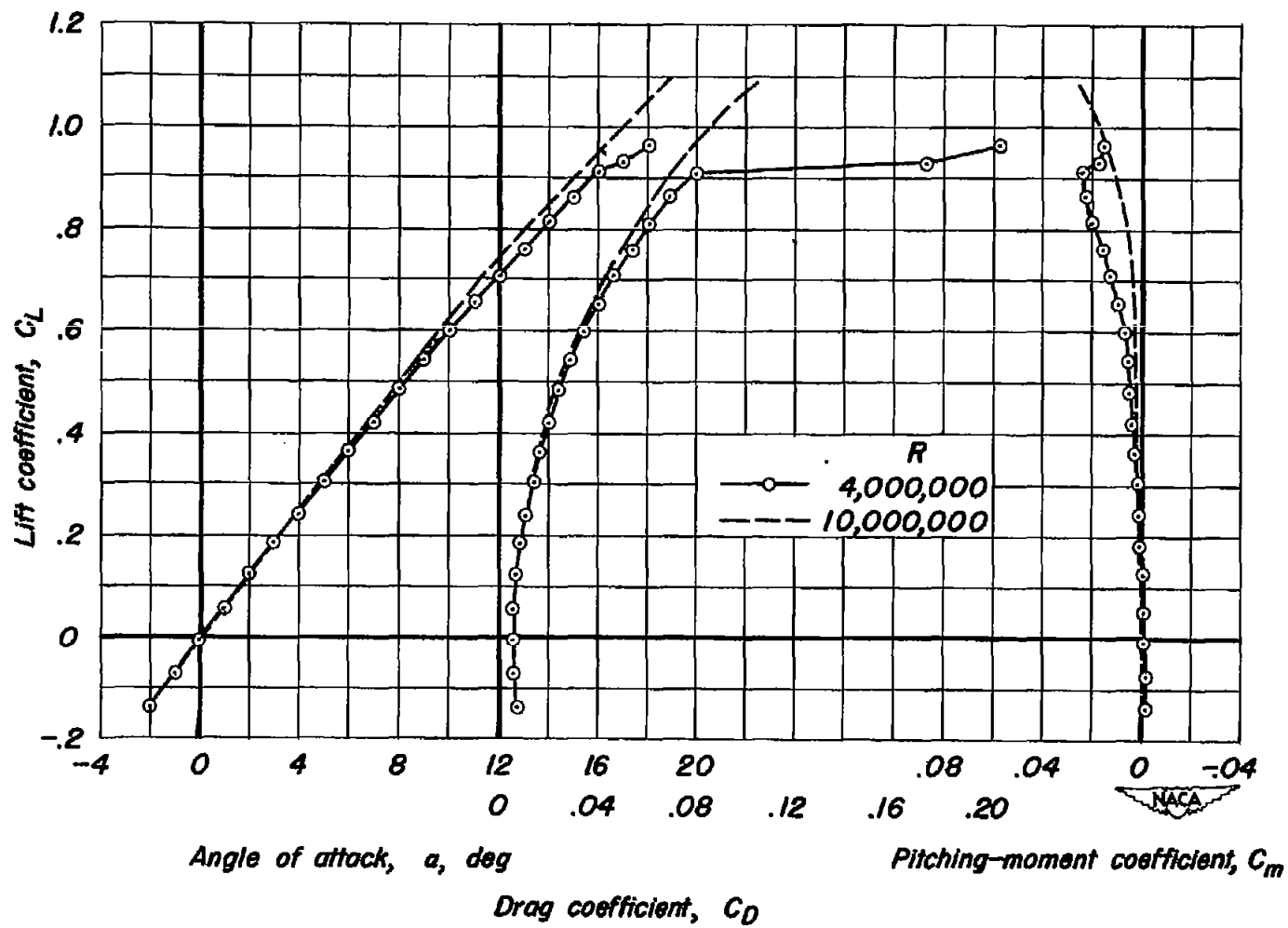
Figure 5.—Continued. $M, 0.25$.



Section pitching-moment coefficient, c_m

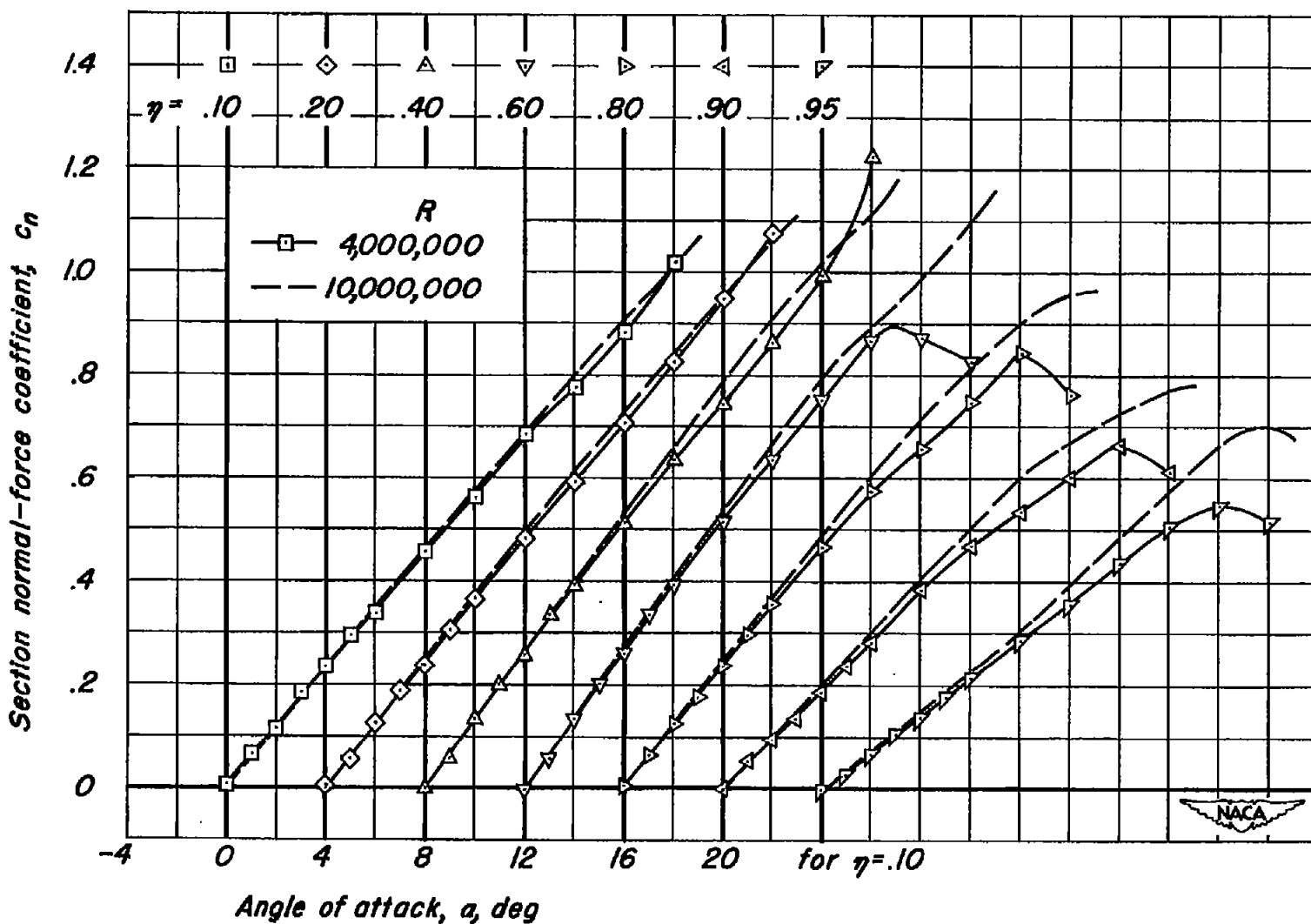
(c) Section pitching-moment characteristics.

Figure 5.- Concluded. $M, 0.25$.



(a) Lift, drag, and pitching-moment characteristics.

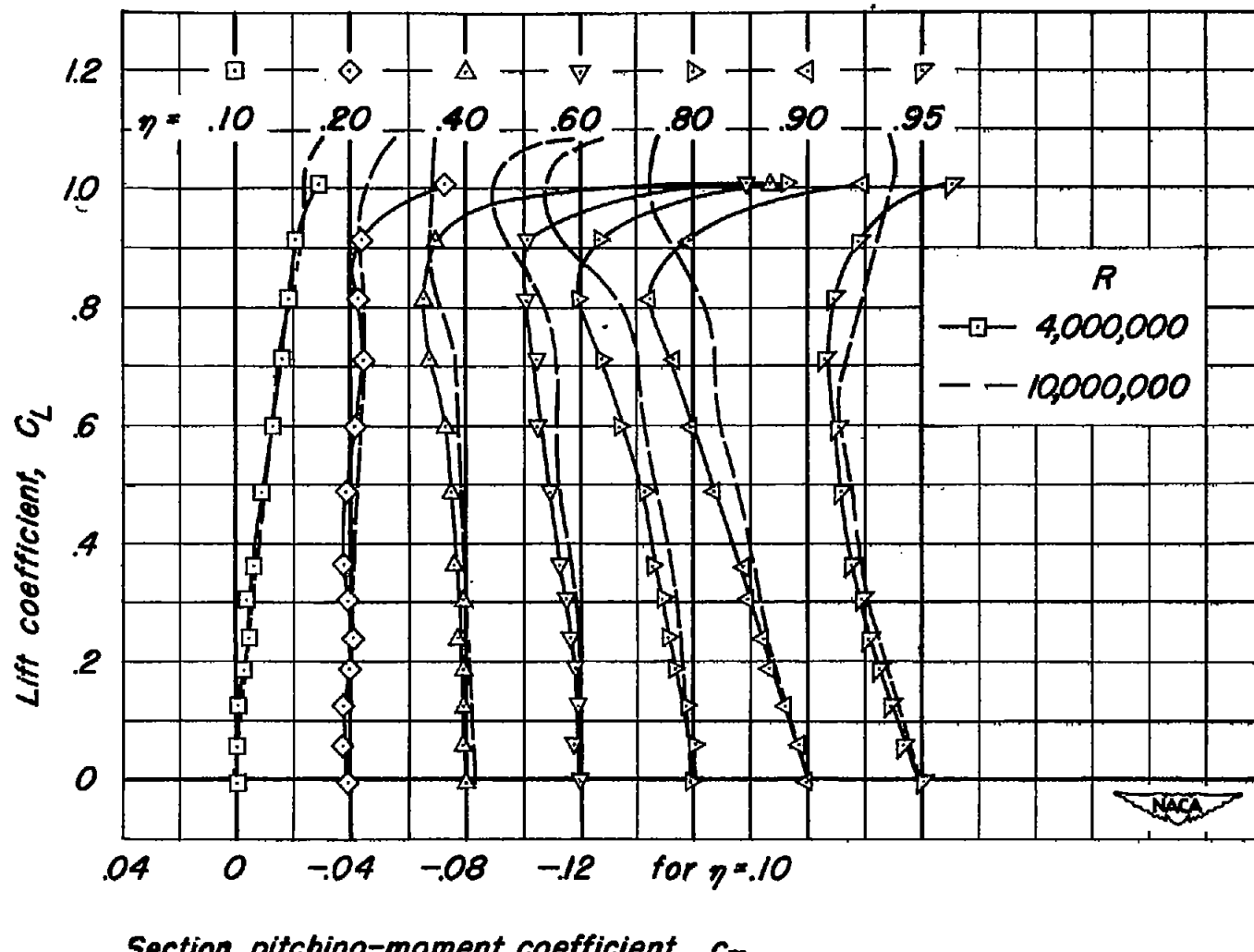
Figure 6. — The lift, drag, and pitching-moment characteristics and the corresponding section normal-force and pitching-moment characteristics for seven sections of the wing. $M, 0.25$.



(b) Section normal-force characteristics.

Figure 6.-Continued. M, 0.25.

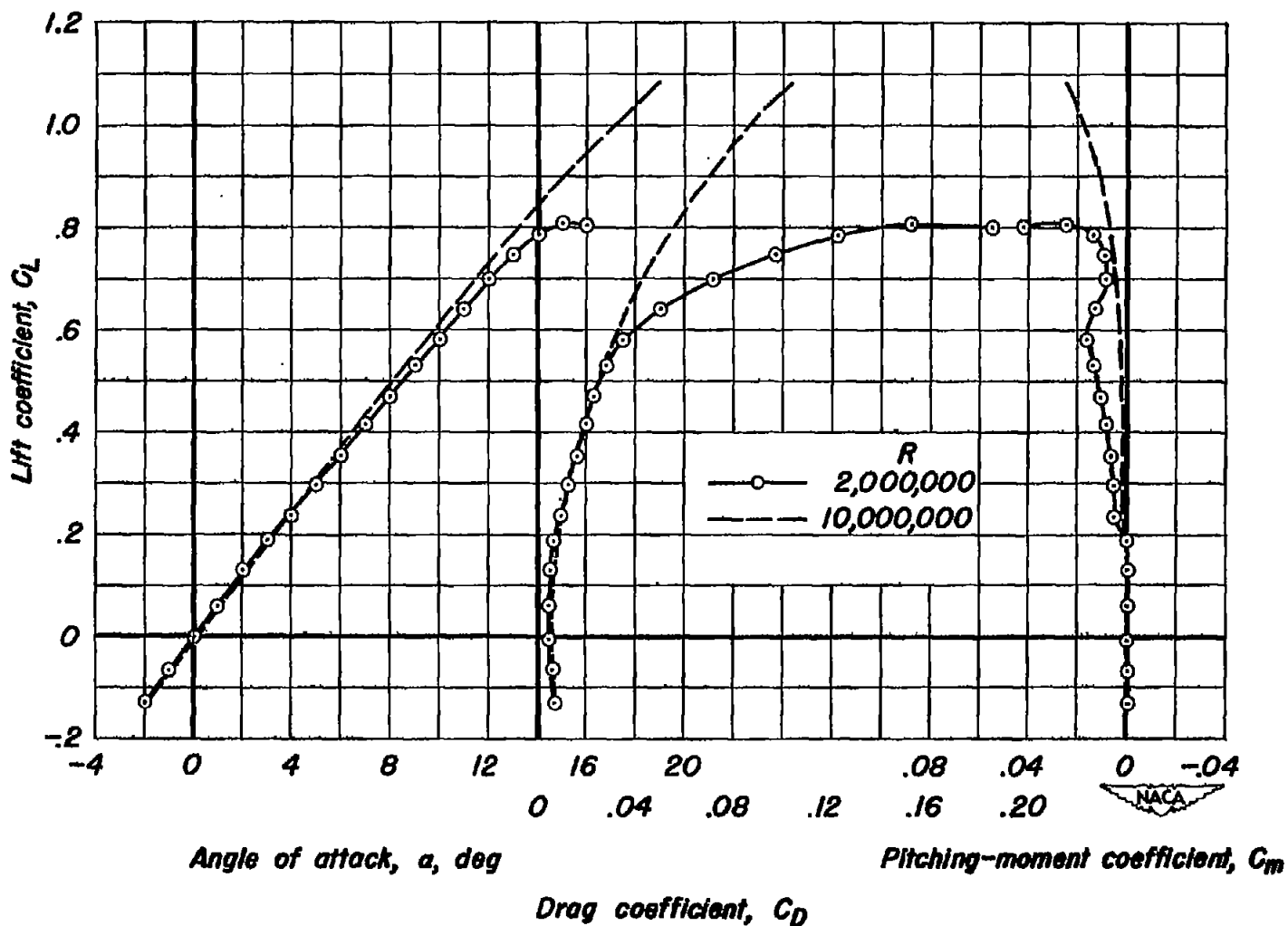
CONFIDENTIAL



(c) Section pitching-moment characteristics.

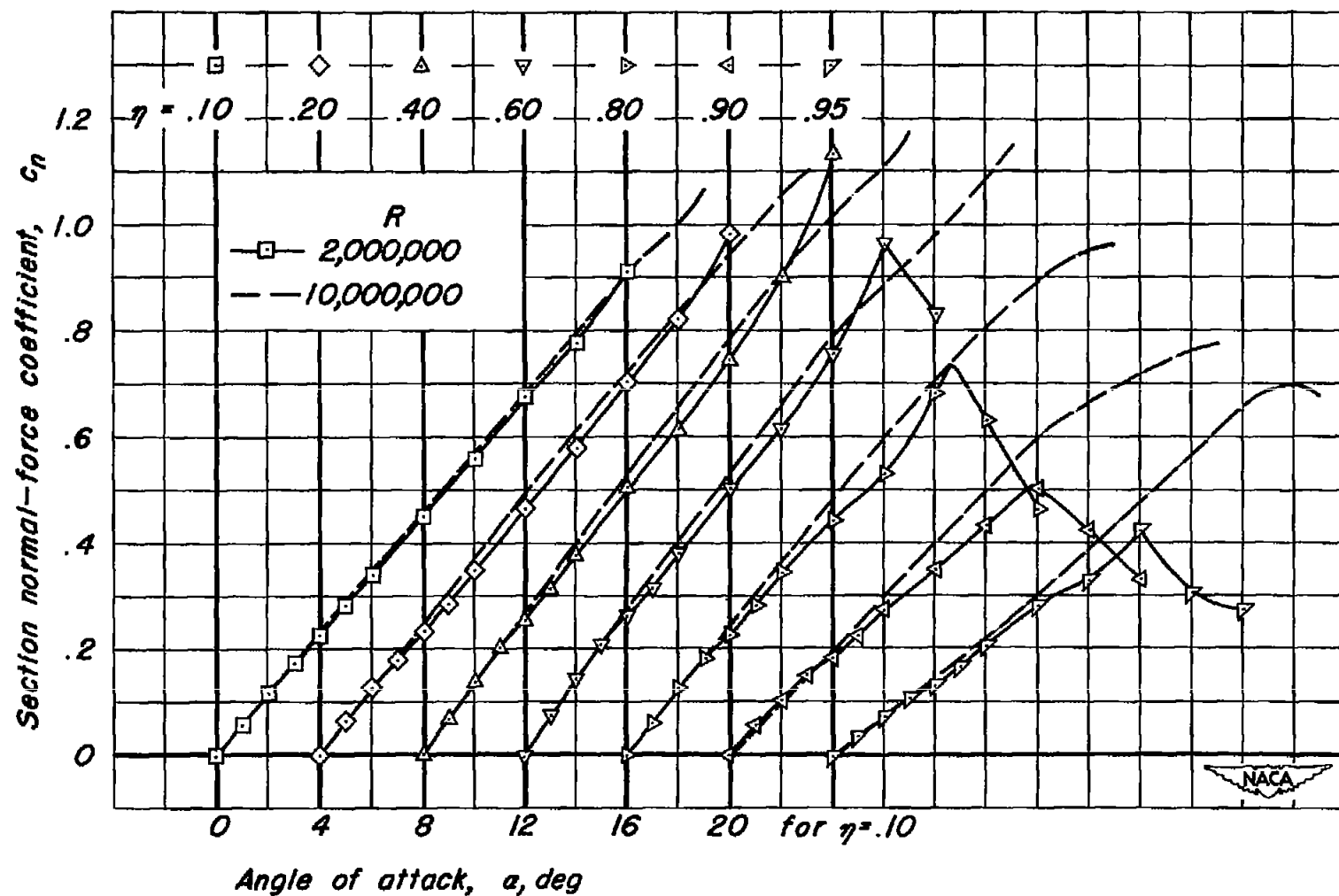
Figure 6.—Concluded. $M, 0.25$.

NACA RM A52B20



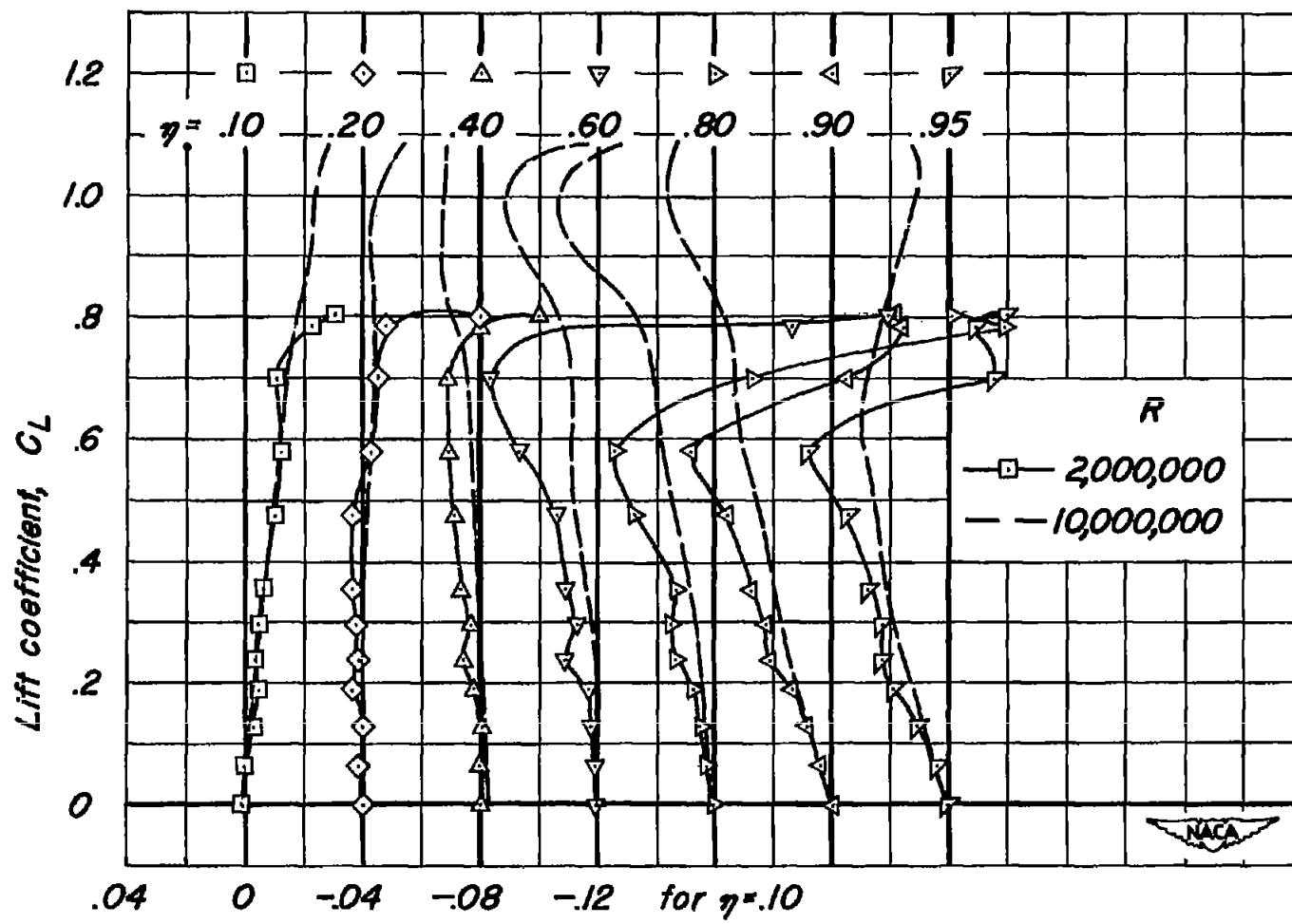
(a) Lift, drag, and pitching-moment characteristics.

Figure 7.— The lift, drag, and pitching-moment characteristics and the corresponding section normal-force and pitching-moment characteristics for seven sections of the wing. $M, 0.25$.



(b) Section normal-force characteristics.

Figure 7.—Continued. $M, 0.25$.



Section pitching-moment coefficient, c_m

(c) *Section pitching-moment characteristics.*

Figure 7.- Concluded. M, 0.25.

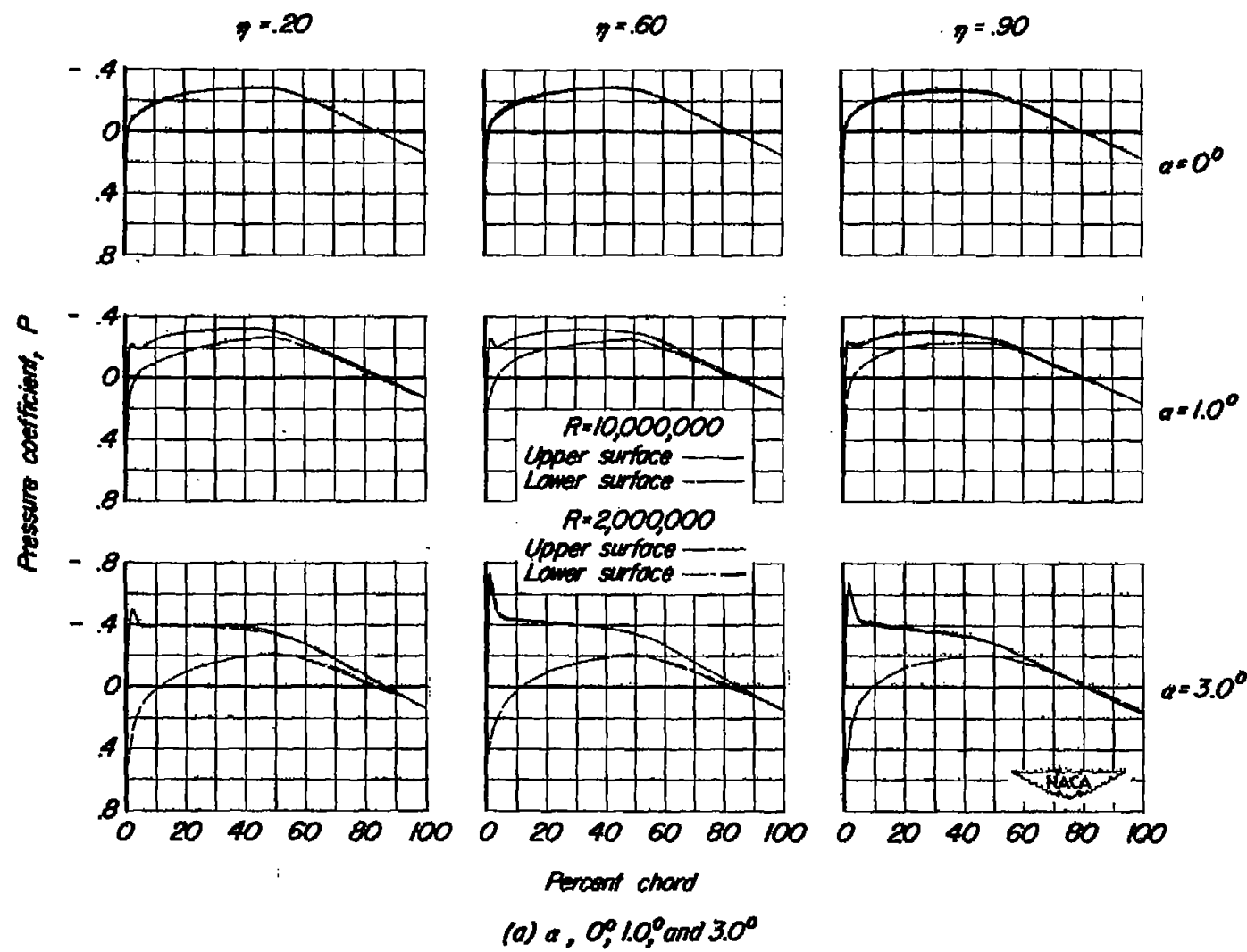
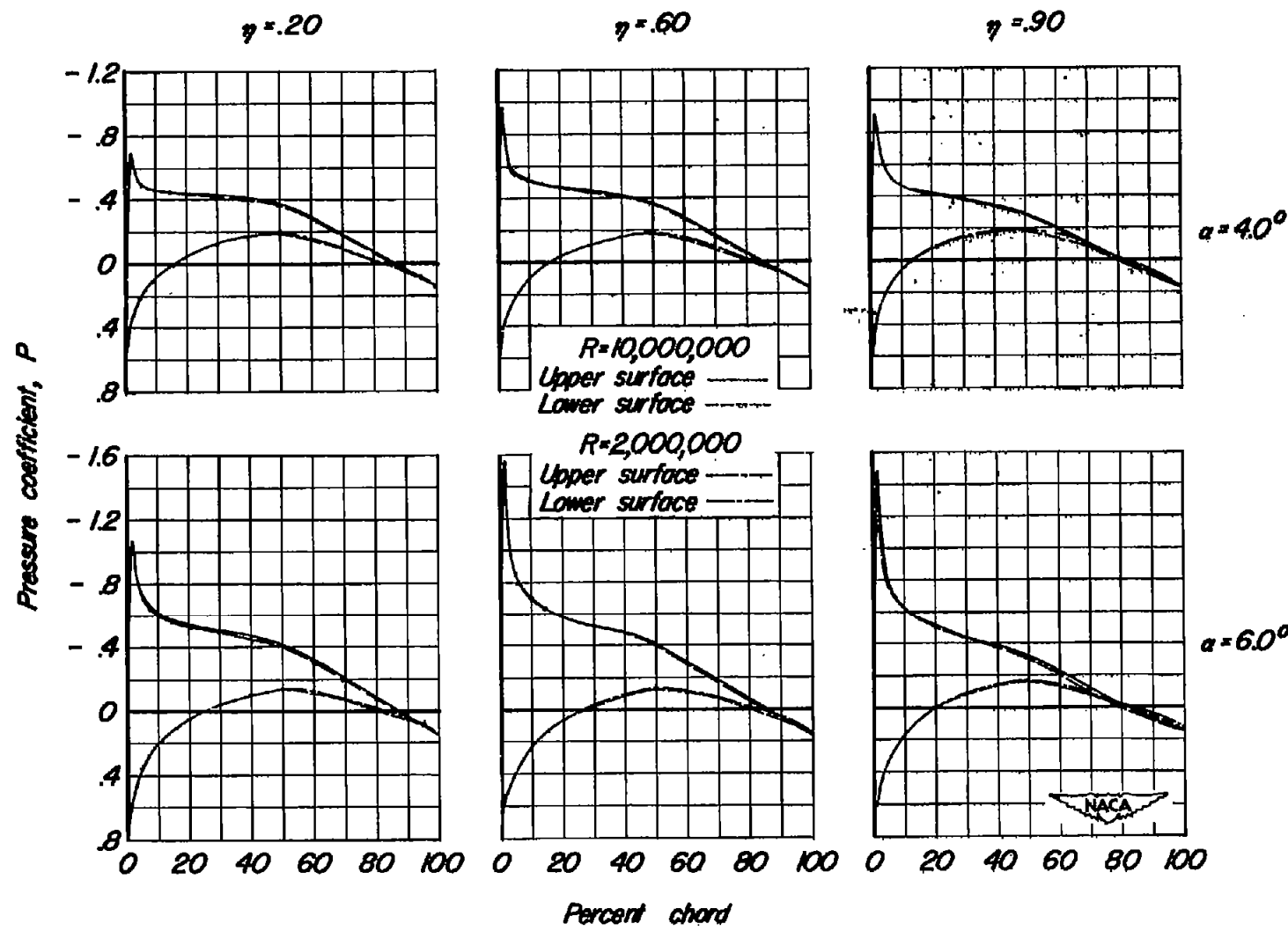
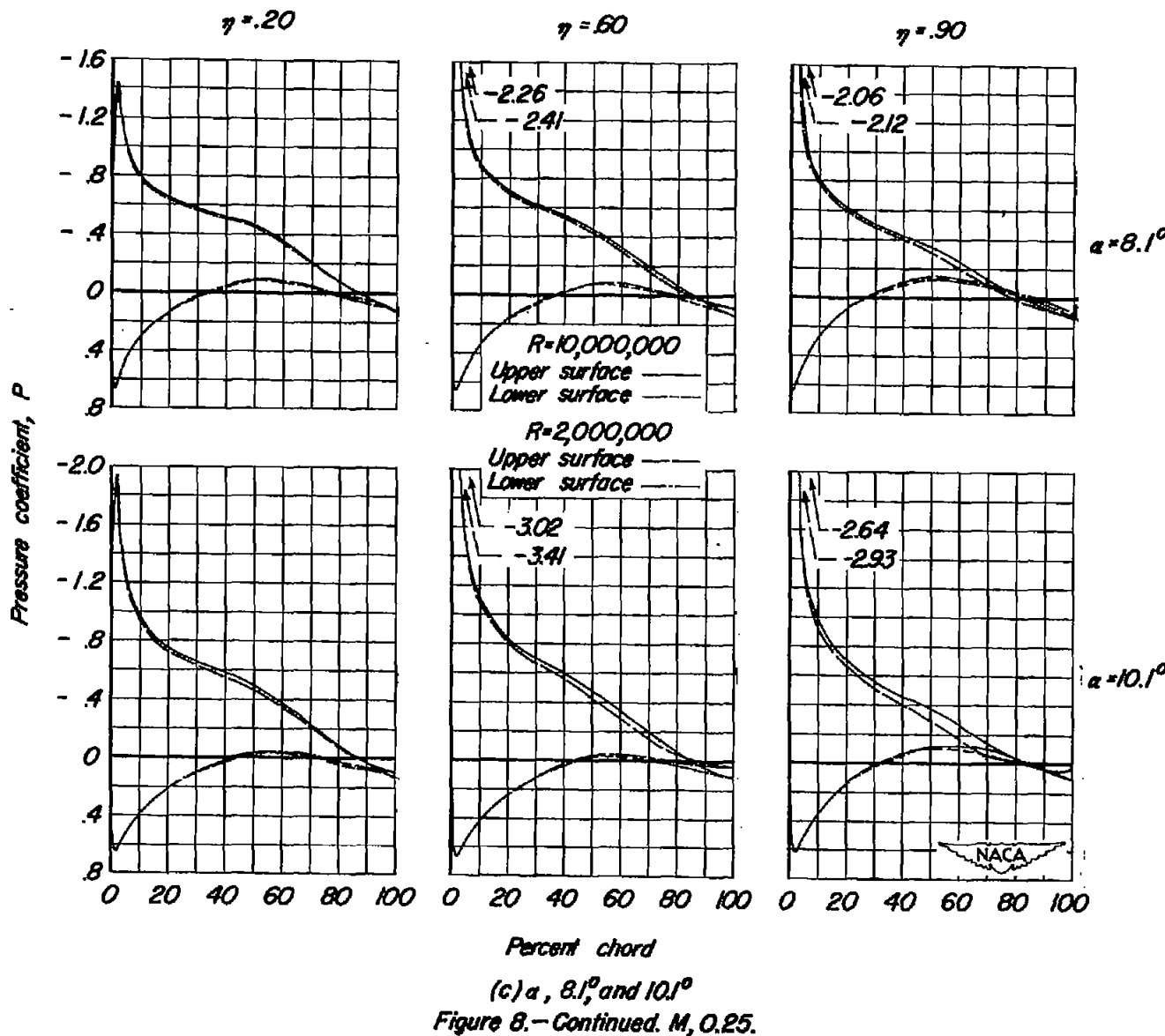
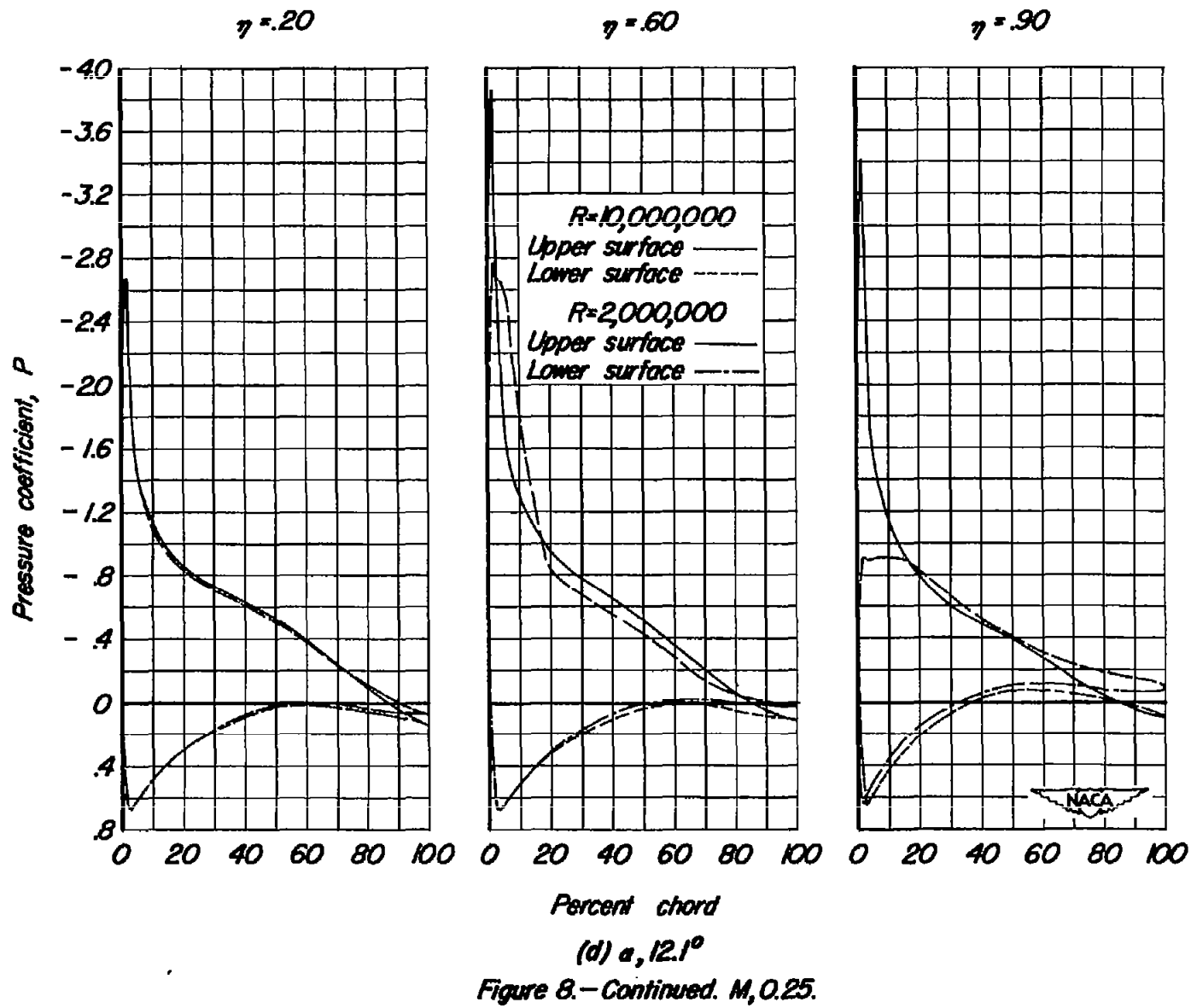


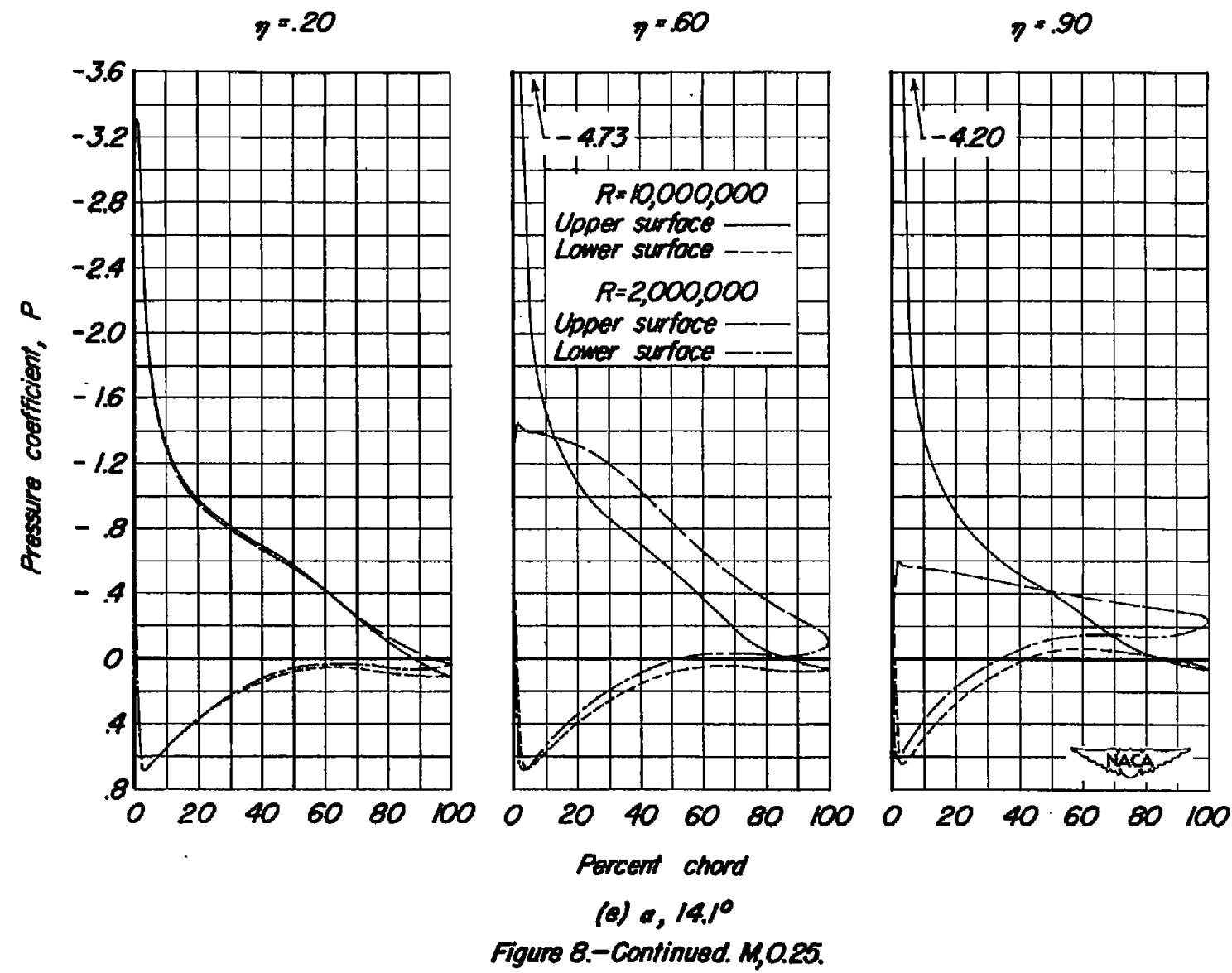
Figure 8.- The chordwise distribution of static pressure coefficient for 20, 60, and 90 percent of the semispan. $M, 0.25$.

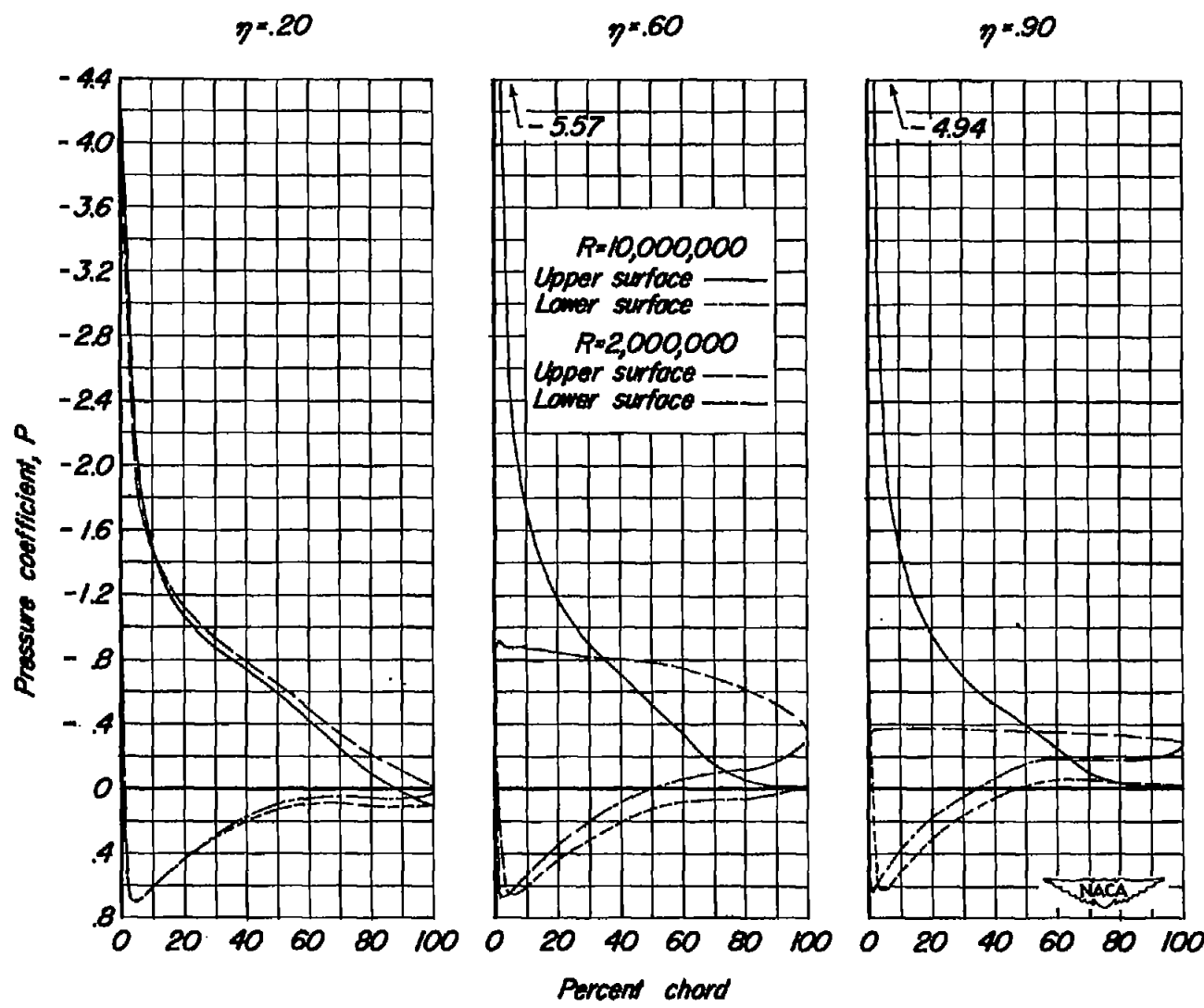
 $(b) \alpha = 4.0^\circ \text{ and } 6.0^\circ$ Figure 8.—Continued. $M, 0.25$.



Figure 8.—Continued. $M, 0.25$.

CONFIDENTIAL





(f) $\alpha = 16^\circ$
Figure 8.- Concluded. $M = 0.25$.

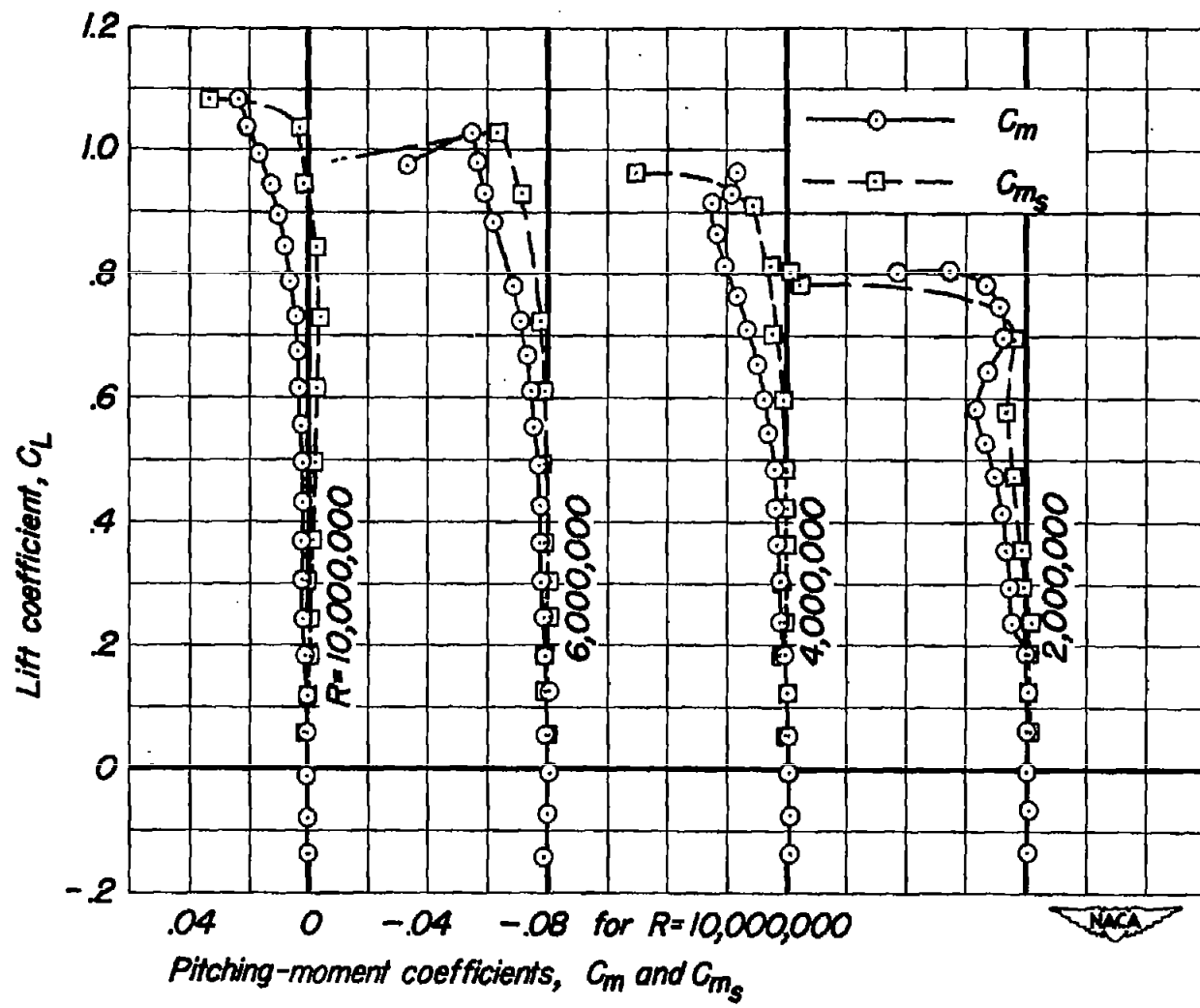


Figure 9.— Comparison of the pitching-moment coefficient, C_m , with the span-load pitching-moment coefficient, C_{ms} . $M, 0.25$.

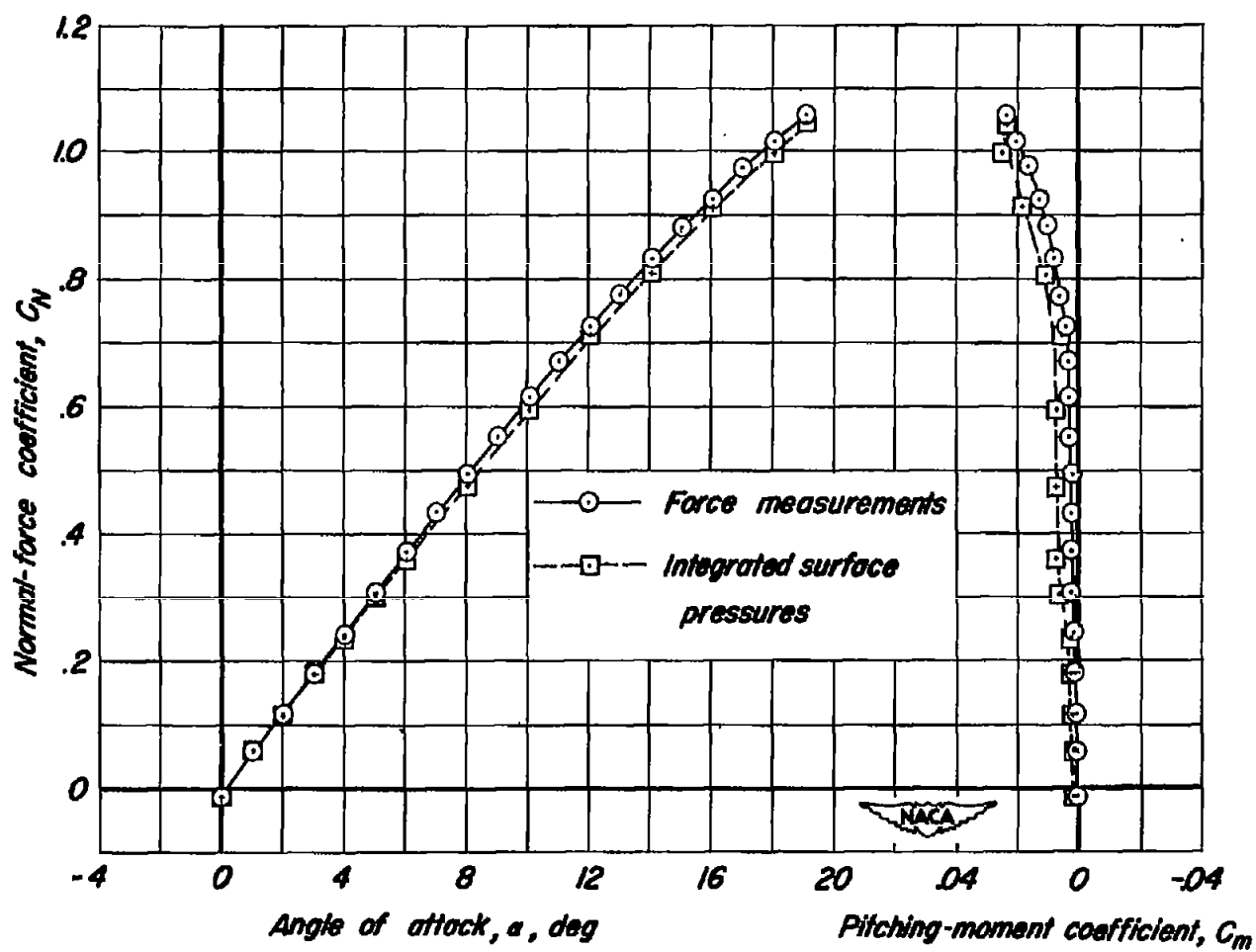
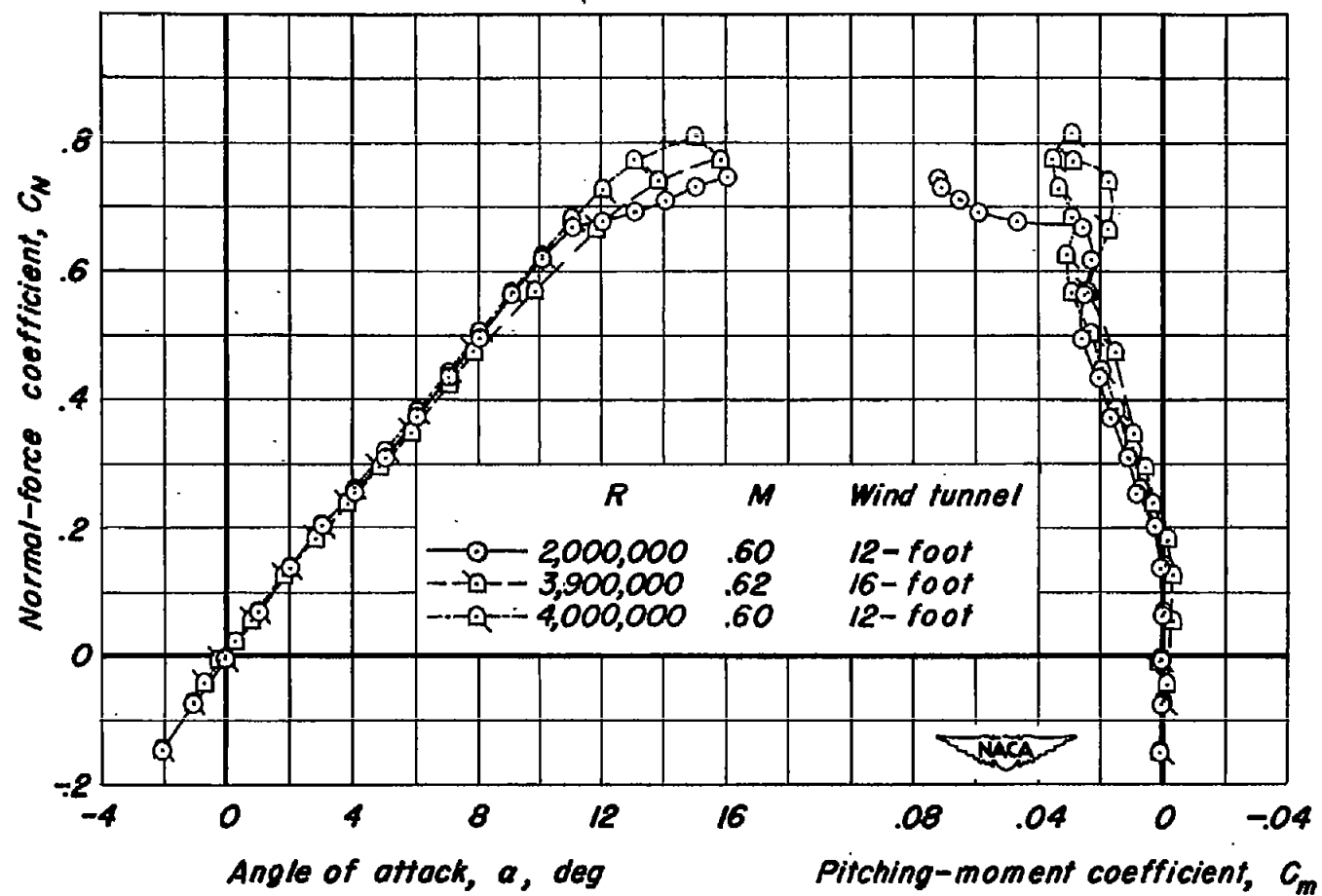


Figure 10.— Comparison of normal-force and pitching-moment data obtained from force measurements with those obtained from integration of surface pressures.

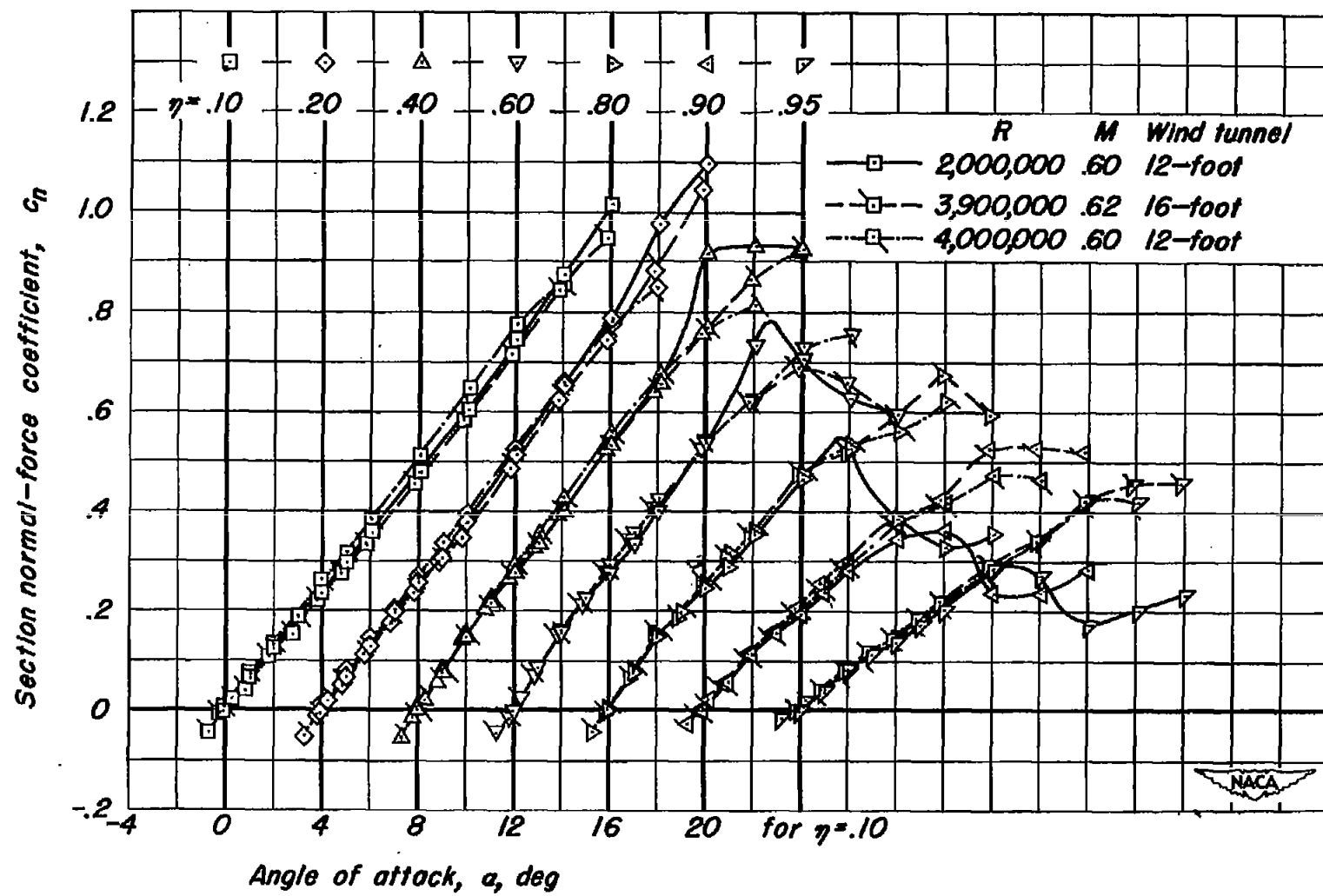
$R, 10,000,000$; $M, 0.25$.

CONFIDENTIAL



(a) Normal-force and pitching-moment characteristics.

Figure 11.- The normal-force and pitching-moment characteristics and the corresponding section characteristics for a Mach number of approximately 0.6 as evaluated from tests in the Ames 12-foot pressure wind tunnel and in the Ames 16-foot high-speed wind tunnel.

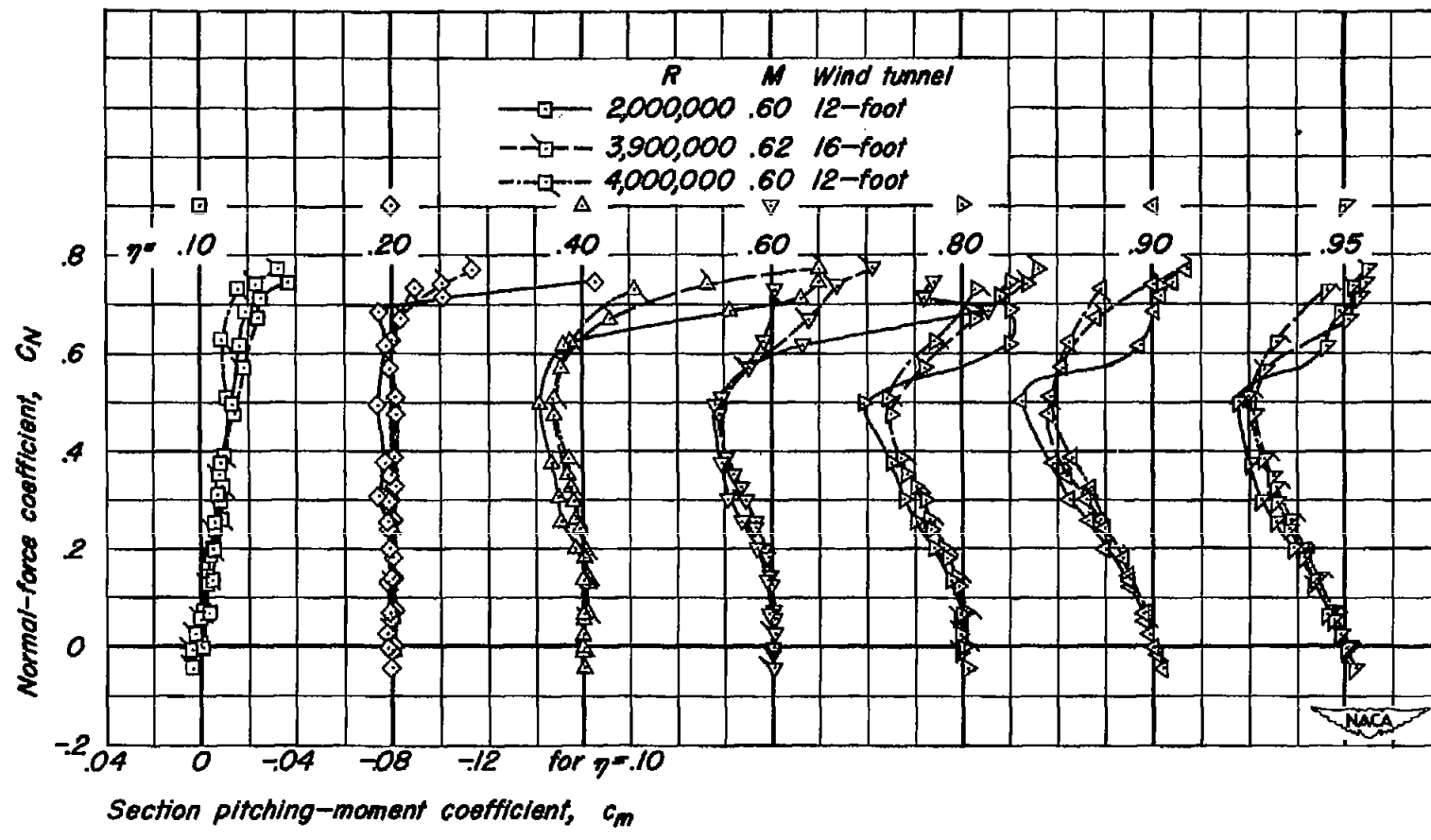


(b) Section normal-force characteristics.

Figure 11.—Continued.

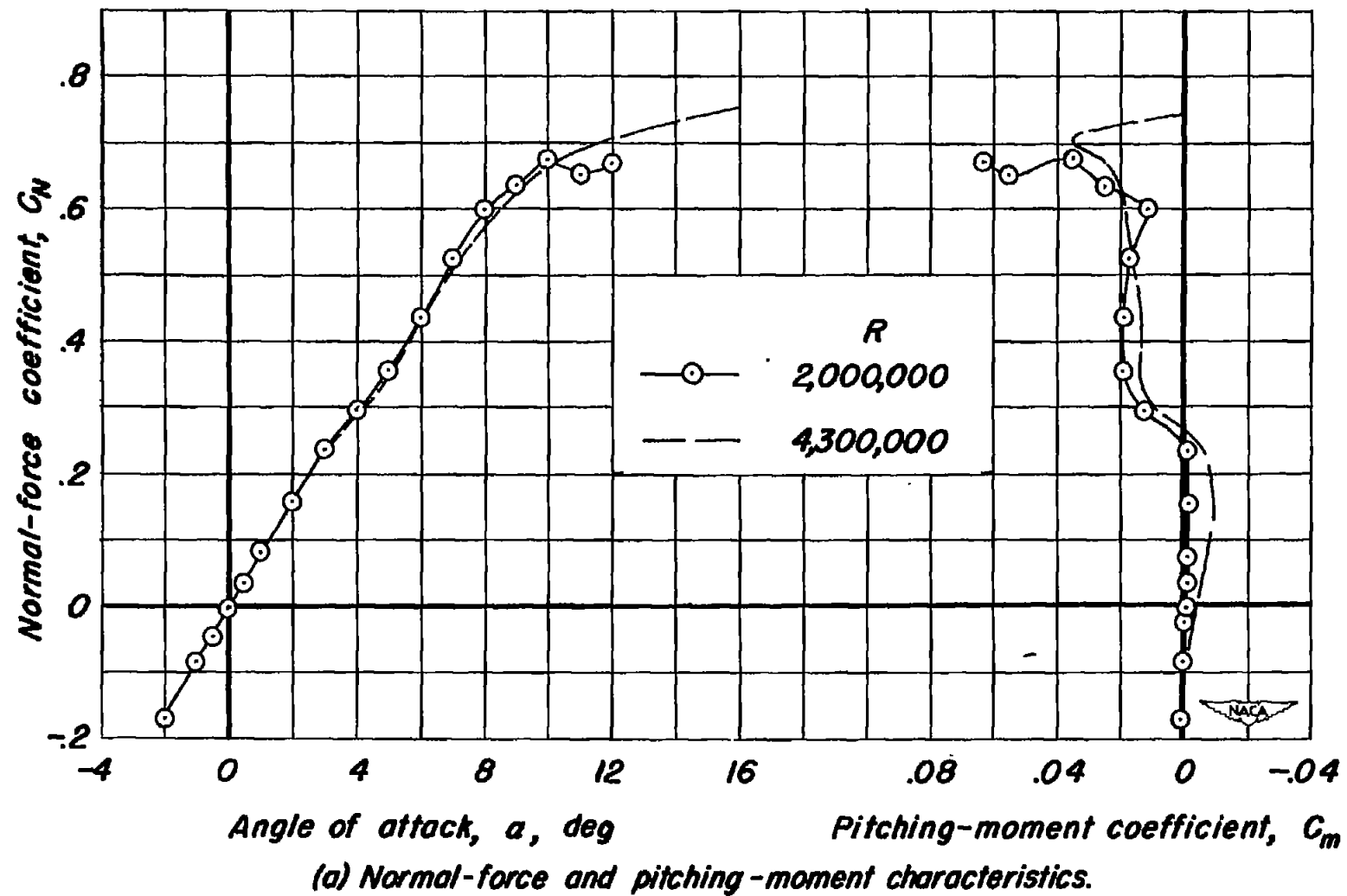
CONFIDENTIAL

NACA RM A52B20



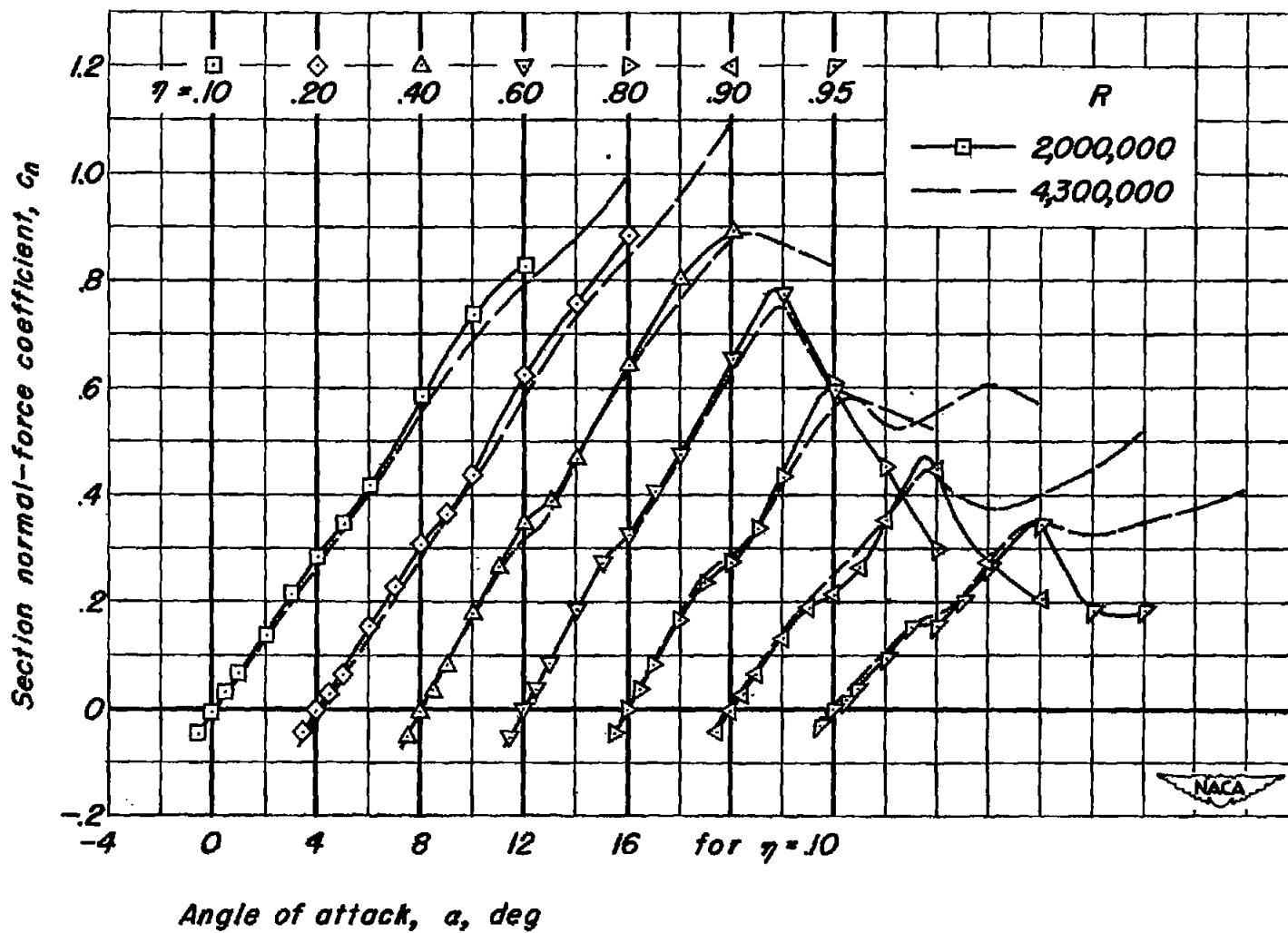
(c) Section pitching-moment characteristics.

Figure II.— Concluded.



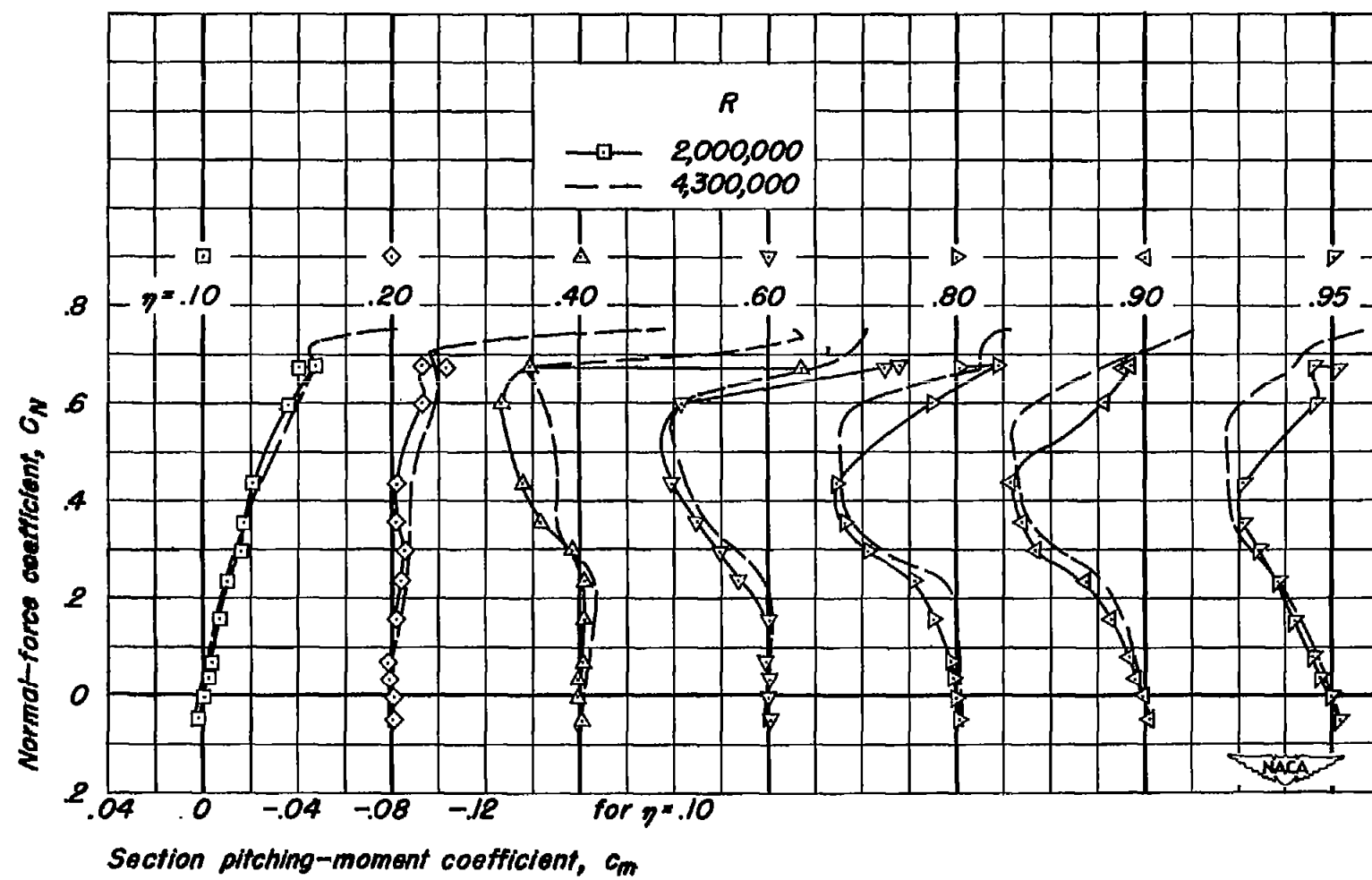
(a) Normal-force and pitching-moment characteristics.

Figure 12.- The normal-force and pitching-moment characteristics and the corresponding section characteristics for seven sections of the wing. $M, 0.80$.



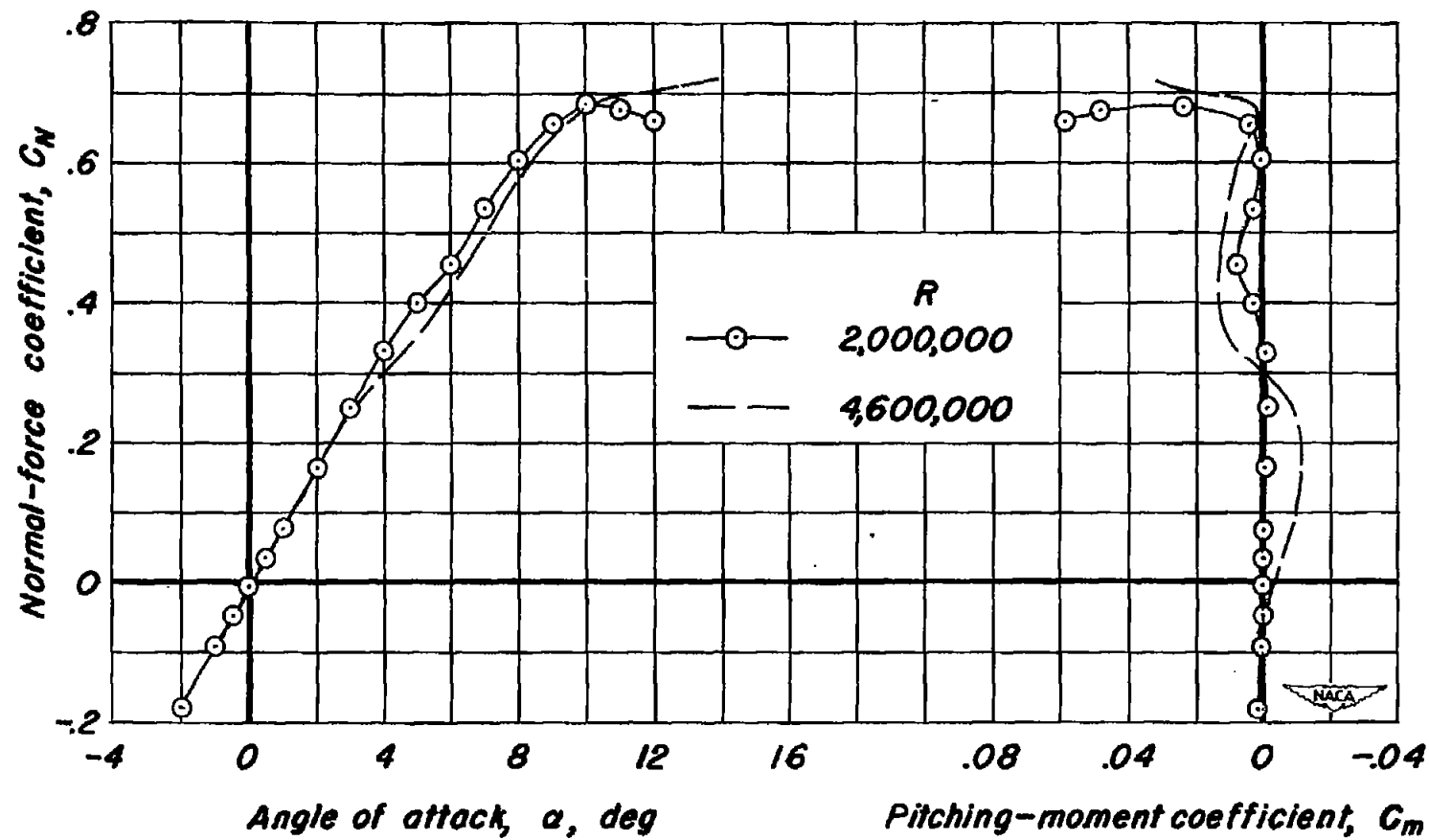
(b) Section normal-force characteristics.

Figure 12.- Continued. M, OBO.



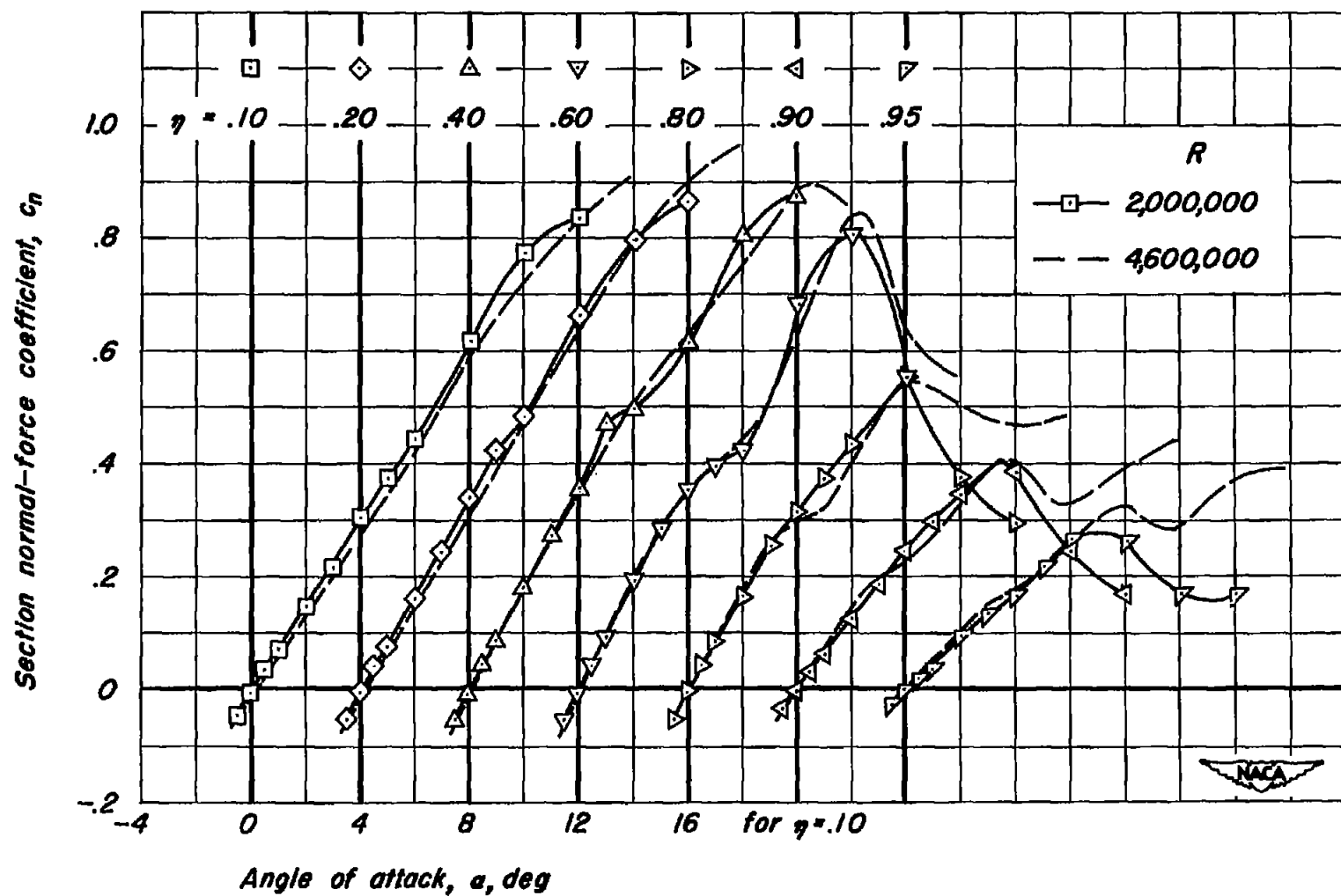
(c) Section pitching-moment characteristics.

Figure 12.- Concluded. $M, 0.80$.



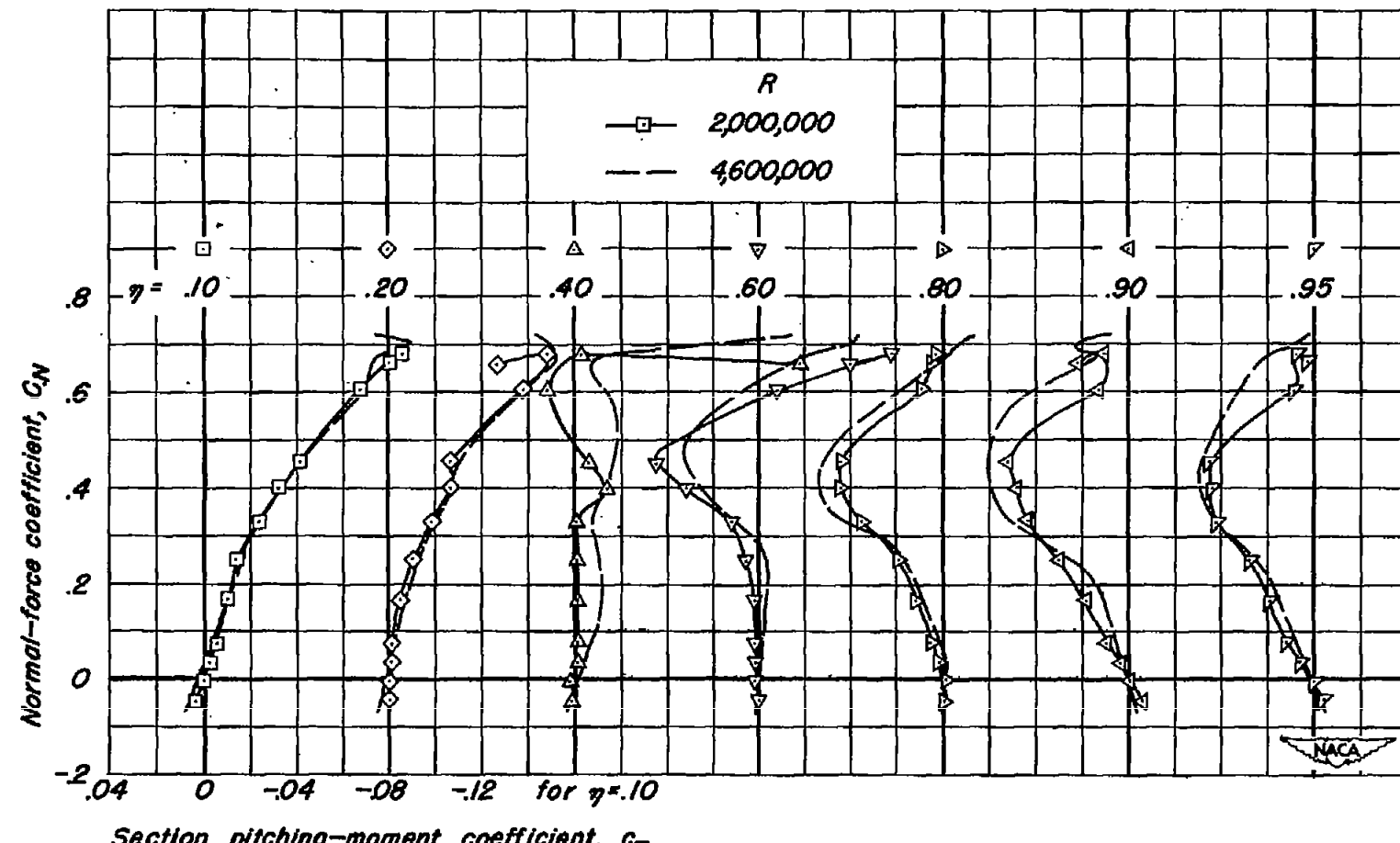
(a) Normal-force and pitching-moment characteristics.

Figure 13.— The normal-force and pitching-moment characteristics and the corresponding section characteristics for seven sections of the wing. $M, 0.85$.



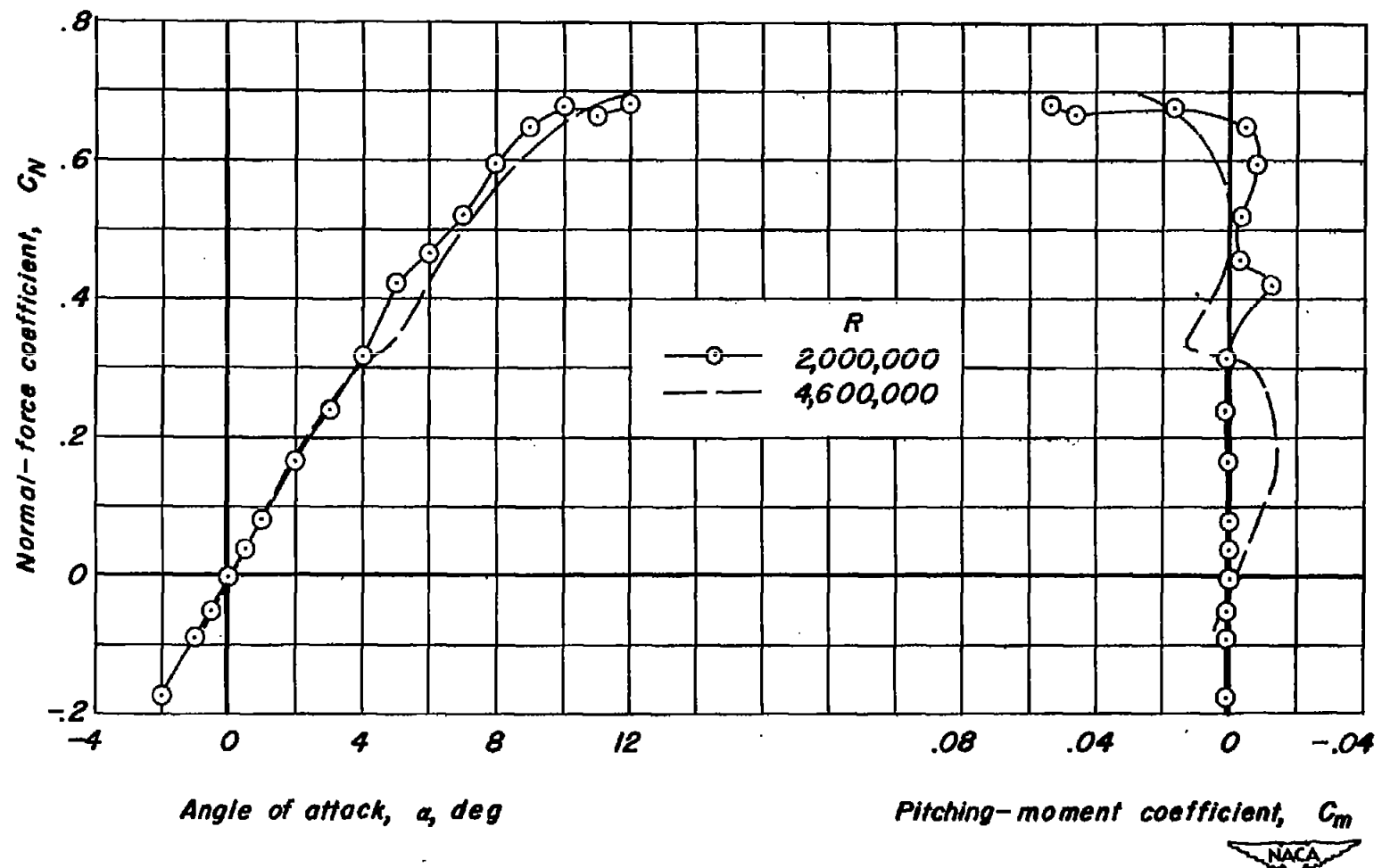
(b) Section normal-force characteristics.

Figure 13.—Continued. $M, 0.85$.



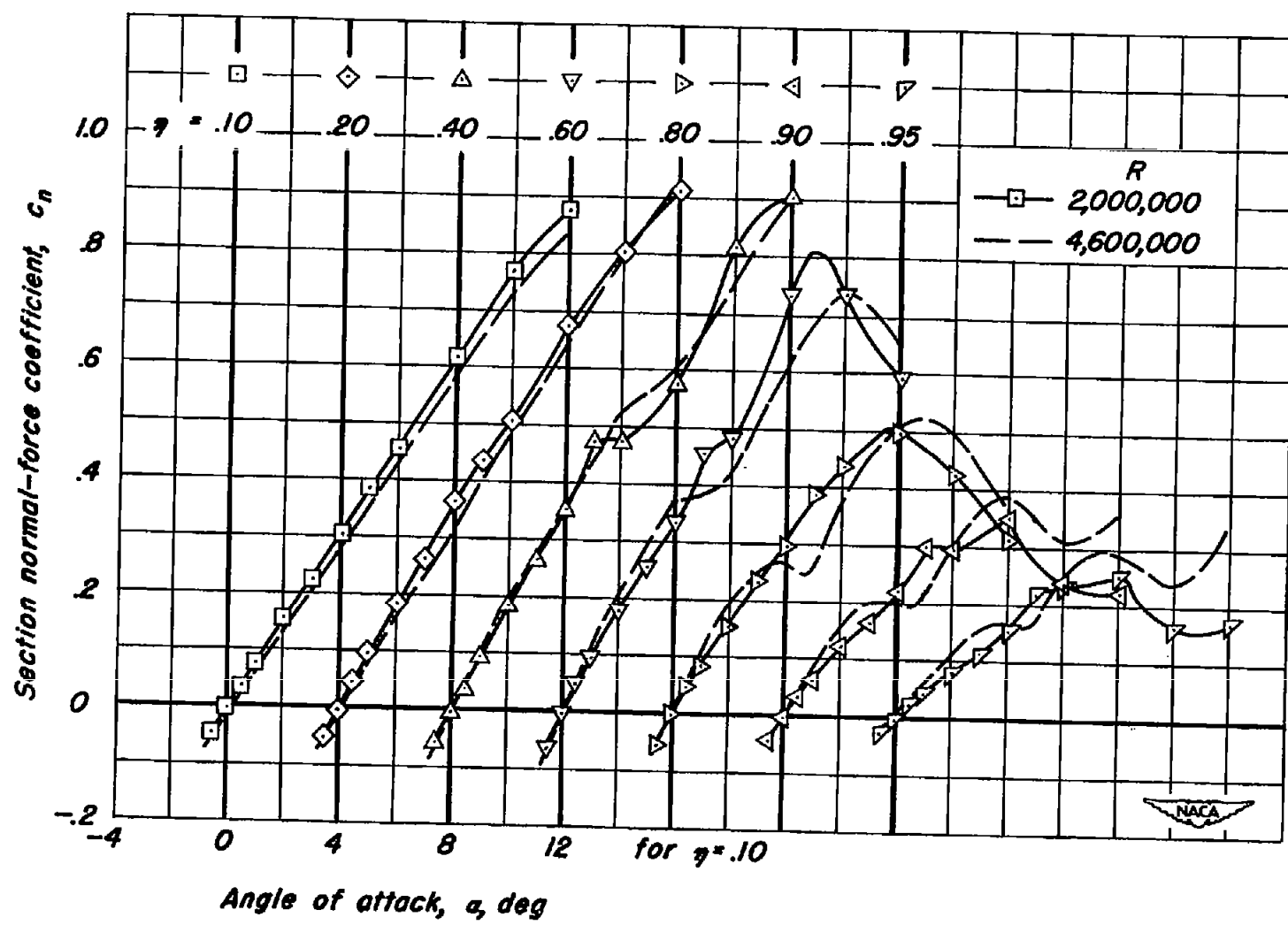
(c) Section pitching-moment characteristics.

Figure 13.— Concluded. M, 0.85.



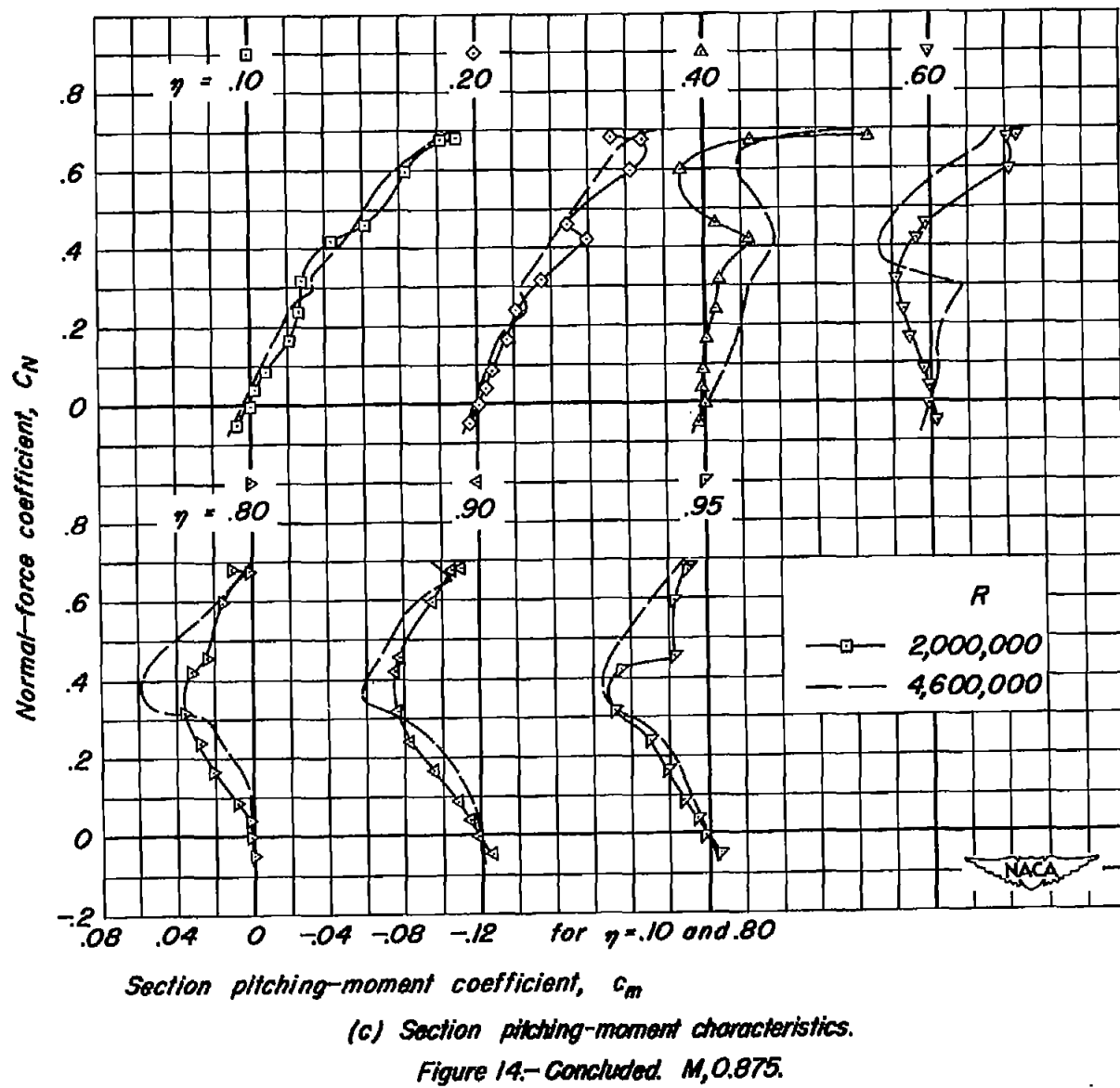
(a) Normal-force and pitching-moment characteristics.

Figure 14. – The normal-force and pitching-moment characteristics and the corresponding section characteristics for seven sections of the wing. $M, 0.875$.

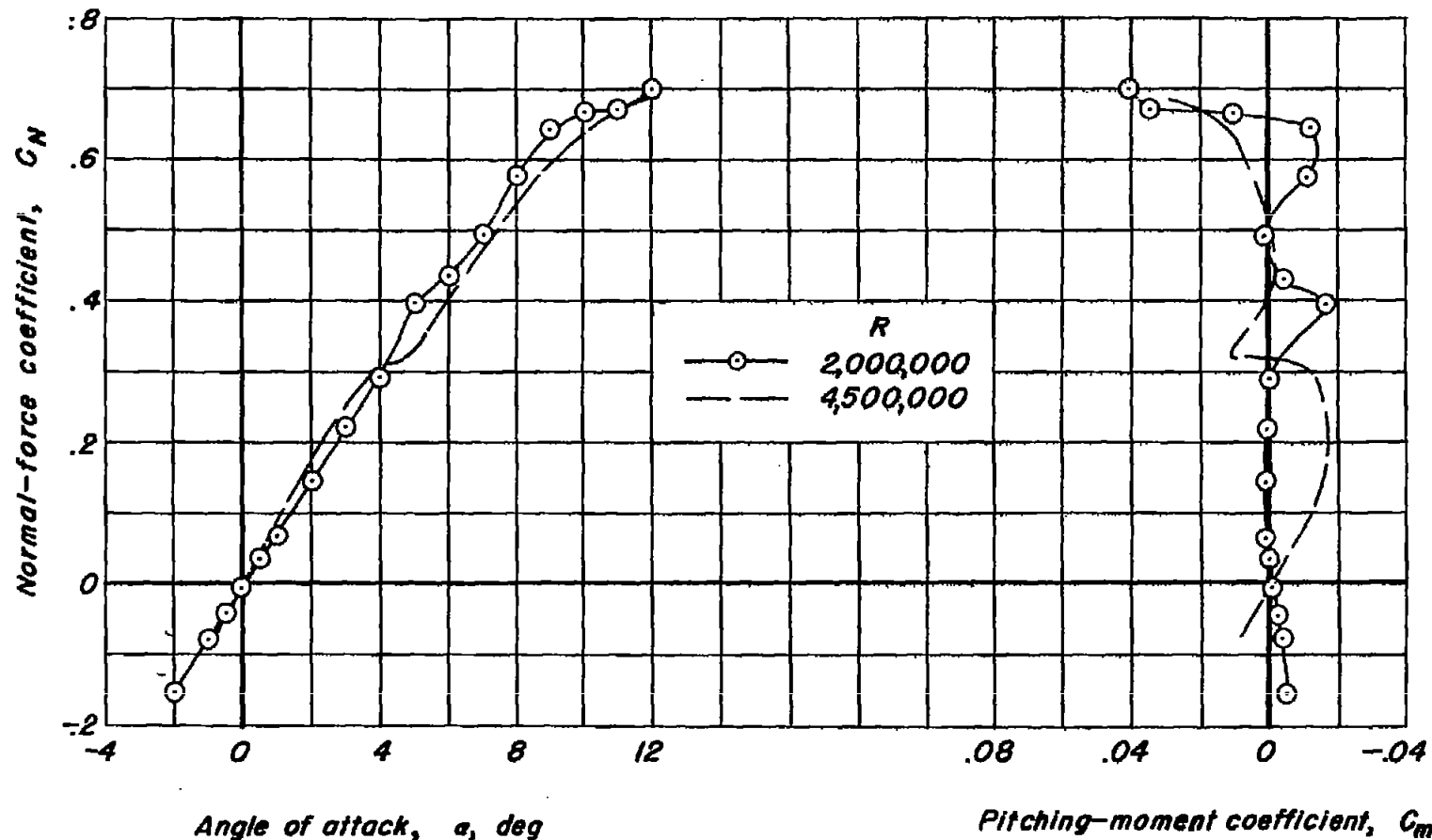


(b) Section normal-force characteristics.

Figure 14.—Continued. $M, 0.875$.

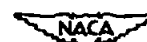


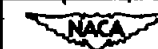
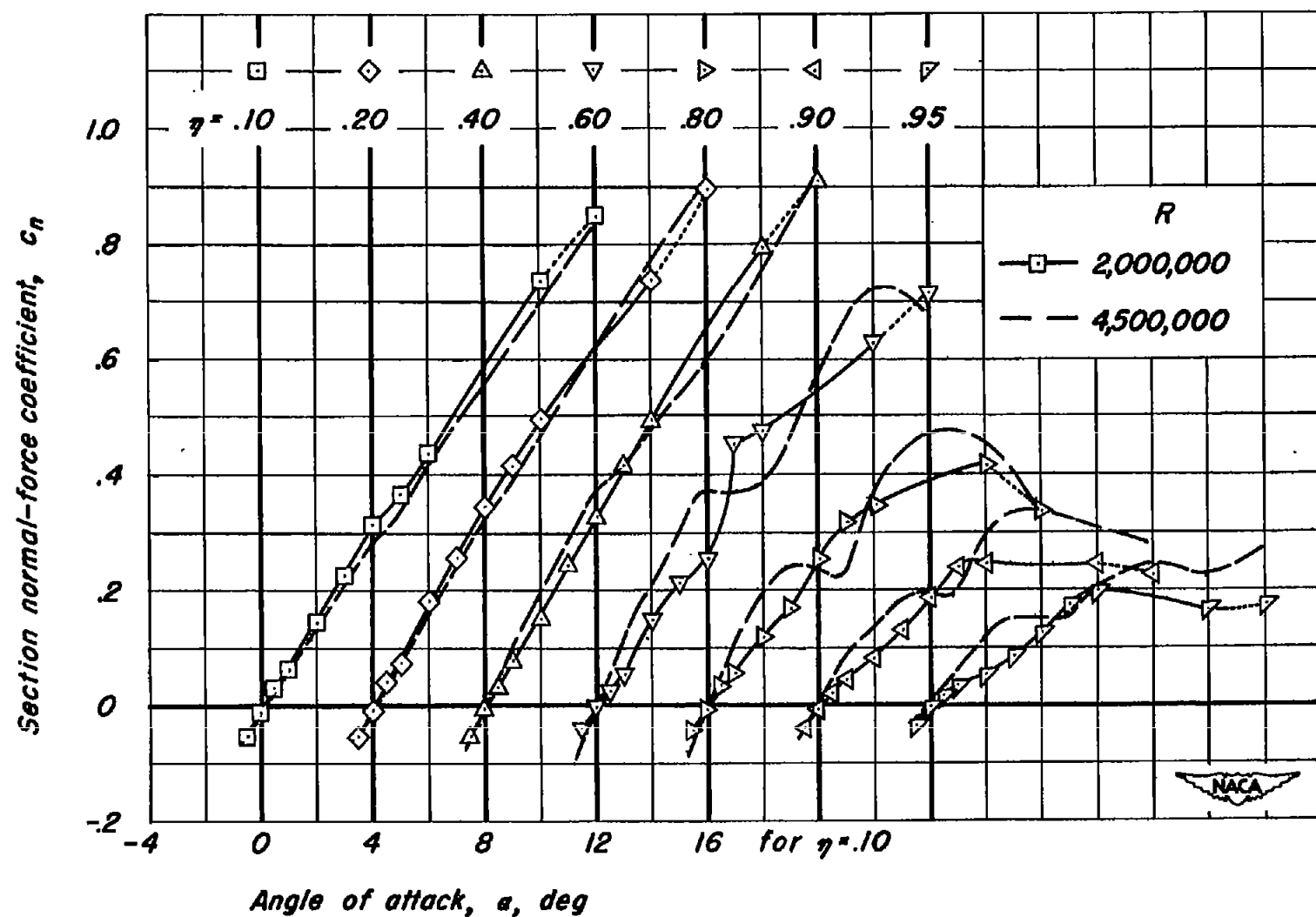
CONFIDENTIAL



(a) Normal-force and pitching-moment characteristics.

Figure 15.— The normal-force and pitching-moment characteristics and the corresponding section characteristics for seven sections of the wing. $M, 0.90$.





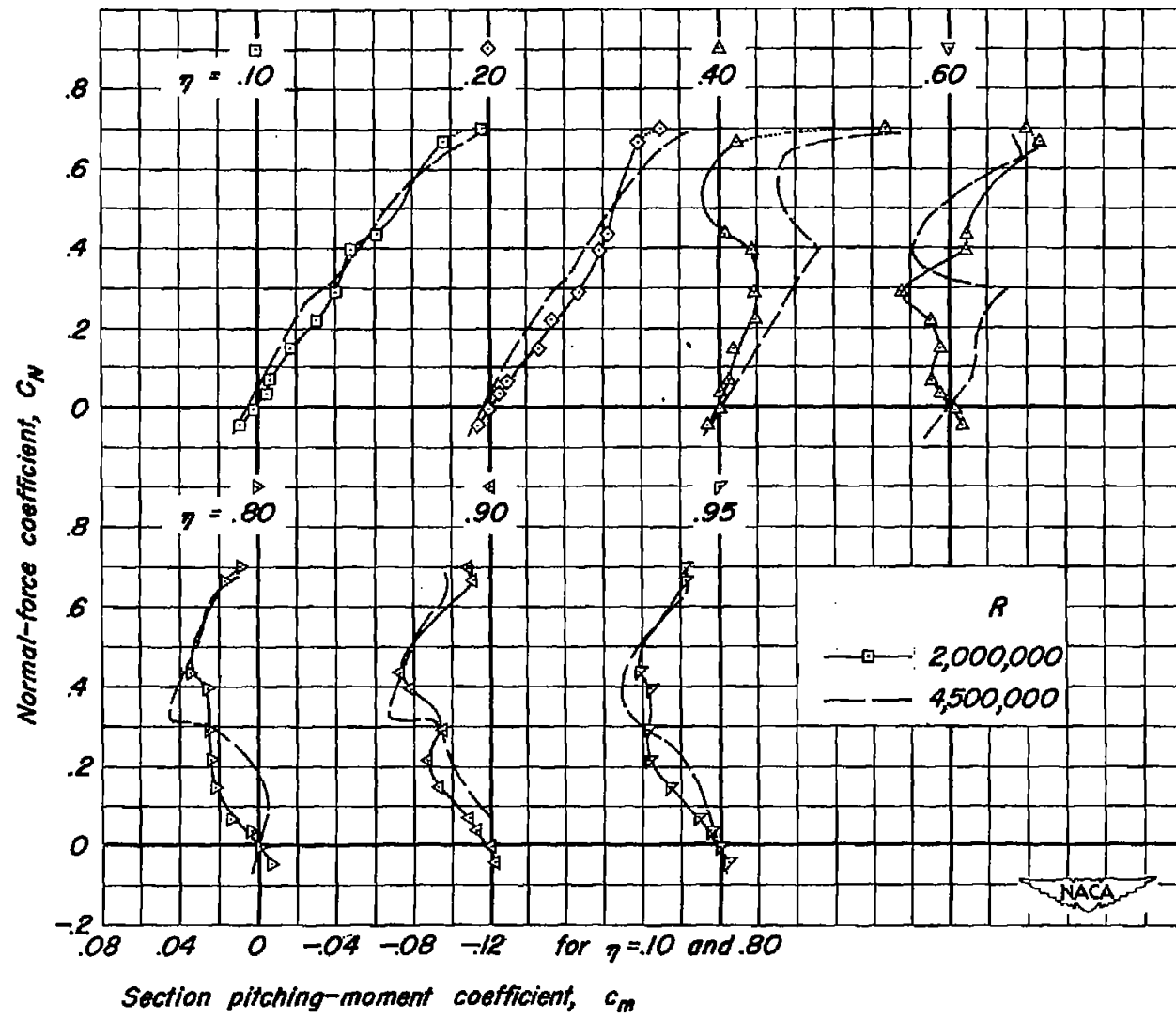
Angle of attack, α , deg

(b) Section normal-force characteristics.

Figure 15.-Continued. M, 0.90.

CONFIDENTIAL

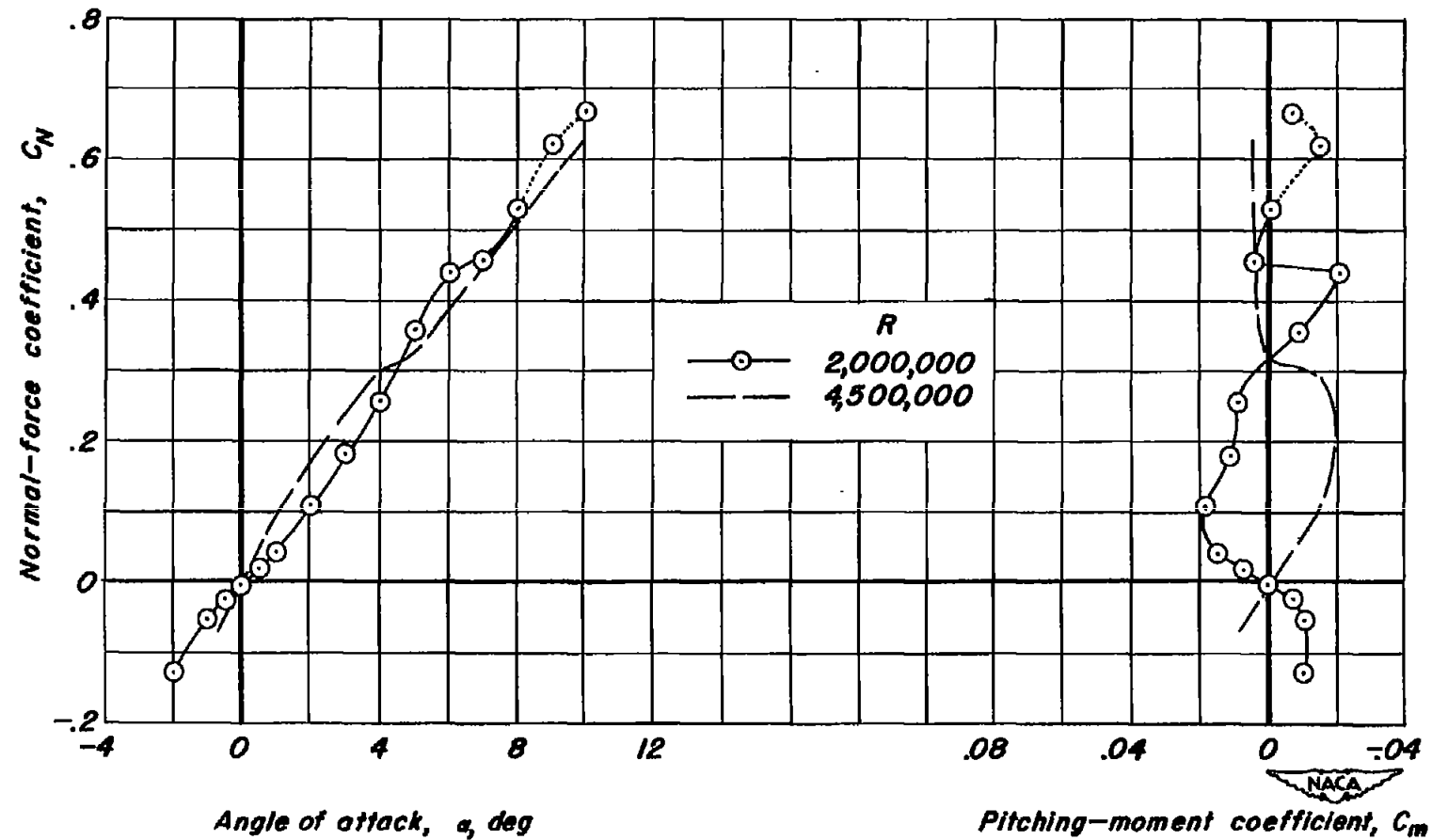
22



(c) Section pitching-moment characteristics.

Figure 15.— Concluded. M, 0.90.

NACA RM 45250

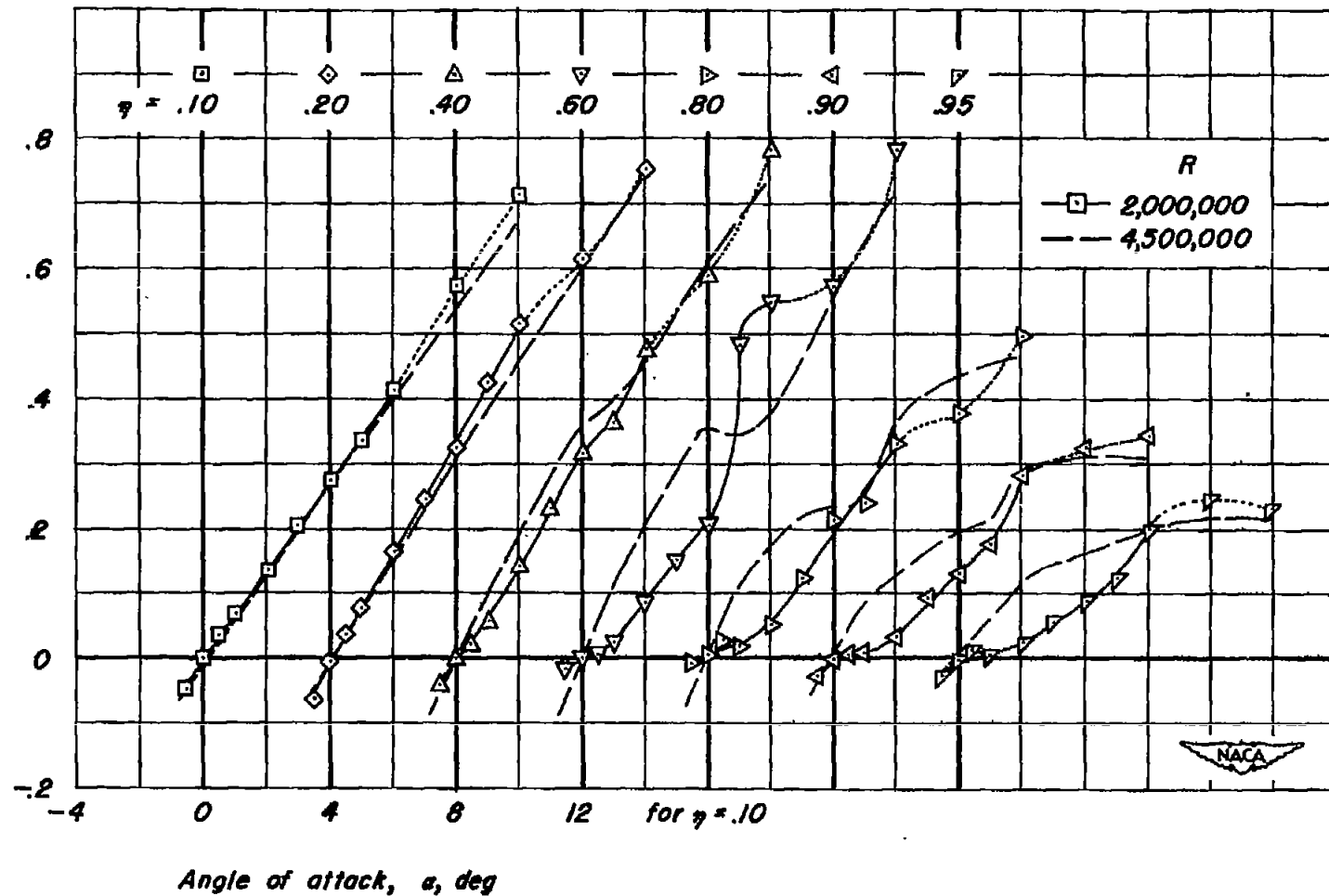


(a) Normal-force and pitching-moment characteristics.

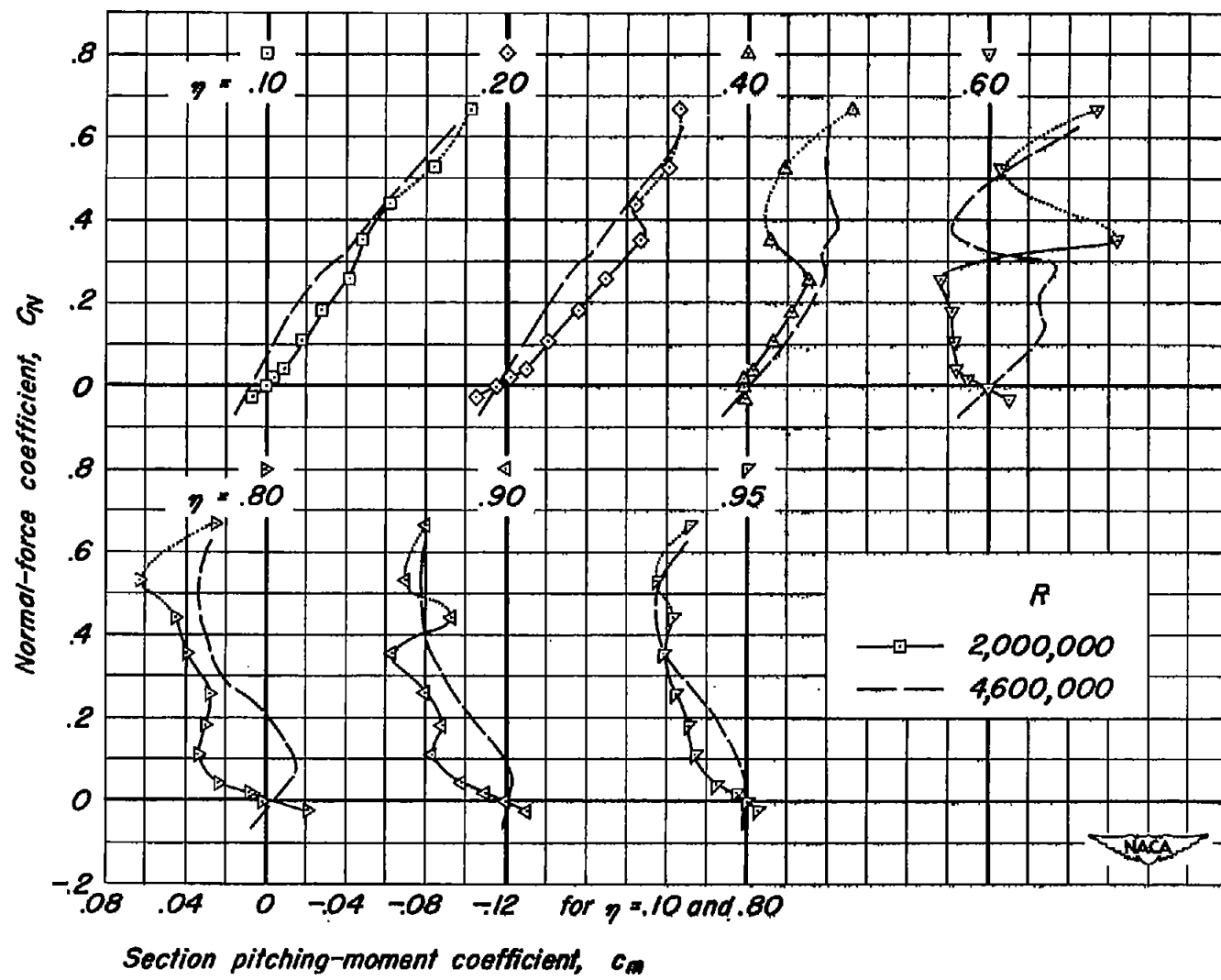
Figure 16.— The normal-force and pitching-moment characteristics and the corresponding section characteristics for seven sections of the wing. $M, 0.92$.

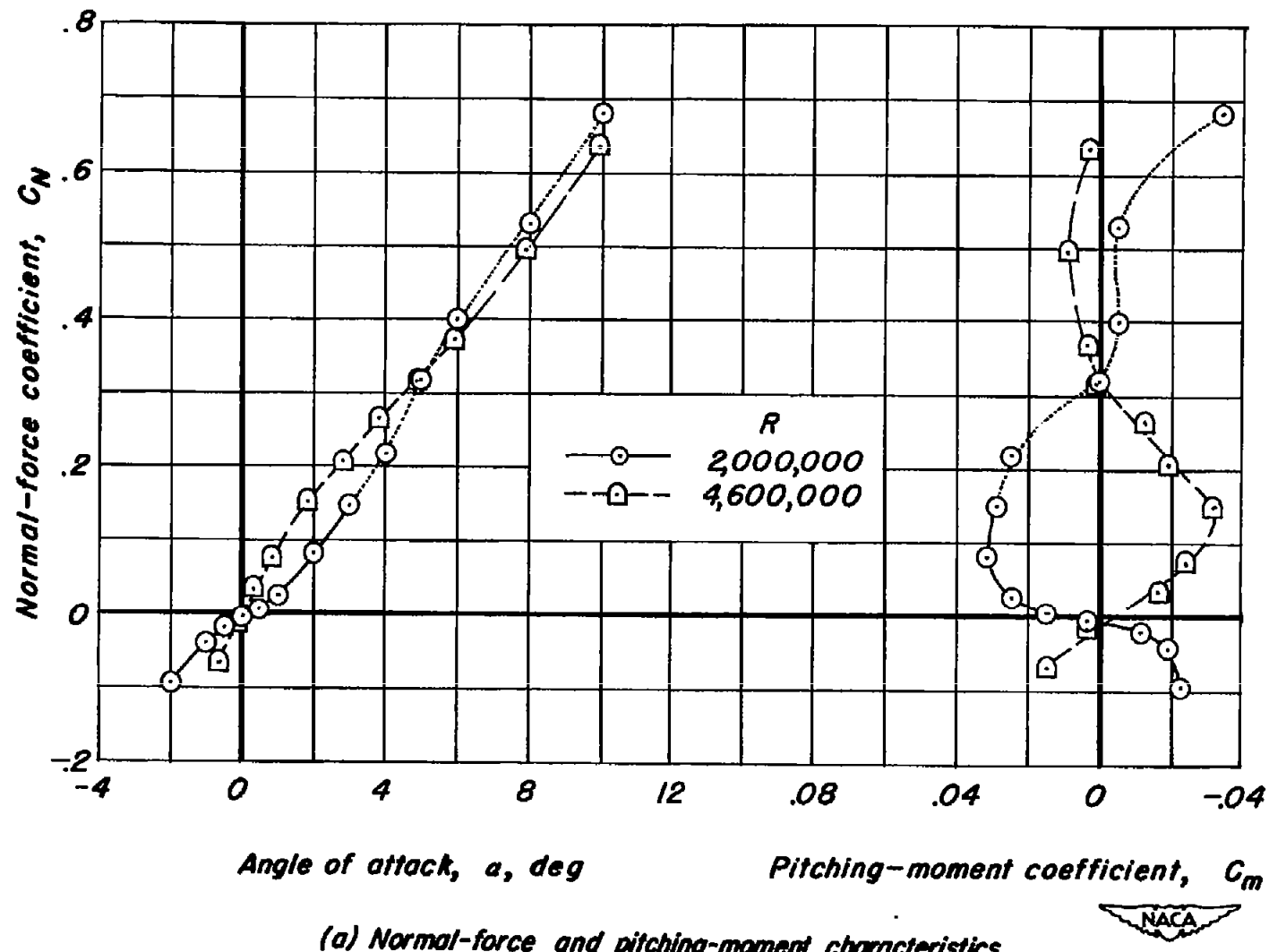
CONFIDENTIAL

U.S. GOVERNMENT PRINTING OFFICE

Section normal-force coefficient, C_N 

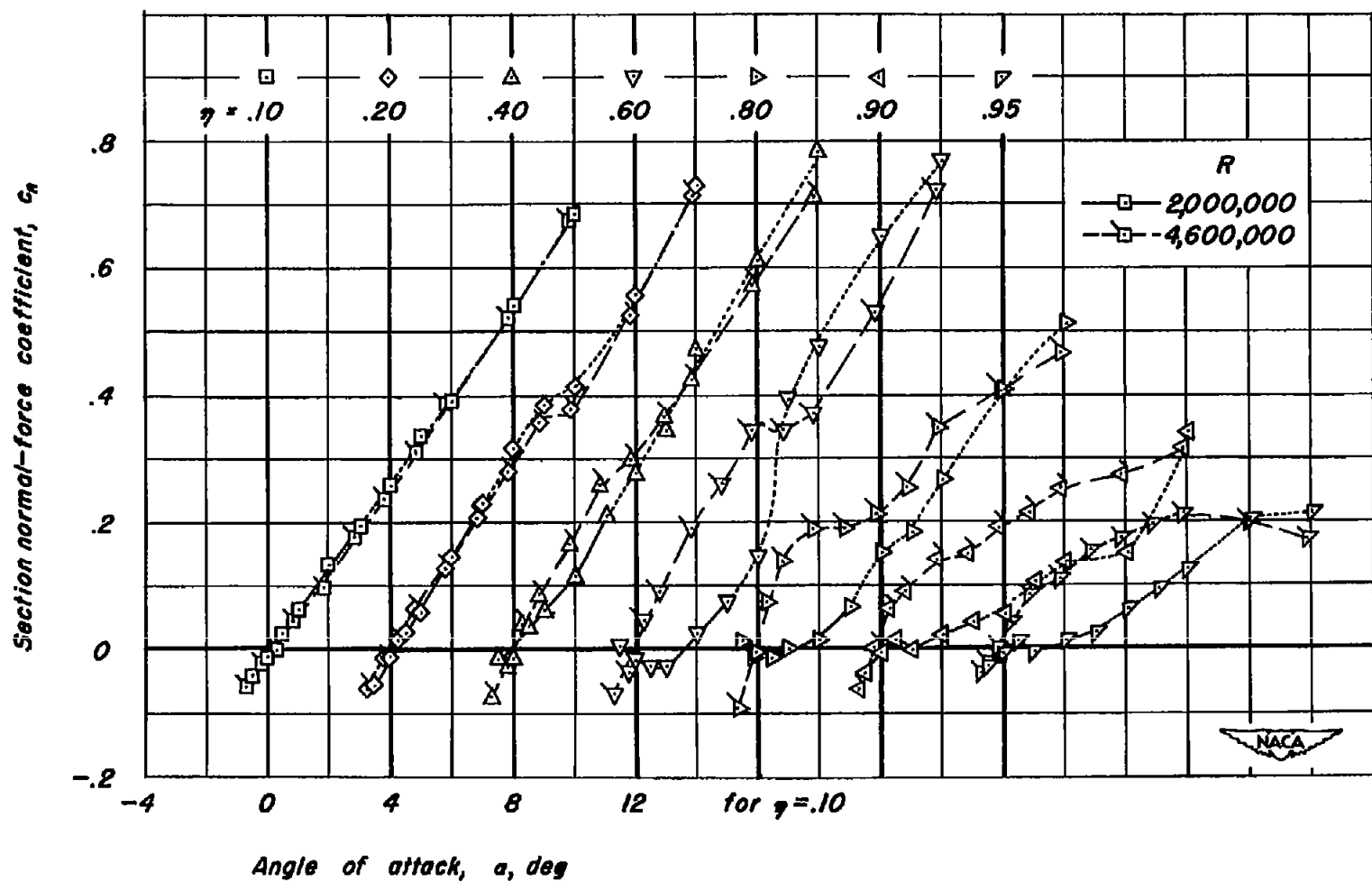
(b) Section normal-force characteristics.
Figure 16.-Continued. $M = 0.92$.



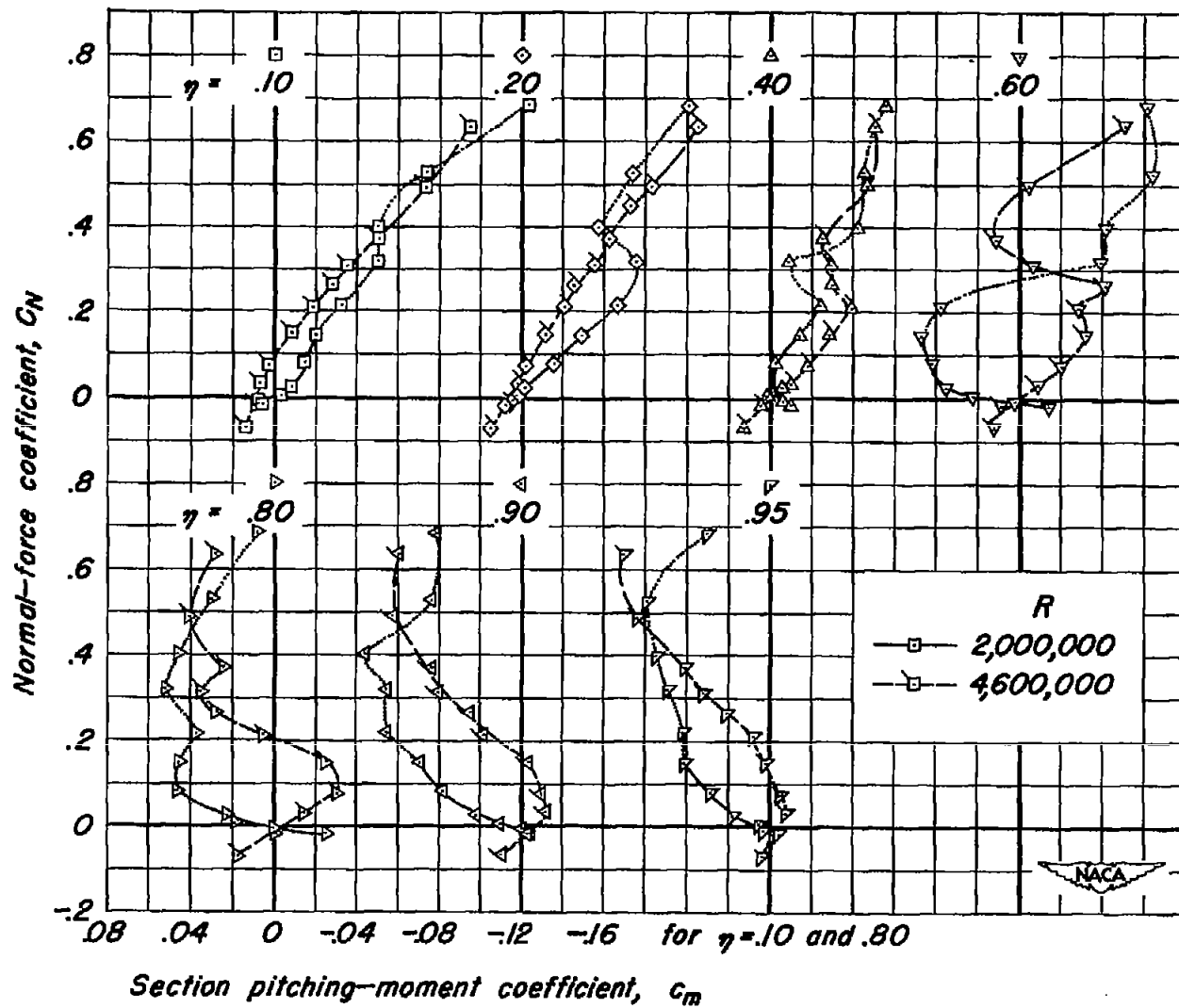


(a) Normal-force and pitching-moment characteristics.

Figure 17.—The normal-force and pitching-moment characteristics and the corresponding section characteristics for seven sections of the wing. $M, 0.94$.



(b) Section normal-force characteristics.
Figure 17.—Continued. $M, 0.94$.



Section pitching-moment coefficient, c_m

(c) Section pitching-moment characteristics.

Figure 17.—Concluded. M, 0.94.

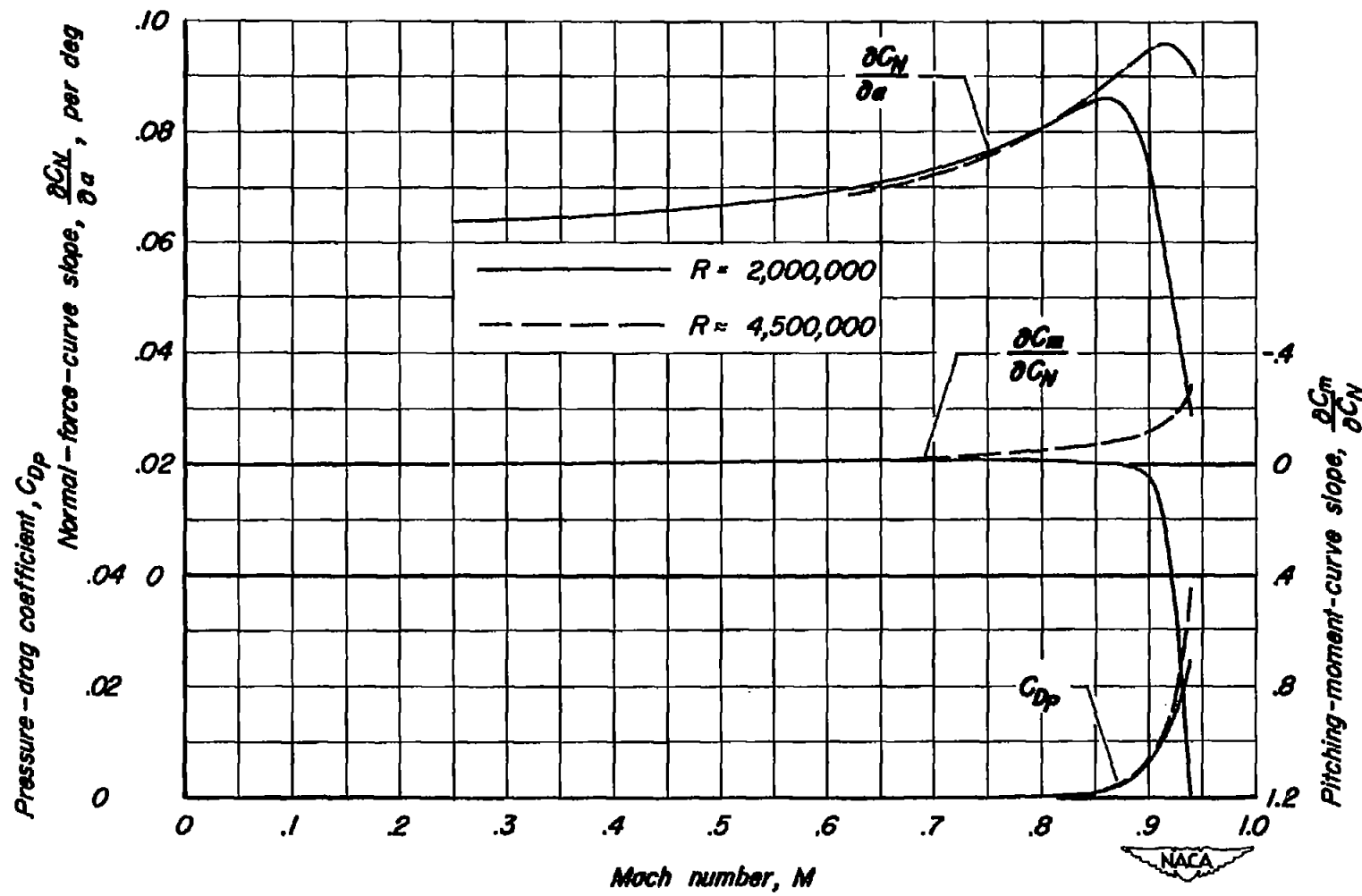


Figure 18.- The effect of Reynolds number on the variation with Mach number of the normal-force-curve slope, the pitching-moment-curve slope, and the pressure-drag coefficient, C_N , 0.

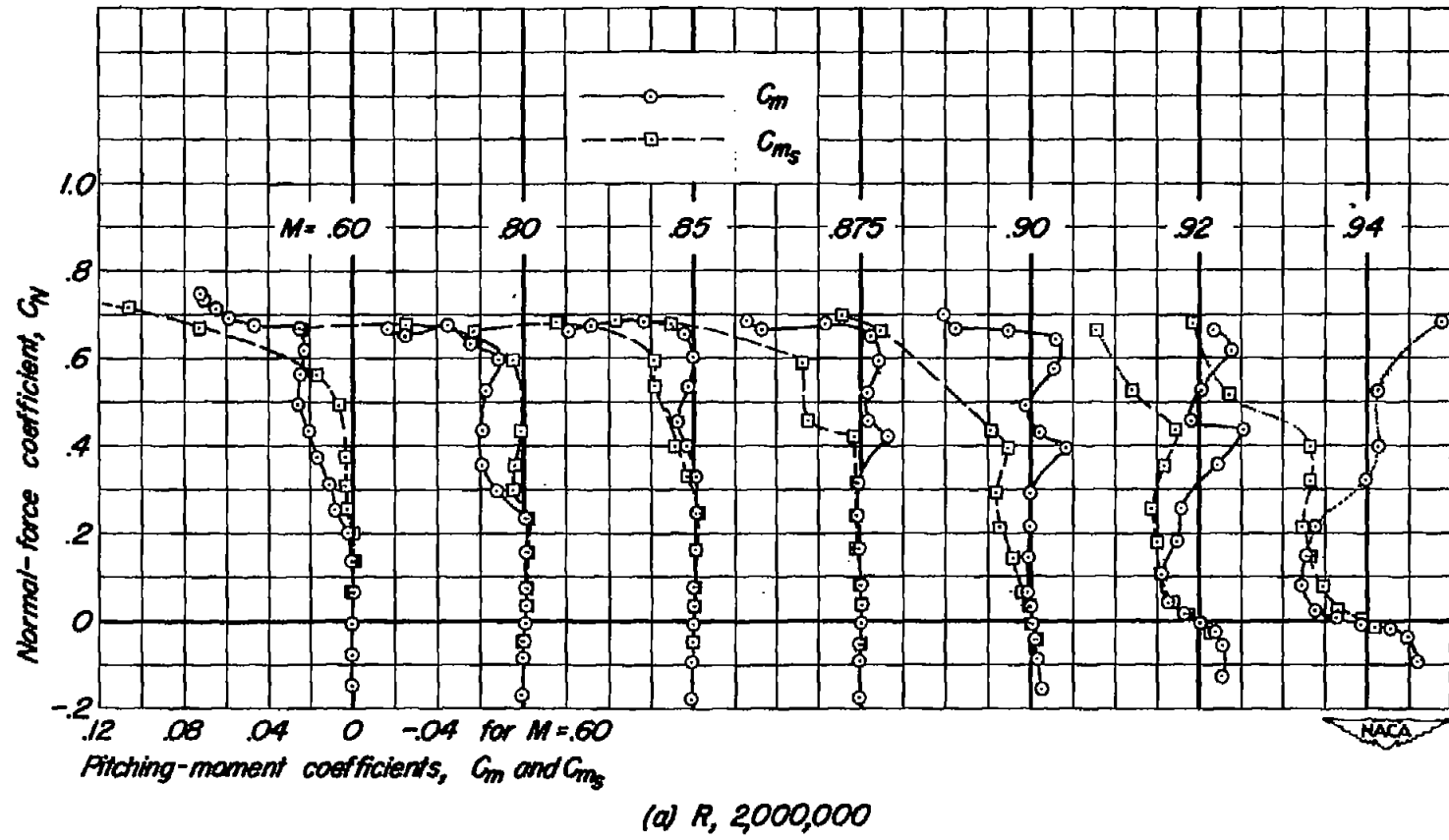
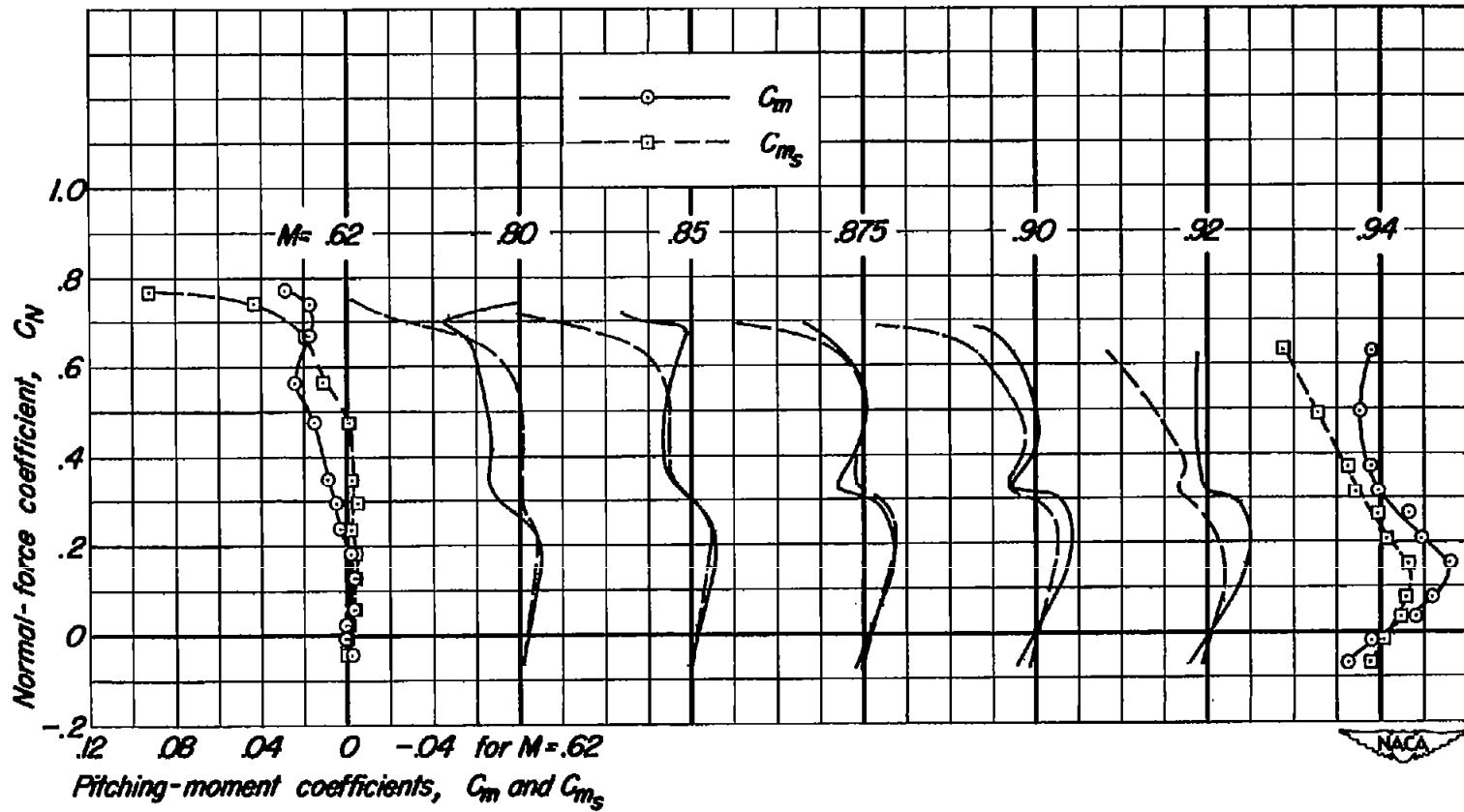


Figure 19 - Comparison of the pitching-moment coefficient, C_m , with the span-load pitching-moment coefficient, C_{m_s} .



(b) R , approximately 4,500,000

Figure 19.- Concluded.

CONFIDENTIAL

NACA RM A52B20

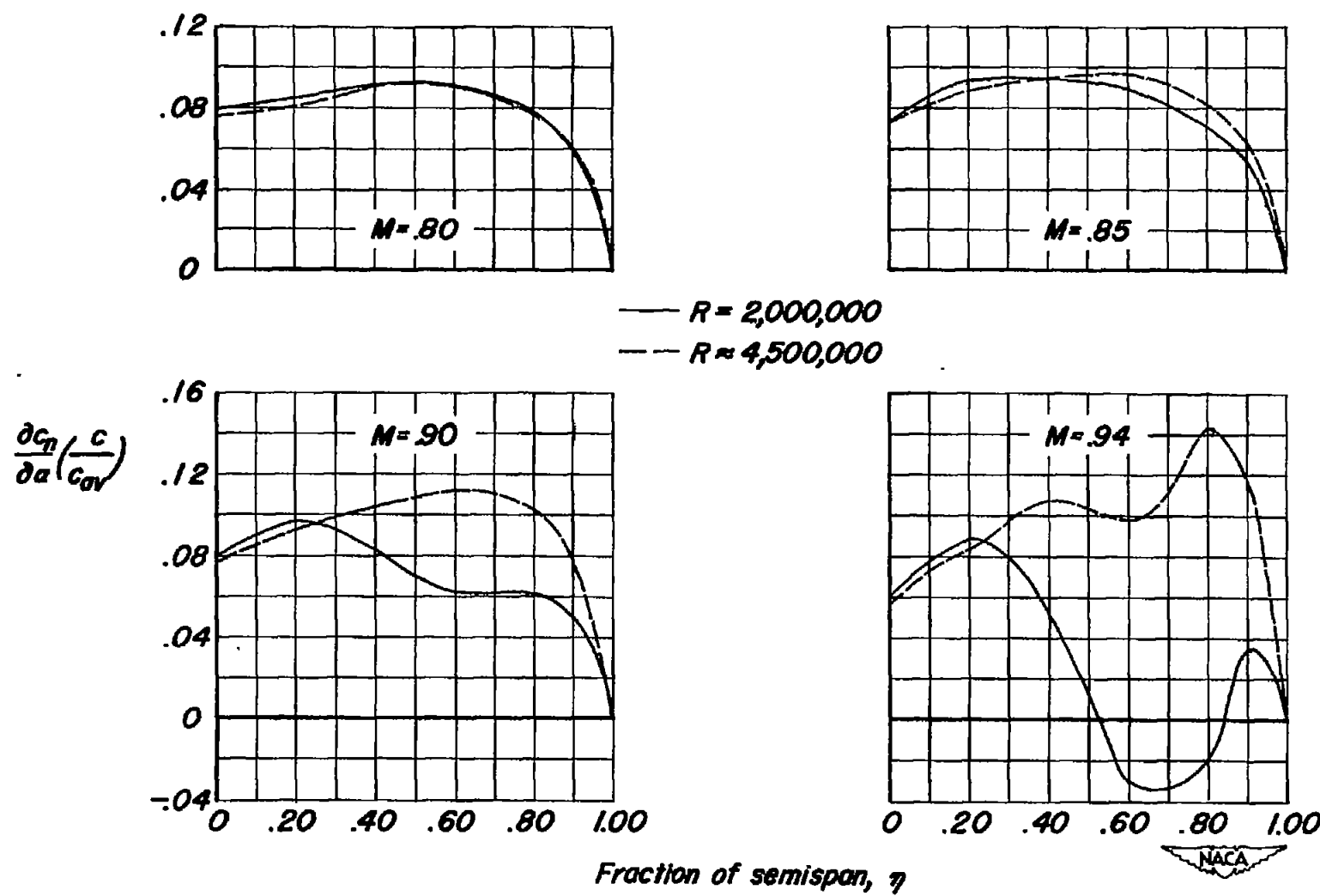


Figure 20.- The spanwise distribution of loading indicated by the slopes of the section normal-force curves at an angle of attack of 0° .

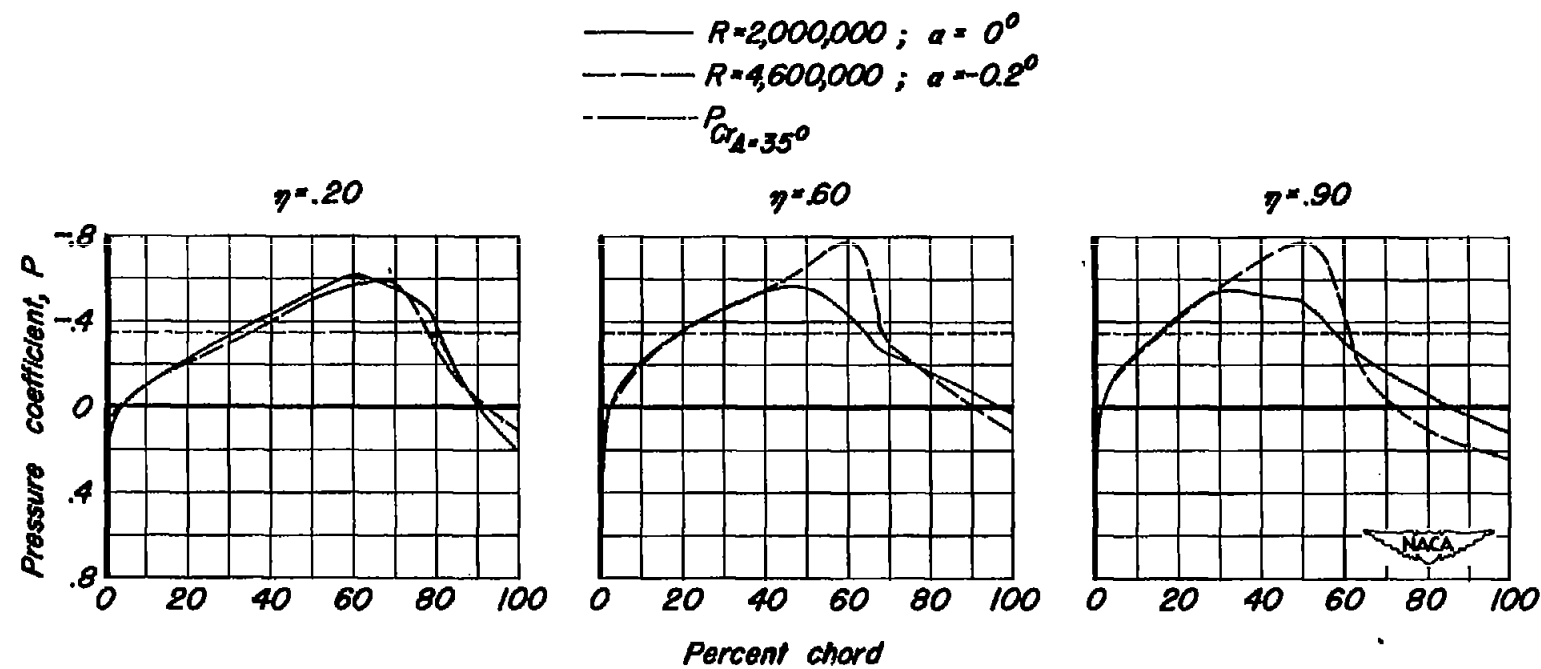


Figure 21.— The chordwise distribution of static pressure coefficient over the upper surface at 20, 60, and 90 percent of the semispan. $M, 0.94$.

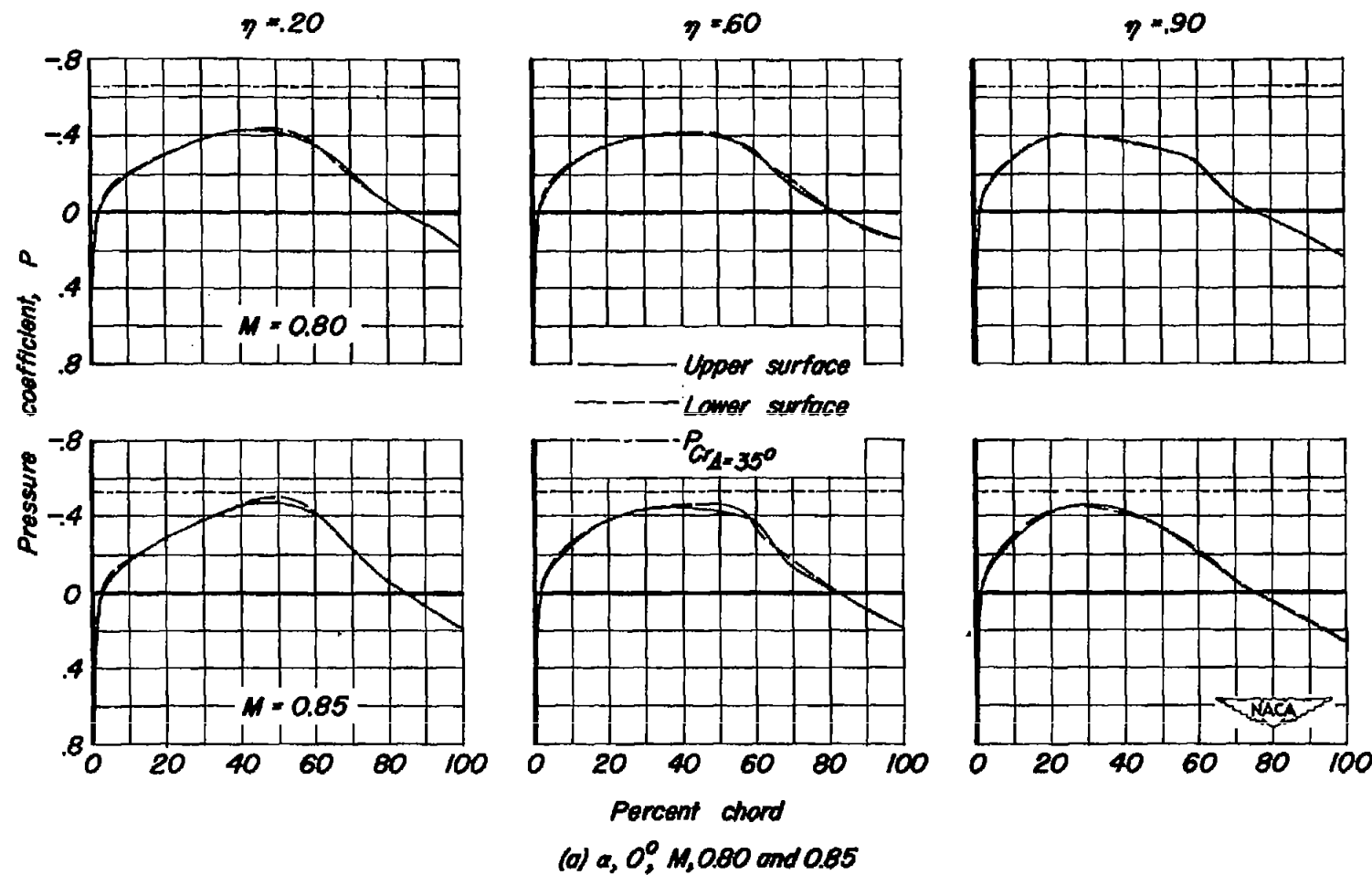
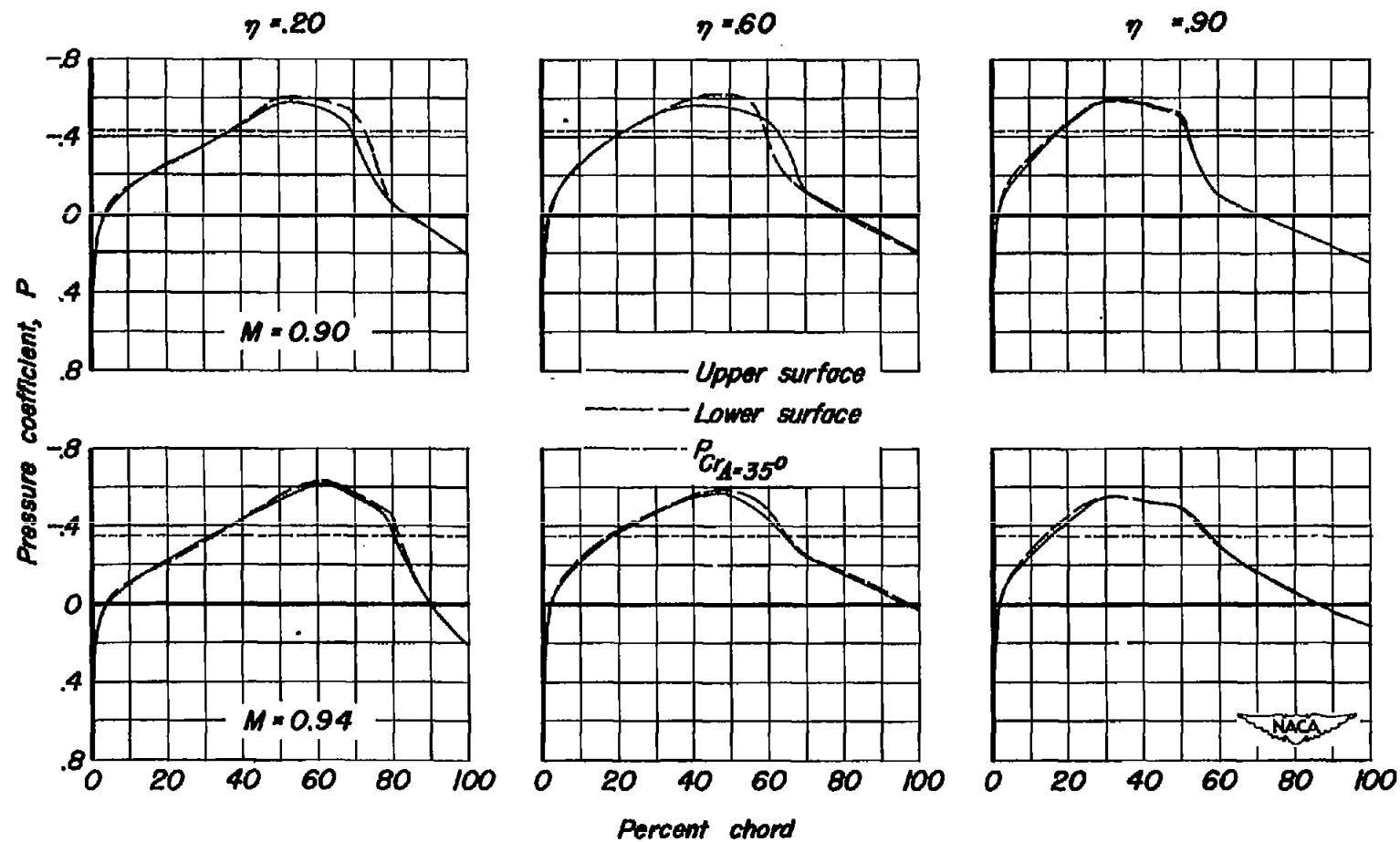
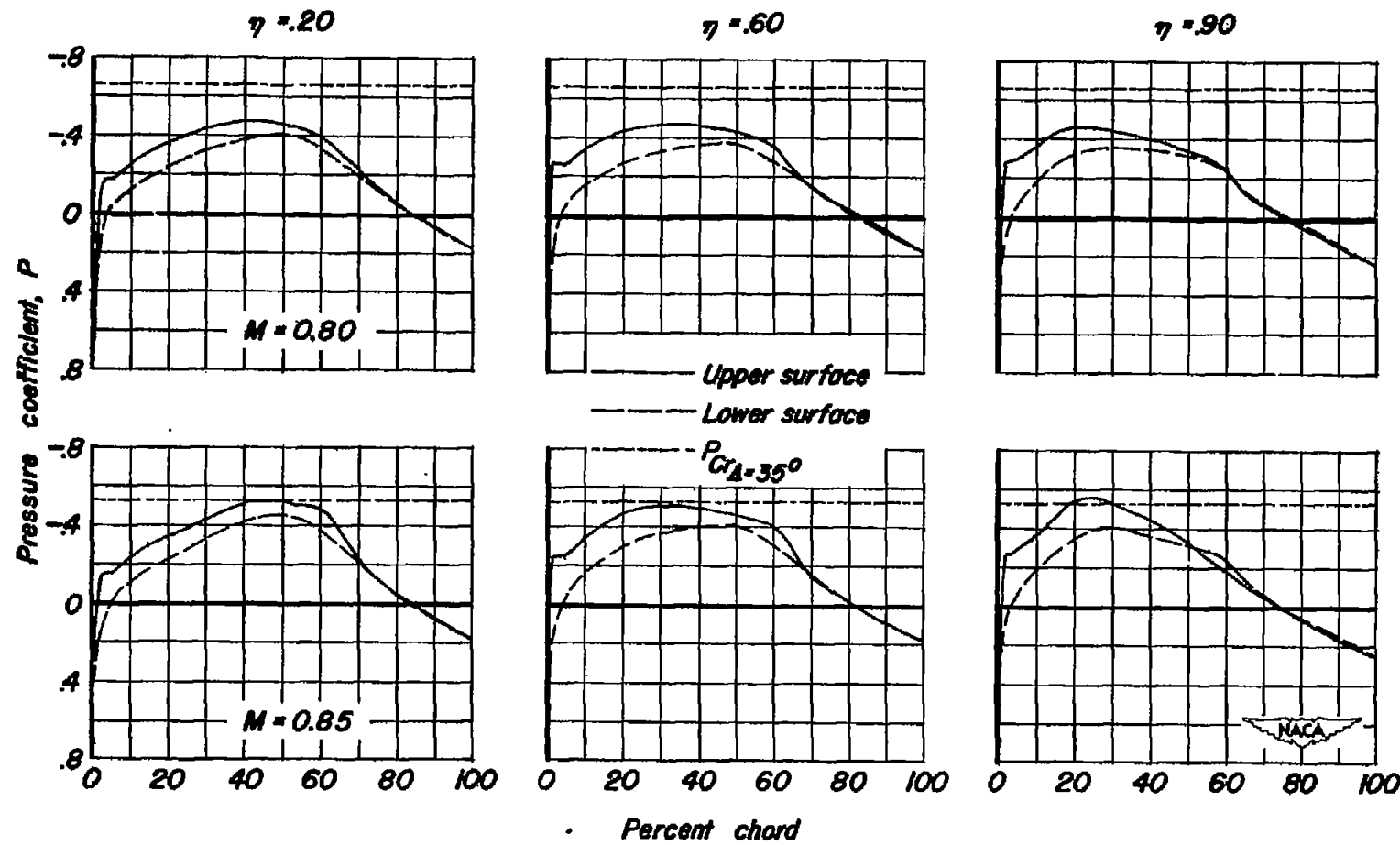
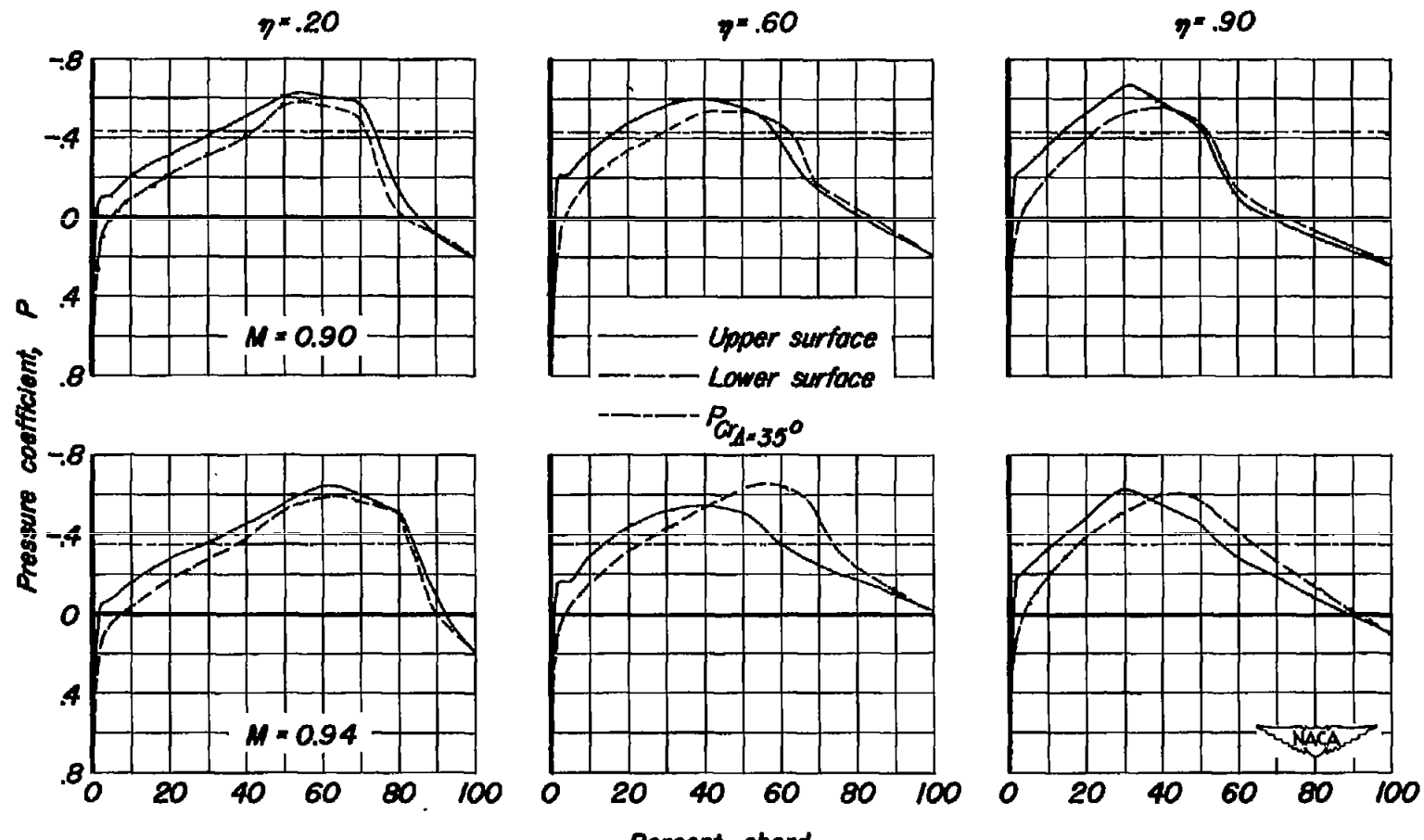
(a) $\alpha, 0^\circ, M, 0.80$ and 0.85

Figure 22.— The chordwise distribution of static pressure coefficient at 20, 60 and 90 percent of the semispan for angles of attack of 0° and 1° at several Mach numbers. $R, 2,000,000$.

(b) $\alpha, 0^\circ; M, 0.90$ and 0.94 Figure 22.- Continued. $R, 2,000,000$.

Figure 22.—Continued. $R, 2,000,000$.

(d) $\alpha, 1^\circ; M, 0.90$ and 0.94 Figure 22.- Concluded. $R, 2,000,000$.

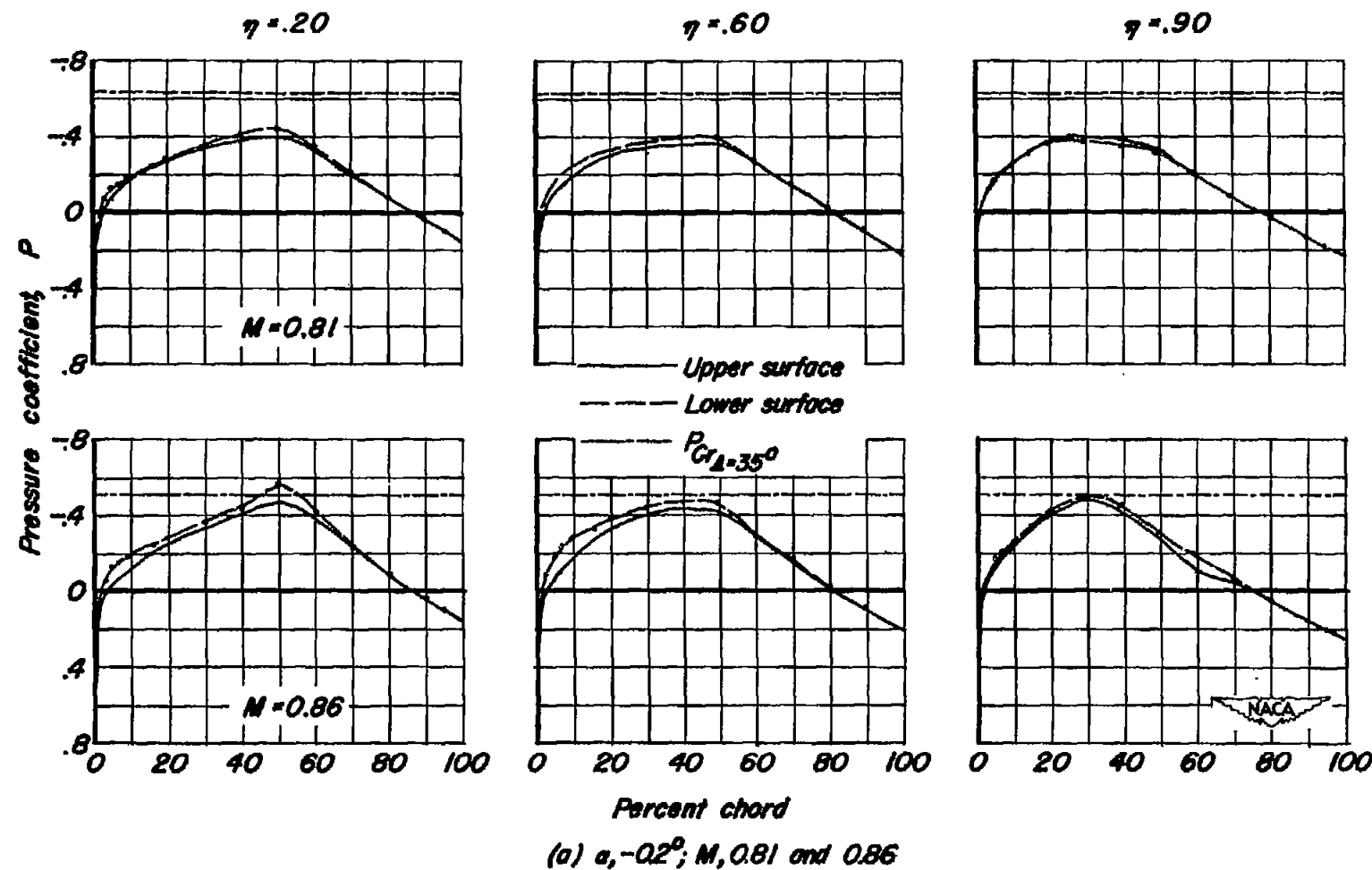
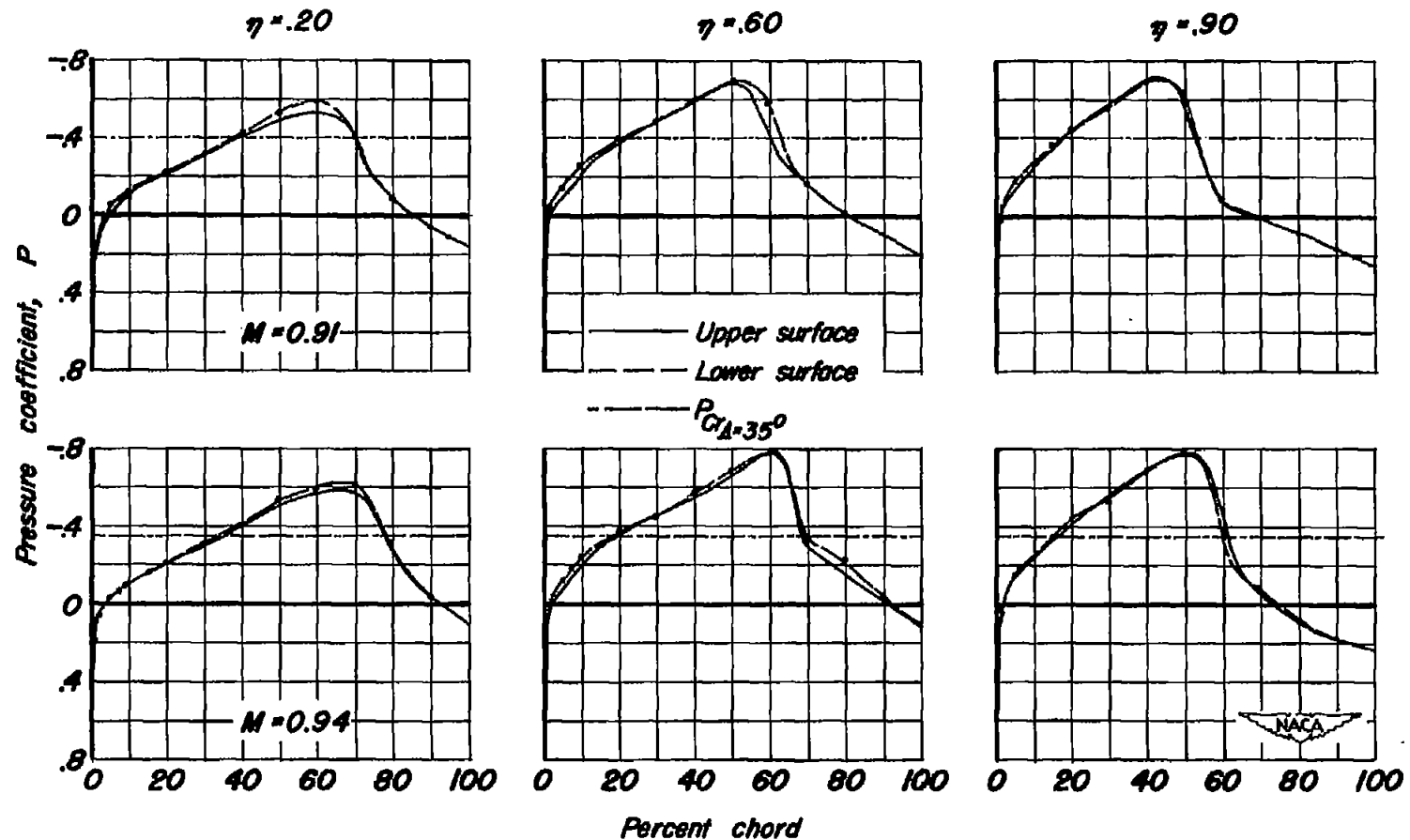
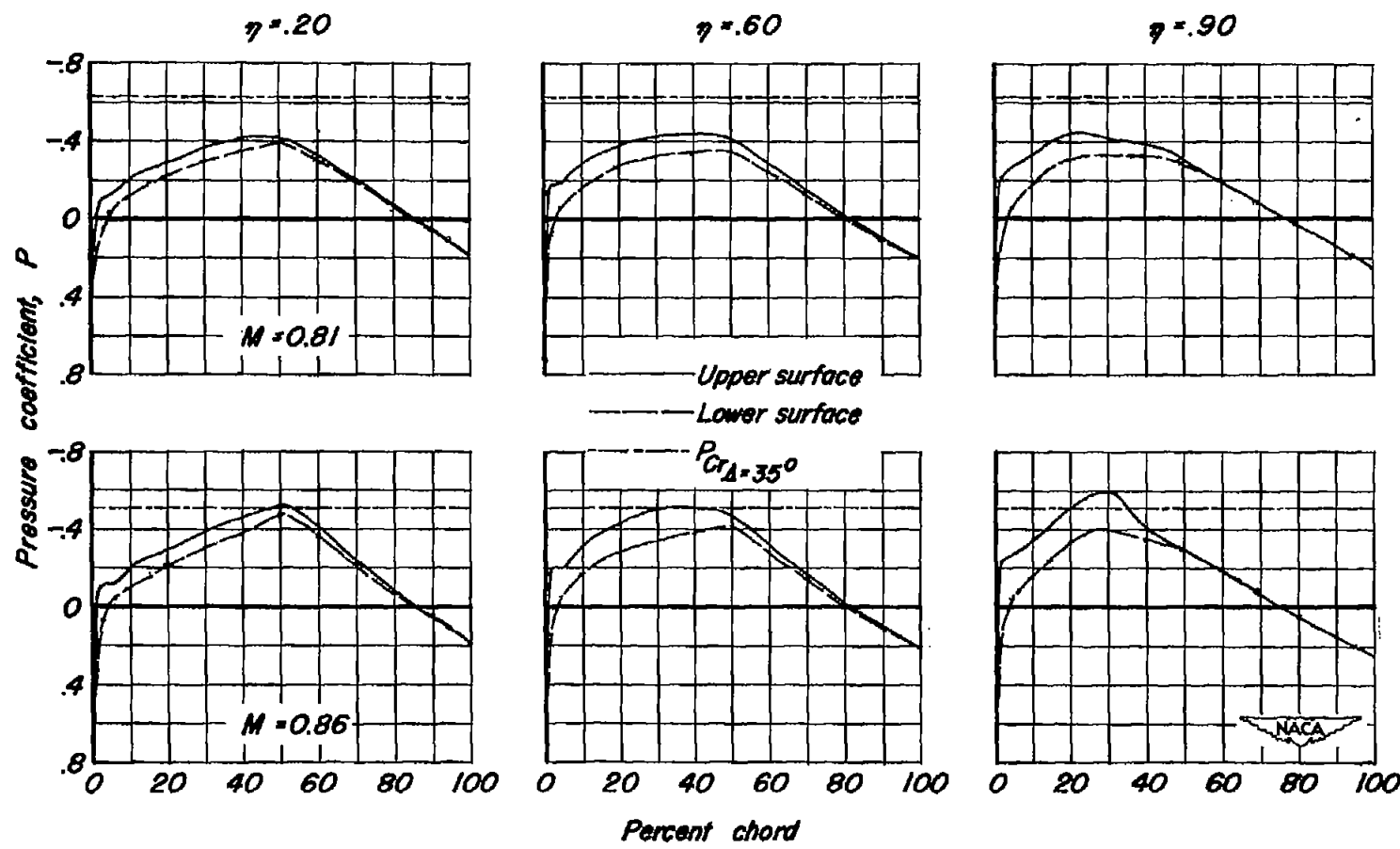


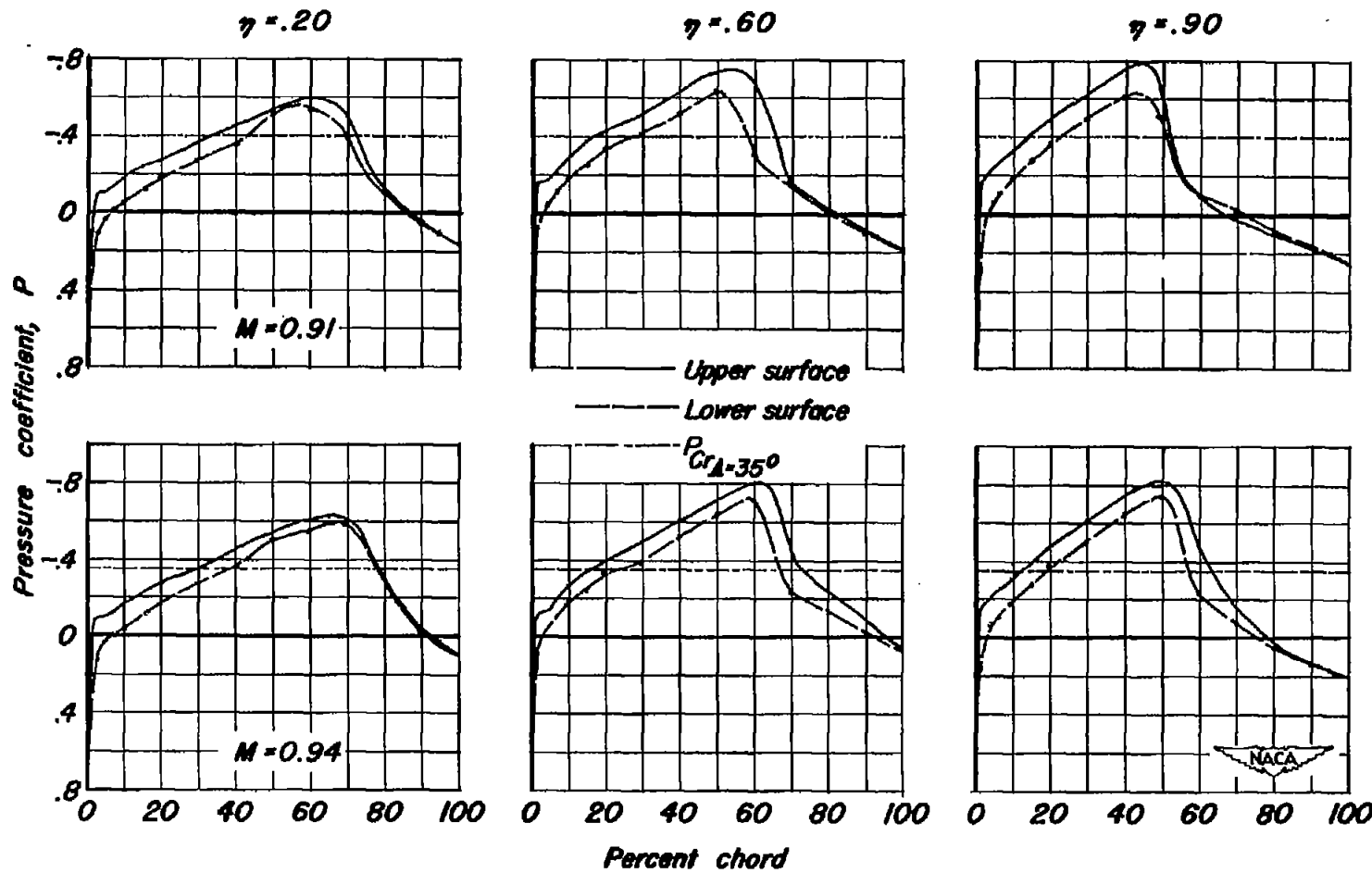
Figure 23.—The chordwise distribution of static pressure coefficient at 20, 60, and 90 percent of the semispan for angles of attack of -0.2° and 0.8° at several Mach numbers. Approximate $R, 4,500,000$.

(b) $\alpha = -0.2^\circ$; $M = 0.91$ and 0.94 Figure 23.- Continued. Approximate $R = 4,500,000$.



(c) $\alpha, 0.8^\circ; M, 0.81$ and 0.86

Figure 23.-Continued. Approximate $R, 4,500,000$.

(d) $\alpha, 0.8^\circ; M, 0.91$ and 0.94 Figure 23.— Concluded. Approximate $R, 4,500,000$.

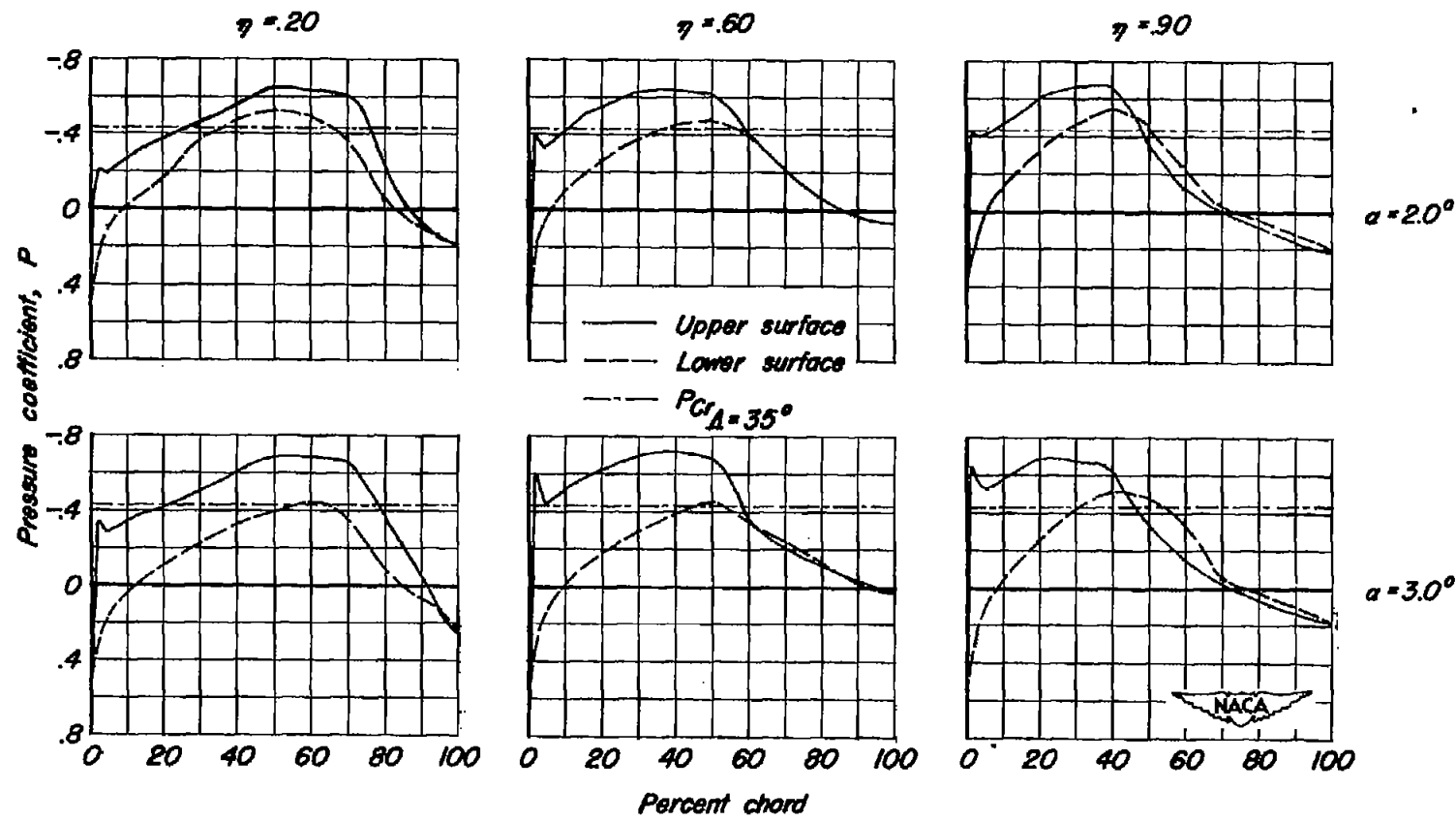
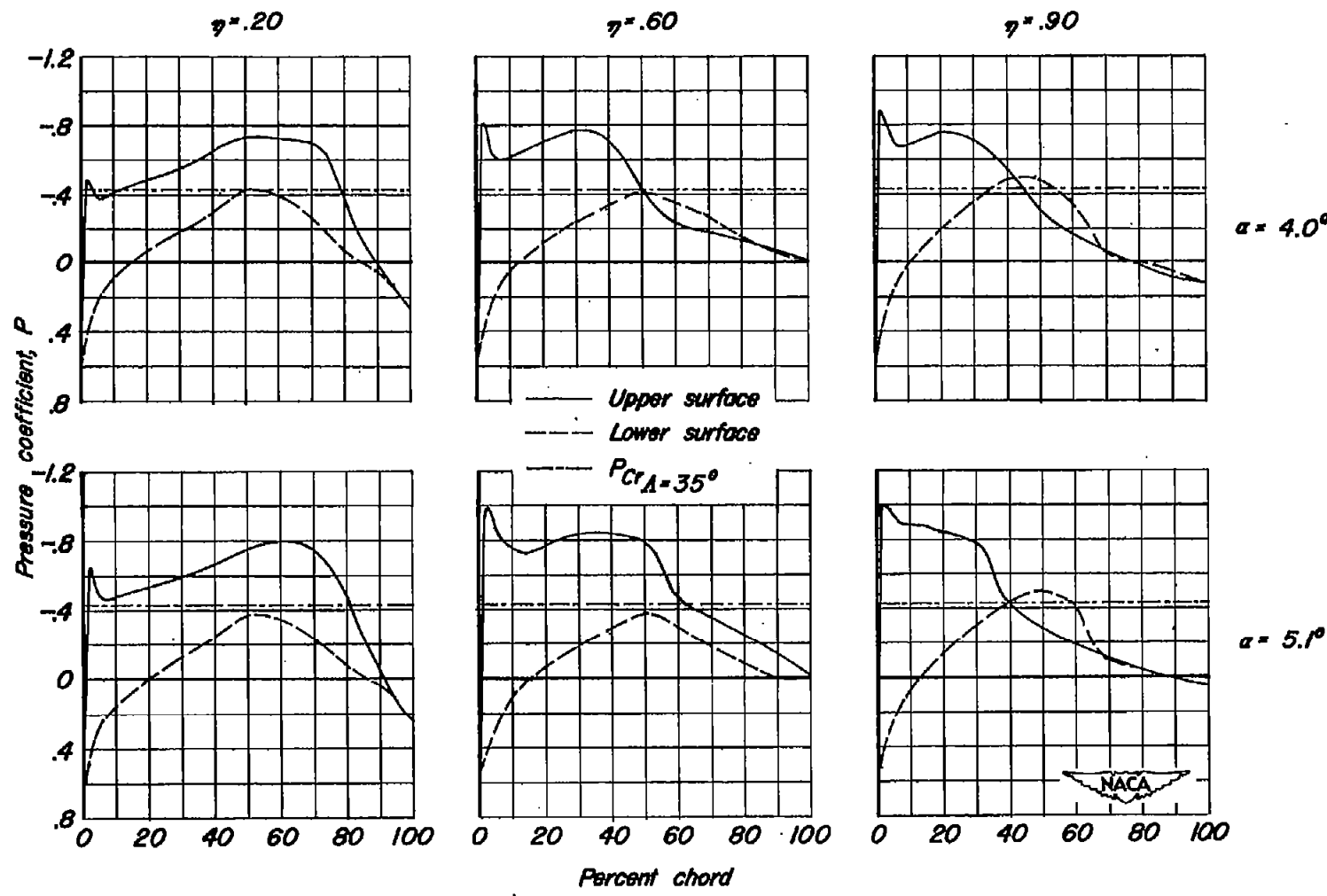
(a) $\alpha, 2.0^\circ$ and 3.0° ; $M, 0.90$; $R, 2,000,000$.

Figure 24.— The chordwise distribution of static pressure coefficient at 20, 60, and 90 percent of the semispan.



(b) $\alpha, 4.0^\circ$ and 5.1° ; $M, 0.90$; $R, 2,000,000$.

Figure 24.—Continued.

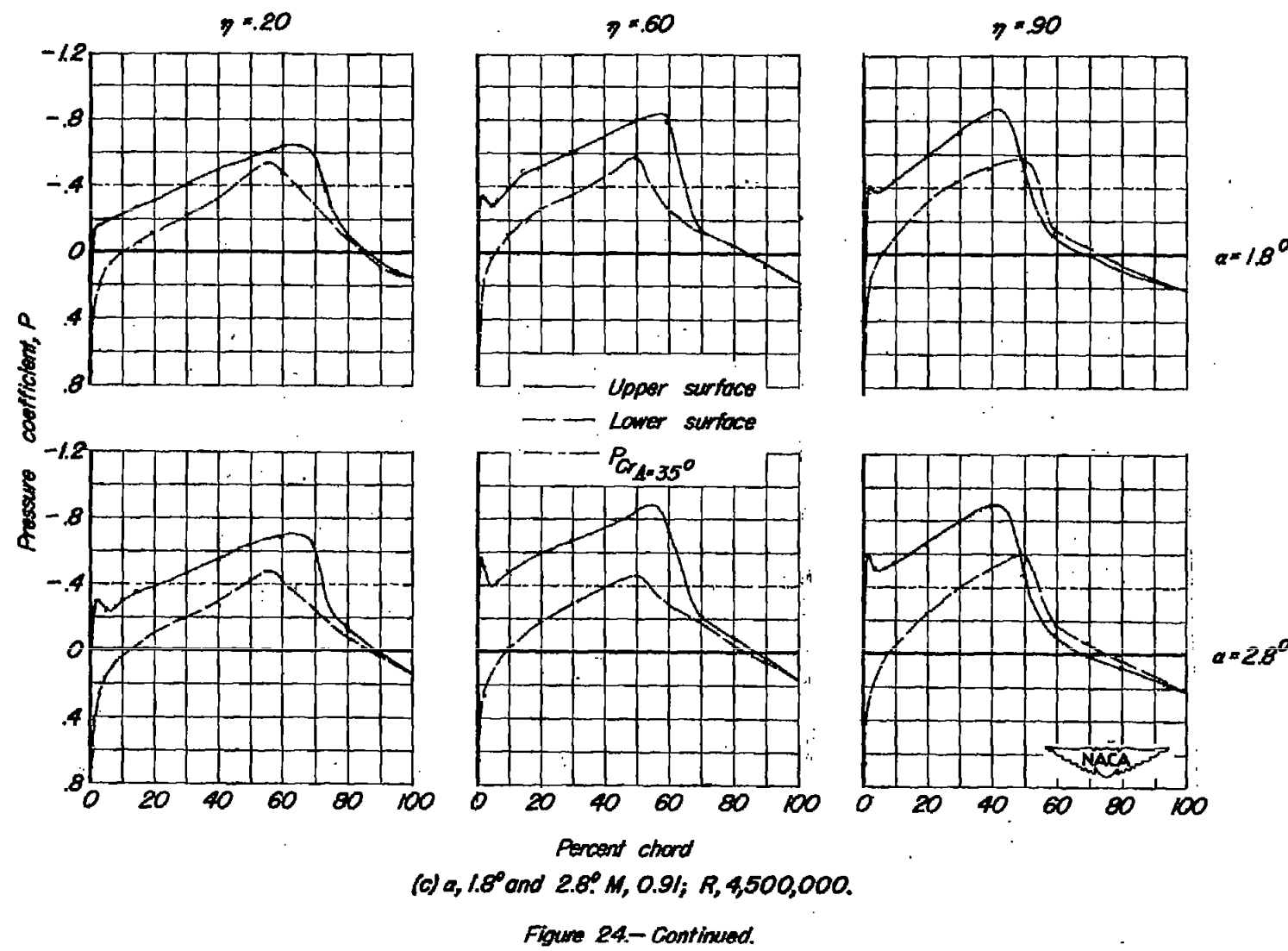
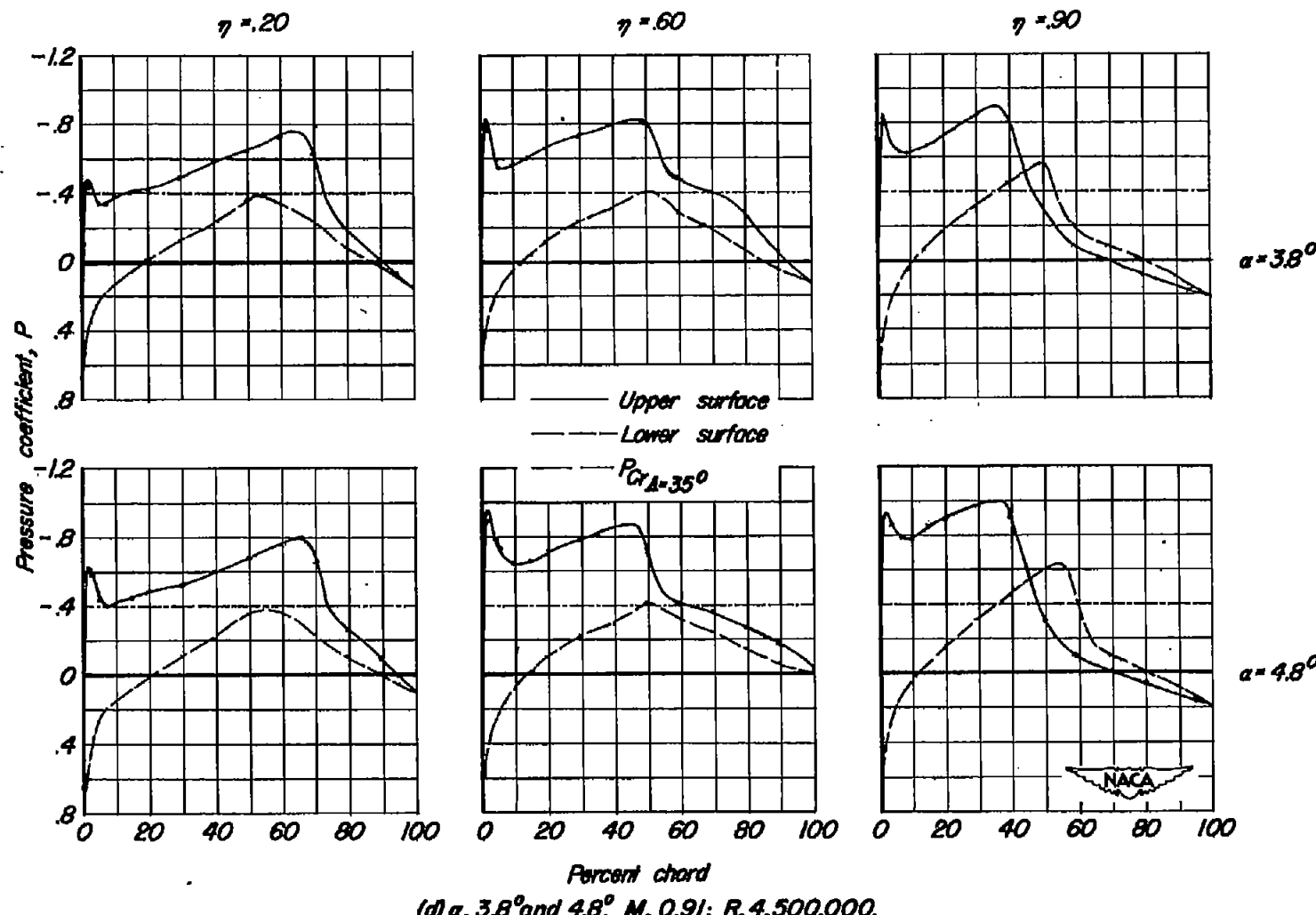


Figure 24.—Continued.



(d) $\alpha, 3.8^\circ$ and 4.8° ; $M, 0.91$; $R, 4,500,000$.

Figure 24.- Concluded.